UNIVERSITY OF LIVERPOOL

Efficient Computation of Cable Electromagnetic Compatibility Problems with Parametric Uncertainty

by

Zhouxiang Fei

B.Eng. M.Sc.

Submitted in accordance with the requirements for the award of the degree of Doctor of Philosophy of the University of Liverpool

January 2018

Copyright

To my beloved wife Xin Li, my mother Weina Zhou, and my father Jingyin Fei. Thank you for everything of my life.

Acknowledgements

The past four years of my PhD study are the most meaningful and successful time in my life. This period has formed my professional research ability and given me a new horizon to view the world. First and foremost, I would like to dedicate my deepest and sincerest gratitude to my supervisor Professor Yi Huang. Thank you for giving me the opportunity to conduct the PhD study under your supervision. Your excellent guidance and generous financial support have helped me achieve numerous successful research outcomes. You have guided me along the correct path of my research and career, and given me a bright future life. Your teaching in research and life has shaped me as a professional academic with nice personality. My thankfulness to you is immeasurable. I would also like to thank my second supervisor Dr. Jiafeng Zhou for your informative feedback on my presentation, your guidance on my research, and your awareness of connecting academic research to industrial applications.

I would like to thank my parents for your support in everything of my life. You have raised me up, taught me right from wrong, and supported me materially and spiritually throughout my life. I also appreciate the encouragement, care, patience, and trust from my beloved wife. You have helped me face every new day with positive attitude.

My thanks also go to my helpful colleagues as well as friends in life. Particularly, I would like to thank Dr. Jingwei Zhang, Dr. Ping Cao, Dr. Qian Xu, Dr. Lei Xing, Dr. Sheng Yuan, Dr. Muayad Kod, Dr. Chaoyun Song as well as Abed Pour Sohrab, Zhihao Tian, Muaad Hussein, Anqi Chen, Yuan Zhuang, Manoj Stanley, Umniyyah Ulfa, Tianyuan Jia, Wenzhang Zhang, Yansong Wang, Jingyuan Jiang, and Qiang Hua for your help in my research and daily life.

Last but not least, the financial support from the Innovate U.K. and the University of Liverpool is gratefully acknowledged.

Table of Contents

List of Figures

Acronyms

CDF	Cumulative Distribution Function
COV	Coefficient of Variance
CST	Computer Simulation Technology
DUT	Device Under Test
EM	Electromagnetic
EMC	Electromagnetic Compatibility
GHz	Giga Hertz (10^9)
MATLAB	Matrix Laboratory
MC	Monte-Carlo
MHz	Mega Hertz (10^6)
MTL	Multiconductor Transmission Line
HIRF	High Intensity Radiated Fields
IEEE	Institute of Electrical and Electronics Engineers
KCL	Kirchhoff's Current Law
kHz	kilo Hertz (10^3)
KVL	Kirchhoff's Voltage Law
PCB	Printed Circuit Board
PCE	Polynomial Chaos Expansion

PDF	Probability Density Function
PVC	Polyvinyl Chloride
RC	Reverberation Chamber
RF	Radio Frequency
SC	Stochastic Collocation
SMA	Subminiature Version A
SROM	Stochastic Reduced Order Model
TEM	Transverse Electromagnetic
TWP	Twisted-Wire Pair
UTLM	Unstructured Transmission Line Modelling
VNA	Vector Network Analyser

List of Publications and Awards

Journal Publications

[1] **Z. Fei**, Y. Huang, J. Zhou, and C. Song, "Numerical analysis of a transmission line illuminated by a random plane-wave field using stochastic reduced order models," *IEEE Access*, vol. 5, no. 1, pp. 8741-8751, 2017.

[2] **Z. Fei**, Y. Huang, J. Zhou, and Q. Xu, "Uncertainty quantification of crosstalk using stochastic reduced order models", *IEEE Transactions on Electromagnetic Compatibility*, vol. 59, no. 1, pp. 228-239, Feb. 2017.

[3] Y. Zhuang, **Z. Fei**, A. Chen, Y. Huang, K. Rabbi, and J. Zhou, "Design of multioctave high-efficiency power amplifiers using stochastic reduced order models", *IEEE Transactions on Microwave Theory and Techniques*, vol. 66, no. 2, pp. 1015-1013, Feb. 2018.

[4] C. Song, Y. Huang, J. Zhou, P. Carter, S. Yuan, Q. Xu, and **Z. Fei**, "Matching network elimination in broadband rectennas for high-efficiency wireless power transfer and energy harvesting," *IEEE Transactions on Industrial Electronics*, vol. 64, no. 5, pp. 3950–3961, May 2017.

[5] Q. Xu, Y. Huang, L. Xing, Z. Tian, **Z. Fei**, and L. Zheng, "A fast method to measure the volume of a large cavity," *IEEE Access*, vol. 3, pp. 1555-1561, Sep. 2015.

Conference Publications

[1] **Z. Fei**, Y. Huang, J. Zhou, and Q. Xu, "Statistical analysis of crosstalk subject to multiple uncertainty sources using stochastic reduced order models", in *Proc. EMC Europe 2016 symposium*, Wroclaw, Poland, Sep. 2016, pp. 690-694.

[2] **Z. Fei**, Y. Huang, J. Zhou, and Q. Xu, "Sensitivity analysis of cable crosstalk to uncertain parameters using stochastic reduced order models", in *Proc. 2016 IEEE International Symposium on EMC*, Ottawa, Canada, Jul. 2016, pp. 385-389.

[3] **Z. Fei**, Y. Huang and J. Zhou, "Crosstalk variations caused by uncertainties in three-conductor transmission lines," in *Proc. Loughborough Antennas and Propagation Conference,* Loughborough, UK, Nov. 2015, pp. 1-5.

[4] H. Jiang, J. Zhou, Y. Huang, Y. Zeng, J. Humphries, Q. Xu, C. Song, L. Xing, **Z. Fei**, and J. Nalborczyk, "Design of a Marx generator for HEMP filter evaluation taking account of parasitic effect of components", in *Proc. EMC Europe 2016 symposium*, Wroclaw, Poland, Sep. 2016, pp. 839-843.

[5] Y. Zhuang, **Z. Fei**, A. Chen, Y. Huang, and J. Zhou,, "Distributed matching network design for broadband power amplifiers", in *Proc. 2017 IEEE Electrical Design of Advanced Packaging & Systems Symposium*, Haining, China, Dec. 2017, pp. 1-3. (Best Student Paper Award)

[6] **Z. Fei**, Y. Huang, J. Zhou, C. Song, and T. Jia, "Efficient stochastic analysis of transmission signal integrity for remote sensing applications", in *Proc. 2018 Joint IEEE International Symposium on EMC and APEMC* (Accepted).

Awards

[1] **Z. Fei**, Y. Huang, J. Zhou, and Q. Xu: the recipient of the Student Scholarship from the IEEE EMC Society to attend the 2016 IEEE International Symposium on EMC, Ottawa, Canada, July 2016.

[2] Z. **Fei**, Y. Huang, J. Zhou, and Q. Xu: the BEST EMC PAPER FINALIST for the 2016 IEEE International Symposium on EMC, Ottawa, Canada, July 2016.

[3] Y. Zhuang, **Z. Fei**, A. Chen, Y. Huang, and J. Zhou, "Distributed matching network design for broadband power amplifiers", in *Proc. EDAPS 2017* (Best Student Paper Award).

Abstract

Cables are heavily used to transmit power and signals in various systems. However, due to the susceptibility of cable to conducted and radiated emissions, unintended response could be provoked in the cable, and therefore, degrade the system operation. This is referred to as the cable electromagnetic compatibility (EMC) problems. Deterministic simulations based on the nominal values of system variables are usually performed to predict the possible malfunction. However, the variables characterising the cable system are naturally random due to, e.g. manufacturing tolerance. As a result of the systemic uncertainty, the induced interference in the cable also becomes a random observable. Therefore, the statistical description of the cable interference is a more reasonable outcome for assessing the system risk. Accordingly, stochastic approaches are needed to produce the required statistical outcome.

The conventional statistical approach to quantify the uncertainty of the system response is the Monte-Carlo (MC) method. However, the computational cost of the MC method could become overly expensive when dealing with a large number of random variables. Thus, the cable EMC problems in large platforms with multiple uncertainty sources cannot be efficiently solved using the MC method. Clearly, an efficient statistical approach needs to be sought to solve the challenging cable EMC problems in the real world. Very recently, the *stochastic reduced order model* (SROM) method was proposed in the field of mechanical engineering, and is known to have merits such as the non-intrusiveness feature and superior efficiency. Therefore, the potential of applying the SROM method for cable EMC problems is very promising, and thoroughly investigated in this thesis.

This thesis presents a comprehensive study of the cable EMC problems. The contributions of this thesis are mainly twofold, comprising the investigation of cable interference caused by: (1) the conducted emission (mainly at intra-system level), and (2) the radiated emission when exposed to incident electromagnetic fields. In the case of parametric uncertainty, the

statistical analysis of the induced interference is efficiently performed using the SROM method.

Specifically, the first main contribution of this thesis is dedicated to the study of crosstalk phenomenon, i.e., the inference induced to a wire by nearby wires in the cable. A parametric study is performed to investigate the effect (i.e., by increasing or decreasing) of the cable configurational changes on the crosstalk variation. The result can also be used to suggest factors causing excessive crosstalk. Under the cable parametric uncertainty, the statistics of crosstalk is successfully predicted using the SROM method. The efficiency of the statistical analysis using the SROM method and its ease of implementation are clearly demonstrated, compared to the conventional MC method and another state-of-the-art statistical approach referred to as the stochastic collocation (SC) method. The sensitivity of crosstalk to different cable variables is efficiently quantified using the SROM method, and then ranked. With this ranking, the feasibility of reducing the complexity of stochastic EMC problems by ignoring weak parametric uncertainties is explored.

The second significant contribution of this thesis is the efficient uncertainty quantification of the interference in the cable caused by random electromagnetic field illumination. The most complex scenario where the incident electromagnetic wave is assumed to be fully random is chosen for investigation. As a response to the random illumination, the statistics of the interference (i.e., the induced current) in the cable is efficiently obtained using the SROM method. The computational cost of the SROM method is shown to be significantly reduced by orders of magnitude, compared to those of the MC and SC methods. The result demonstrates the potential of the SROM method for the general problems of the cable system response to the random radiation field.

Overall, the research presented in this thesis has successfully advanced the uncertainty propagation techniques for EMC problems, especially in the case of the cable interference. Based on the performance discussion, this thesis has also provided an in-depth knowledge about the merits and disadvantages of different stochastic methods, which helps EMC engineers perform the efficient statistical analysis for their specific problems.

Chapter 1 Introduction

1.1 Electromagnetic Compatibility

At the starting point of this thesis, it is of great significance to understand the meaning of electromagnetic compatibility (EMC) [1], [2]. To start with, everyone may have had the experience that noise or interference can be induced to electronic devices (such as radio receivers and televisions) when lightning happens nearby. This is a typical example of electromagnetic emission sources imposing interference to unexpected receptors. In this example, the lightning acts as the source of the electromagnetic emission, and the electronic device becomes the victim of such an emission. The electromagnetic emissions can exist in different forms, such as by nature or artificiality, and cause interference into electronic devices. In severe scenarios, the induced interference may even result in the malfunction of the victim device. Taking the baseband system communication via cables for example, the transmission error may occur if the interference picked by the cable distorts the form of the signal severely.

Therefore, before releasing an electronic device to the market, it is important to evaluate the EMC performance of this device, in order to remove the potential malfunction. Specifically, to credit a device with approval, two aspects of the EMC performance need to be evaluated. The first aspect is to evaluate the electromagnetic emission [3] from the device. The aim is to ensure that its electromagnetic emissions do not cause intolerable interference in other systems in that environment. The second aspect is concerned with the susceptibility of the electronic device to its working environment. The device is required to be not susceptible to emissions from other systems. In other words, when ambient devices (acting as the sources of interference emission) interfere with the electronic device under test, the electronic device should still function normally. This aspect is becoming very crucial due to the increasing complexity of the electromagnetic environment. As a result, the potential vulnerability of the electronic device to the harsh electromagnetic environment must be examined before

releasing to the market. If an electronic device satisfies the requirements of the aforementioned two aspects, we claim this device to be electromagnetically compatible with other electronic devices in its working environment.

In industry, to evaluate the EMC performance of an electronic device, EMC tests need to be performed. The outcome of the EMC test judges if this electronic system can be released to the market. Due to the significance of EMC in the product quality evaluation, an increasing amount of effort is paid to enhance the research of EMC in different aspects. For example, relevant EMC standards and testing technologies need to be developed to deal with new emerging electronic products.

Due to the development of the EMC subject, comprehensive guidelines are available to conduct EMC analyses. Generally speaking, interference (i.e., unintended electromagnetic energy) can be coupled from the emission source to the circuit in the victim device by two main coupling mechanisms. In the first mechanism, interference is transferred through direct conduction of the common metallic paths shared by the emission source and victim circuit. This mechanism commonly happens in intra-system scenarios. In addition to the interference delivered through direct conduction, the second mechanism for inducing interference is by the radiation of electromagnetic waves. In this mechanism, the emission source takes the form of incident electromagnetic fields generated naturally or artificially, for example, by lightning pulses or radio station antennas. The in-depth explanation of the second mechanism is that distributed voltage/current sources are generated in the victim circuit as a response to the electromagnetic illumination. Due to these distributed sources, undesired signals (i.e., the interference) are produced and may cause the malfunction of the circuit.

Based on the definition of EMC, each electronic device can act as an emission source as well as victim, depending on which EMC aspect of this device is being evaluated. On the other hand, the interference can be induced to the victim circuit by conducted coupling (i.e., the first mechanism) and radiated coupling (i.e., the second mechanism). This gives rise to the four main subdivisions of the EMC subject: (1) the radiated emission; (2) the radiated susceptibility; (3) the conducted emission; and (4) the conducted susceptibility [1].

This thesis is focused on the susceptibility of the electronic system to the radiated and conducted electromagnetic disturbance. This is because the aim of this thesis is to analyse the induced effect in the victim device, and thus, to ensure that the induced effect does not cause the victim device to malfunction.

1.2 Cable EMC

Having understood the general EMC scope, let us focus on cable EMC aspects in this thesis. It would be of interest to investigate the EMC performances of different types of electronic components. Amongst these numerous components, the ongoing dedicated research has been focused on the EMC performance of cable bundles. This is because engineers from aeronautic and automotive industries are facing the demand of introducing more components to the system [4]. The components usually include interconnecting cables for transmitting signals and power. Cable bundles are the key components to realise the transmission function in modern platforms.

Specifically, cables are heavily used to transmit signals (e.g. for control and communication purposes) and electrical power between different components in large systems such as airplanes, ships, and vehicles. Each cable is an assembly of many wires compactly bundled together for e.g. conserving space. The wires in the cable are usually from different categories, such as single wires, twisted wire pairs, and coaxial cables, and serve different purposes. Fig. 1-1 provides an understanding of the heavy consumption of cables in typical large platforms. For example, in a commercial airplane, the total length of cables on board can reach 500 km to support increasingly sophisticated avionics and even the demand of on-board entertainment facilities [5]. For example, the information from sensors monitoring different working conditions (such as temperature, pressure, and fuel) is conveyed through a significant usage of cables to the processing centre of the aircraft. Fig. 1-2 shows engineers planning the topology of the cable interconnecting system inside an aircraft. The scale of the typical cable length in an aerospace environment is demonstrated in Fig. 1-2. Fig. 1-3 shows a typical configuration of cable bundles for aerospace applications. Even in a modern vehicle, the cable length can be accumulated to 4 km [6]. Fig. 1-4 shows a cable system example for communicating the vehicle engine to the control units in the centre console of the vehicle. The numerous cables shown in Fig. 1-4 are used to interconnect pervasive computing units in modern vehicles in order to deliver new desirable functions, such as the monitoring of the vehicle working condition [7]. Fig. 1-5 demonstrates the complexity of cable wiring system, taking the satellite scenario for example.

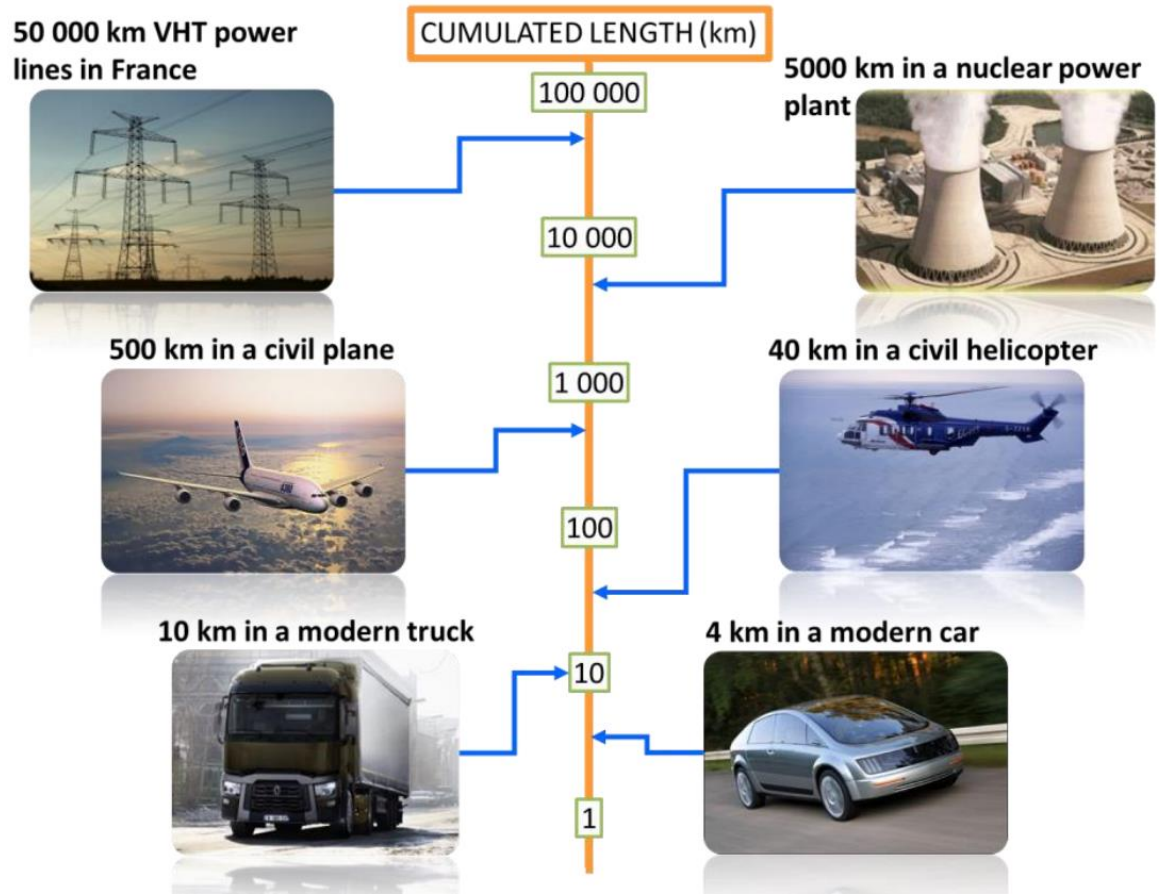

Fig. 1-1. Accumulated cable lengths in different industrial platforms [8].

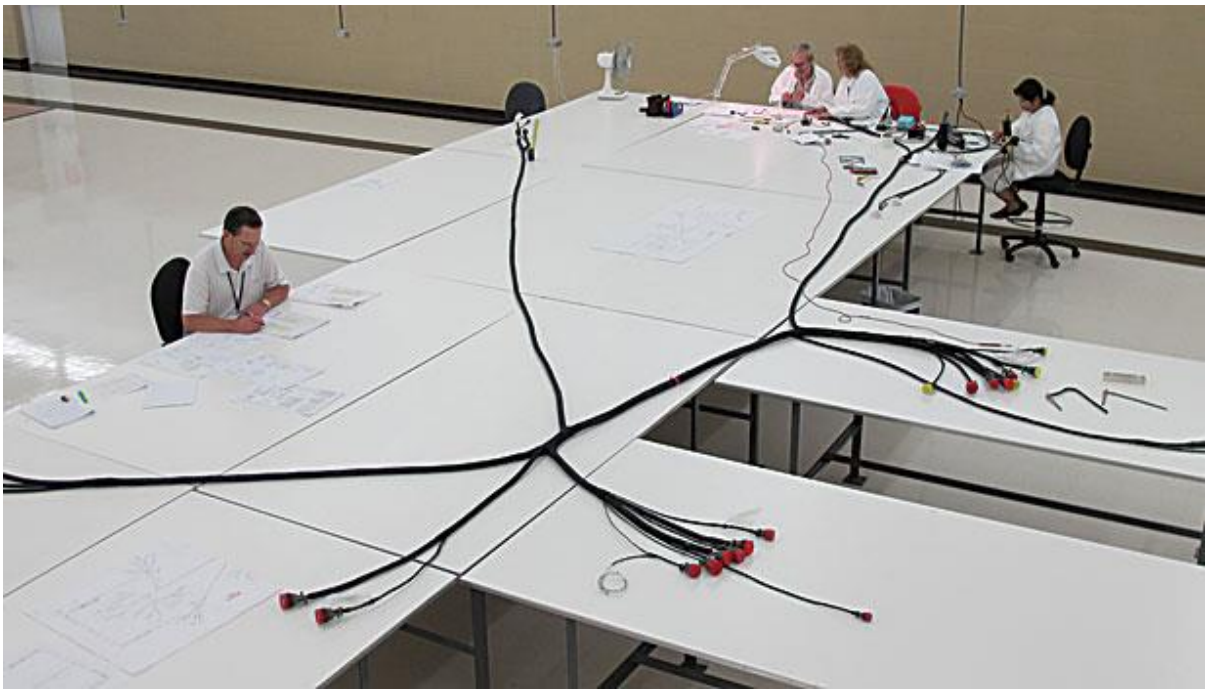

Fig. 1-2. Planning of the cable installation topology for aerospace environment [9].

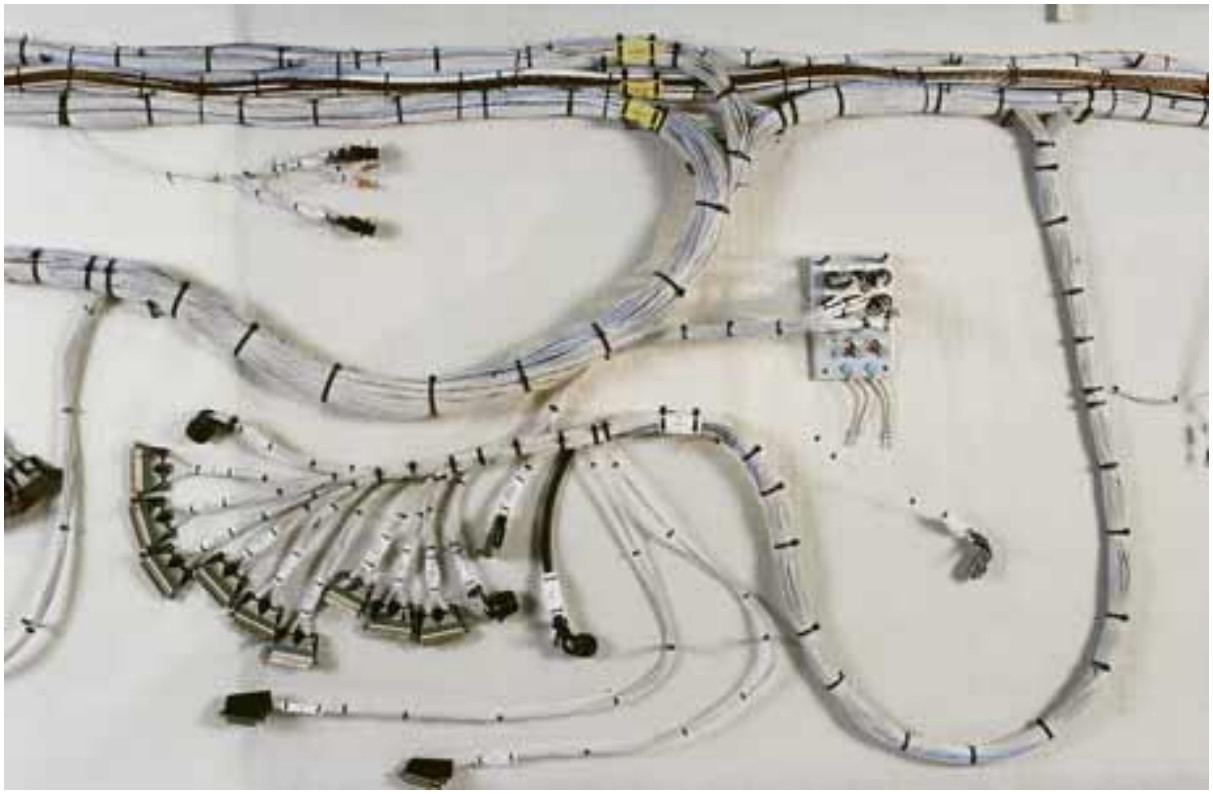

Fig. 1-3. Example of aircraft wiring interconnection [10].

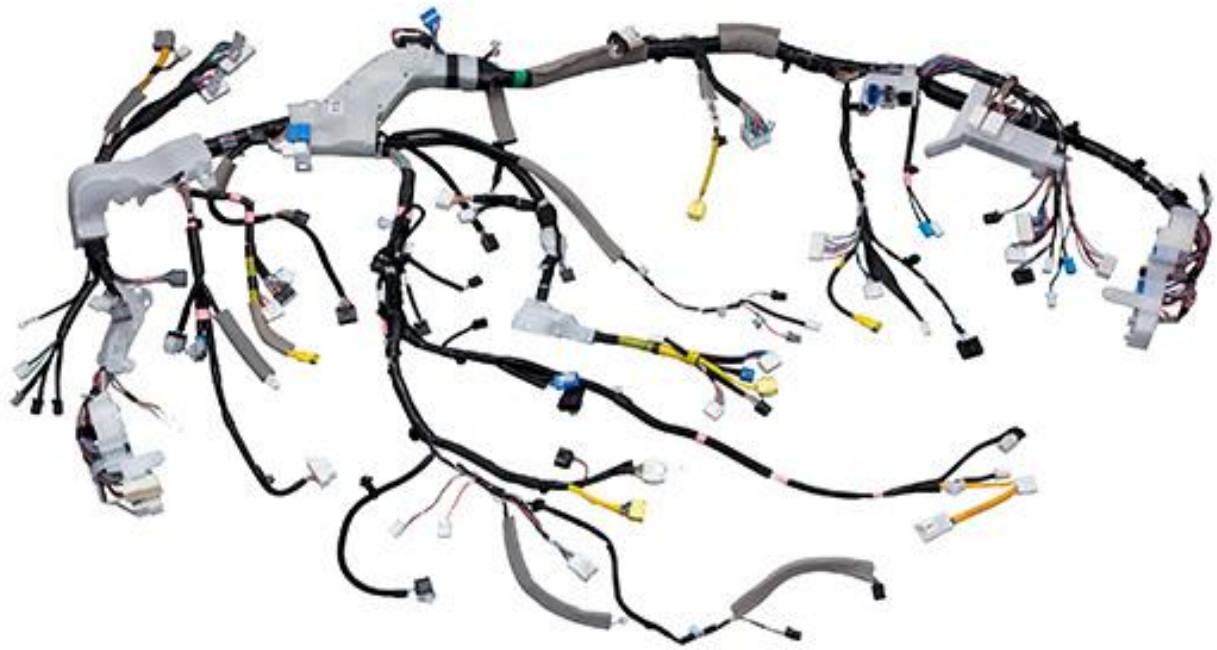

Fig. 1-4. Example of the cable interconnecting system in automotive environment [11].

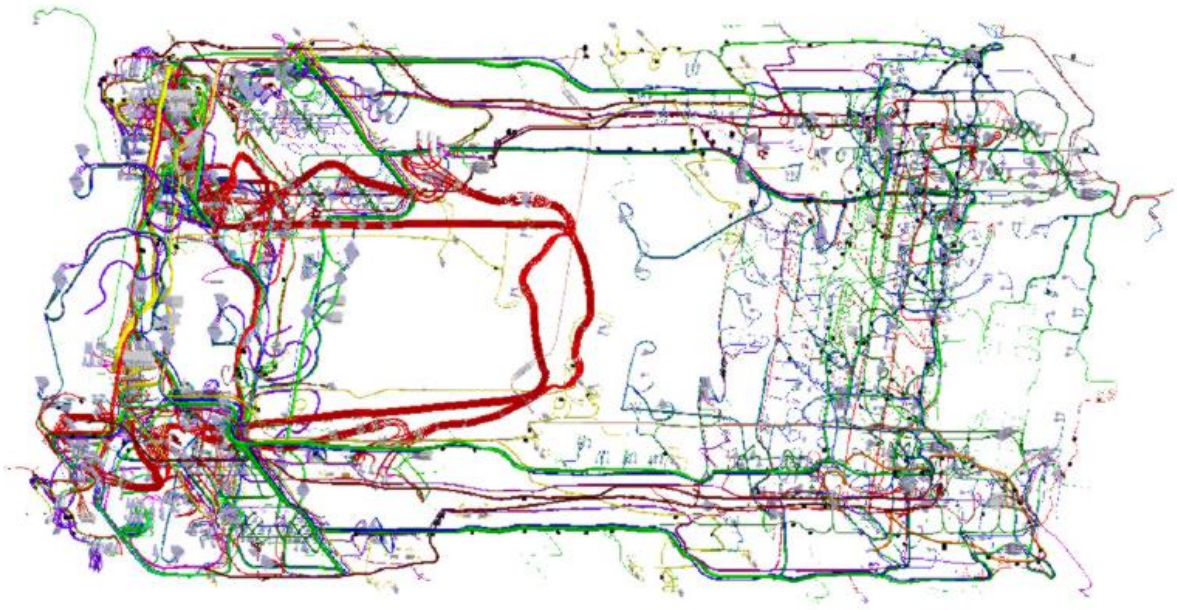

Fig. 1-5. Complex harness bundles in a large communication satellite [12].

However, due to the wide usage of cables in industry, there is a significant demand to assess the system risk raised by cables. In a real system, interference is inevitably introduced to the cable, and could be fatal to cause systemic failures [3]. For this reason, industrial manufacturers are placing stringent EMC regulations on cable system testing. The risk assessment of the cable system can be used to minimise the risk of malfunctions.

The emission source may take different forms based on the investigated scenario. The difference in the form of the emission source is reflected by the name of the coupling mechanism, i.e., the wire-to-wire coupling [13] and the field-to-wire coupling [14].

Let us first introduce the wire-to-wire coupling phenomenon. In a cable interconnecting system, each wire in the cable connects a designated pair of the signal source (usually with a source impedance load) and the termination load at the two ends of the wire. Let us choose an arbitrary wire in the cable as the victim (i.e., receptor) of the interference. Ideally, the voltage coupled to the termination load is intended to be only contributed by the signal source of this wire. However, due to the interaction of the electromagnetic fields generated by the current in this victim wire and in other nearby wires, unintended electromagnetic energy is also coupled to the victim wire. This coupled energy acts as unexpected voltage/current sources in the victim wire, and produces unintended signals at the termination load of the victim wire. This phenomenon is referred to as crosstalk to represent the interference in the wire-to-wire coupling scenario. Consequently, the intended transmission signal at the termination of the

victim wire is distorted. This effect may lead to the malfunction of the electronic component connected by the victim wire.

Although a specific victim wire is nominated in the aforementioned explanation of crosstalk, in fact each wire in the cable can behave as a victim and an emission source simultaneously. At least two separate circuits are needed (one circuit acting as the generator and the other one acting as the receptor) for crosstalk to occur [15]. As cables are usually used to transmit power and signal within a system, the crosstalk is essentially an intra-system interference phenomenon. In other words, crosstalk mainly degrades the function of the components in the same system.

Unlike the crosstalk generated and received at intra-system levels, the interference can also be induced to cables from an electromagnetic emission source outside the system. This gives rise to the second coupling mechanism referred to as the field-to-wire coupling. Telecom base station and radar antennas, as well as lightning pulses, are typical examples to generate incident electromagnetic waves in the field-to-wire coupling phenomenon. The mechanism of the field-to-wire coupling phenomenon can be explained as follows: when the incident wave illuminates an electric system, distributive voltage/current sources are excited along the wires in the cable, and result in coupled signals (i.e., the interference) at the termination components of the wires. Similar to the wire-to-wire coupling scenario, these unwanted signals may lead to disastrous consequences.

Due to the pervasive presence of electromagnetic fields in the real-world, engineers are concerned with the electromagnetic energy coupled from the field into the cables. One example is that avionic engineers pay great attention to the susceptibility of airplanes to strong electromagnetic radiation. This is because airplanes (especially military aircraft) can be exposed to very intensive electromagnetic fields from radars and lightning strikes. The resultant overwhelming interference can be fatal for such a high-precision system and bring disastrous consequences. In the analysis of the field-to-wire coupling phenomenon, the incident electromagnetic field is usually represented by a uniform plane-wave field [16].

The hazards of the cable interference (induced either by the wire-to-wire or field-to-wire coupling mechanism) can be different depending on the application. For example, if the wires in the cable are used to transmit signals between subsystems, the interference can distort the original properties (such as the amplitude) of the transmitted signal. Such a change in the signal may cause transmission error and degrade the function of the circuit connected to the

termination of the wire. Another example of the interference hazard can be illustrated using a power distribution system with a lightning strike or high intensity radiated fields (HIRF) nearby [17]. In the power distribution system, the wires in a cable are used to deliver electrical power to households and industry plants. When a lightning strike occurs, the radiated emission from the lightning may induce noise currents with extremely high magnitude into the power cable. This interference can be further coupled through conducted emission to the electric devices connected to the power system. As a result, the device on the user side, despite already being approved with EMC regulation, may still suffer unexpected strong interference and experience degraded operation. This example also shows that the cause of some EMC problems may not be comprehensively explained using a single coupling mechanism. In fact, the mechanisms for most of interference phenomena can be very complex. In such cases, it may be due to multiple interference sources delivering noise signals to the victim device via different coupling mechanisms [1].

Therefore, considering cable EMC is required in various systems. Taking the military aircraft for example, it would be of great significance to prevent the electromagnetic energy entering the cable in the fuselage from radars or hostile aircrafts. Any interference leaking into such a delicate control system may result in tremendous loss. Having understood the threats of interference to electronic systems, it is clear that the prediction of the interference level in the cable system is needed. The aim of performing interference prediction is to ensure the reliable function of the system. The interference prediction result helps engineers understand the potential interference level. Based on this information, EMC analysts can forecast whether the system will behave in the intended manner. If the prediction result is alarming, the redesign of the system is needed to eliminate any potential malfunctions.

The interference prediction is suggested to be performed in the early stage of the cable system design. At this stage, the potential degraded operation can be resolved with little cost. This is because by resolving a problem at this stage, a series of possible interference problems in the subsequent process can be avoided. If necessary, even the redesign of the system may be affordable at the early phase. However, the cost of solving the interference problem increases with the product design process proceeding, due to the increasing complexity of the coupling mechanism. The worst case is that the completed design of a product without interference prediction fails the relevant EMC regulation and faces redesign. At this point, the redesign of the product could be unaffordable for the involved cost and

time. Therefore, performing the interference prediction at the early stage to foresee potential functional degradation is of great significance in the product design process.

As discussed above, the prediction of interference is an important task for EMC engineers to identify the potential malfunction. In addition to knowing the potential risk, EMC engineers also need to investigate how to reduce the conducted and radiated emissions. If the emission level is successfully reduced to conform to the relevant EMC standard, the product can be released to the market and produce profits for the company. There are different techniques to minimise the effect of emissions on the cable system. For example, shielding can be used to prevent interference entering the circuit, and therefore, to avoid the subsequent detrimental effect on the circuit.

It is clear that developing techniques to reduce the interference to/from the cable system in order to comply with EMC regulations is very crucial to the industry. However, the scope of this thesis is focused on the investigation of the interference level due to the wire-to-wire coupling and field-to-wire coupling, caused by conducted and radiated emissions, given that the information about the investigated electromagnetic environment is partially known. This is explained in the next section.

1.3 Necessity of Considering Uncertainty

The cable interference prediction is essentially a workflow of calculating the interference, based on the information of the electromagnetic environment. Here, the information of the electromagnetic environment should give explicit description of the emission source, the receptor of the emission, and the coupling route from the source to receptor. Having known the detail of the electromagnetic environment, a methodology is needed to guide the calculation of the interference. One of the most effective methodologies for interference prediction was developed using the multiconductor transmission line (MTL) theory detailed in [18]. An informative description of the MTL theory is given in Section 2.1 in this thesis. The MTL theory provides a solid foundation for the deterministic prediction of the interference level. With this theoretical foundation, engineers may develop personalised computational electromagnetics codes to predict the interference level. Alternatively, they can seek help from commercial electromagnetic simulation software products, such as Computer Simulation Technology (CST) [19] and FEKO [20].

The first step of simulation is essentially a process of constructing a mathematical model. This mathematical model defines a mapping from the variables characterising the investigated problem to the output response. Clearly, before performing a simulation, the variables describing the attributes of the electromagnetic environment need to be defined.

Typically, an EMC problem is described by a set of variables characterising different attributes of the investigated problem, together with the observable of our interest. The mathematical model of the investigated EMC problem takes in the value of each variable and produces the value of the output response. If the values of variables are available, the simulation can be started to produce the value of the output response, which is the interference level in this thesis. Such a simulation process is conventionally categorised as a deterministic analysis.

For the deterministic analysis, it is assumed that the value of each variable characterising the electromagnetic environment is accurately known and uniquely exists. In other words, the unique value assigned to each variable is believed to truly represent the quantity of the variable. In the deterministic analysis, as each variable takes only one nominal value, the simulation result is also unique (i.e., taking only one value), accordingly.

The deterministic analysis is useful if the nominal values of the system parameters are the same as or very close to the real values of these variables. In this case, the prediction result of the interference level is accurate and convincing. Now the deterministic analysis is very powerful, as the latest numerical simulation tools allows the detail of the cable bundle structure to be represented with better accuracy in the simulation model.

However, for practical applications, the result of deterministic analysis may not be enough. This is because the nominal values of the system variables only define a fixed configuration of the electromagnetic environment. In real scenarios, there is inevitable uncertainty embedded in each of the system variables [21]. As a result, it is difficult to describe the values of the system variables precisely. Due to the uncertainty, there is always a difference to some extent between the nominal and real values of the system variable. Therefore, how the variability of the system variable affects the interference level needs to be understood and quantified.

Although the uncertainty in one of the system variables may have a very weak influence on the overall system definition, the effect of all the parametric uncertainties on the system

description can be significant. As a result, the simulated electromagnetic environment defined using nominal values could be very different from the real electromagnetic environment under analysis. Accordingly, the simulation result based on the nominal system description may deviate significantly from the true result given by the accurate values of the system variables, and therefore, becomes untrustworthy.

The uncertainties may rise from many different aspects during manufacture, assembly, and installation processes. Accordingly, the cable variables affected by uncertainty are not only limited in the electrical aspects, but also includes the cable geometry, routing, material, etc.

The materials used to make different parts of the cable come from a wide range, and therefore, are potential sources of uncertainty. The geometry of the wire (such as the thickness of the insulation layer and the diameter of the inner conductor) could also experience variation due to the accuracy tolerance of the manufacturing facility.

Fig. 1-6. Example of the manual assembly process of cables by workers [9].

Another reason for the introduction of uncertainty is that human labour is involved in the assembly process of cable bundles. It may be intuitively envisaged that cable bundles are fabricated from highly automated assembly line. Based on this view, there is supposed to be no difference between final cable products. However, in the assembly process, the manual insertion of workers is introduced, causing the difference in the form of the final cable product. Specifically, during the assembly process, the wires in the cable are cut, twisted, and

corded in different manners depending on personal working skills. This artificial effect unpredictably changes the location of each wire in the cross-section at each position along the cable length. In other words, the wires irregularly exchange positions along the longitudinal direction of the cable, adding variations to the wire position within the cable. As a result, the uncertainty of the cable bundle structure arises. Although the manual work unpredictably determines the final format of the cable product, there are no specific requirements for workers to constitute a certain geometric layout for the cable. In practice, workers are only responsible for compacting the wires into a cable product. Fig. 1-6 shows an example of the chaotic manual work involved in the assembly of the cable product.

Clearly, the manual insertion in the assembly process makes the final form of the cable product less repeatable. As a response to the variability of the wire position, the interference level in the cable also becomes uncertain. In this scenario, it is very difficult to obtain accurate geometric information of the cable cross-section as it is randomly non-uniform. Due to the lack of the explicit cable bundle structure, the accurate interference prediction becomes difficult to achieve.

Fig. 1-7. Example of a complex working environment for cable installation in the F-35 JSF military aircraft [22].

Uncertainty may also be introduced from the installation process of the cable. Fig. 1-7 demonstrates the complexity of the environment for cable installation in the F-35 JSF military aircraft. In practice, although a general guideline regarding the cable route is provided to the installer, the flexibility of installing the cable still remains with the installer. Therefore, the actual cable routing in the application platform is largely dependent on the skill of the specific worker. As a result, the actual cable route in the system may deviate from the definition in the simulation model. Even after installation, the route of the cable may experience further variation from future maintenance. The cable routing is also affected by the physical route available in the platform varying from the vehicle chassis to fuselage, depending on the application. As a result, the variability is introduced to the cable position with respect to the platform structure. Now we understand that the uncertainty of cable routing is pervasive in practical applications.

Finally, the ageing of the cable is also a key issue to bring uncertainties to cable properties. This is because the properties of the cable coating material and inner conductor degrade over time [23]. For example, the corrosion of the materials due to long time exposure to the working environment is one reason for degradation. This accumulated degradation is reflected by the changes in the conductivity, permittivity, and permeability of the material. Therefore, the material property of the cable could be different throughout its life cycle. This potential variation in the cable material property along the timeline can significantly affect the interference level. However, in the interference prediction analysis, the age of the cable is usually unknown. Also, the information of how the cable material properties vary over time is usually confidential within cable manufacture companies. The unavailability of this first-hand knowledge limits engineers from taking into account the uncertainty caused by ageing. In practice, to simplify the interference prediction analysis, the uncertainty from the ageing effect is usually ignored, and the nominal values of cable material properties provided by the manufacturer are used. Some of the typical uncertainty sources causing cable interference to vary are summarised in Fig. 1-8.

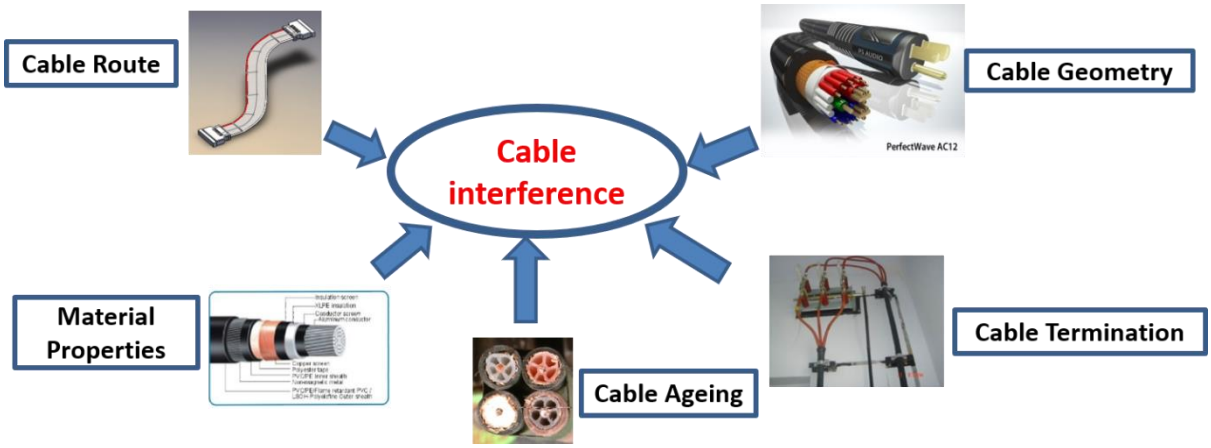

Fig. 1-8. Typical uncertainty sources contributing to the variation of cable interference.

It is worth noting that the aforementioned uncertainty sources in Fig. 1-8 are embedded either in the cable itself, or in the working environment of the cable. In fact, the source of the electromagnetic emission could also be subject to uncertainty. This is particularly true in the field-to-wire coupling phenomenon. For the field-to-wire coupling problem, the information about the impinging electromagnetic field (i.e., the source of the radiated emission) is always lacking [24]. For example, in practice the incident electromagnetic field could potentially illuminate the cable interconnecting system from many different directions. In addition to the random incidence direction, the information about the field strength and polarisation angle of the incident field could also be very obscure in a practical scenario.

In summary, to obtain the accurate simulation result, precise values of system variables are required to build the simulation model. However, due to the uncertainty in the real-world working environment of the cable, the true values of cable variables rarely match the setting of the simulation, resulting in the difference between the numerical simulation and actual result. This is because many variables cannot be precisely defined, making the accurate prediction difficult to achieve. Therefore, although accurate modelling of the electromagnetic problem is desired, it is unrealistic to achieve in reality due to the vague description of the system. As a result, instead of producing a seemingly accurate prediction result, it is more appropriate to proceed with statistical analysis and give a statistical description of the cable interference [25]. Only in this way the parametric uncertainty can be taken into account, and the significance of each parameter variation may be predicted.

1.4 Motivation of This Work

From Section 1.3, it is clear that in the analysis of the cable interference problem, the uncertainty (either caused by nature or manual intervention) pervasively exists in the cable itself, in the working environment of the cable, and even in the source of the electromagnetic emission. In general, the parametric uncertainty results in a random variation of the system response. The system response can be an arbitrary physical quantity that the engineer needs to know from the system model. In this thesis, the system response refers to the cable interference when analysing cable EMC problems.

As the input uncertainty causes the variation of the system response, the single-valued result produced using the nominal values of the input variables is only one of the possible results in practice. This is clearly demonstrated in Fig. 1-9, where the dashed black line refers to the nominal system response given by nominal input values, and the grey shaded area is the overlapping of all the possible results caused by the input uncertainty. This seemingly correct nominal result (marked by the dashed black line) is unable to give a comprehensive description of the system response. Taking the cable system as an example, the uncertainty in each variable causes the interference level to vary in a range rather than having a specific value. Therefore, the uncertainty embedded in cable variables needs to be taken into account in the interference prediction.

Since the nominal system response of an uncertainty-embedded system is unconvincing, a statistical description of the system response is desired. This statistical description can reveal the statistical properties of the system response, such as the mean value, standard deviation, and cumulative distribution function (CDF) [26]. In other words, one can know the possibility of the system response taking values in a certain range. These types of information are more suitable than the single-valued result to describe the randomness of the system response, as the effect of the input uncertainty is taken into account.

Clearly, the statistical property of the system response is dependent on the statistics of the input variable. To obtain the uncertainty of the system response, one needs to propagate the input uncertainty through the deterministic solver [27]. Here, the deterministic solver can be imagined as a mathematical model governing the investigated problem, and is used to produce the value of the system response from the values of input variables. In practise, the deterministic solver can take different forms, such as a software simulation.

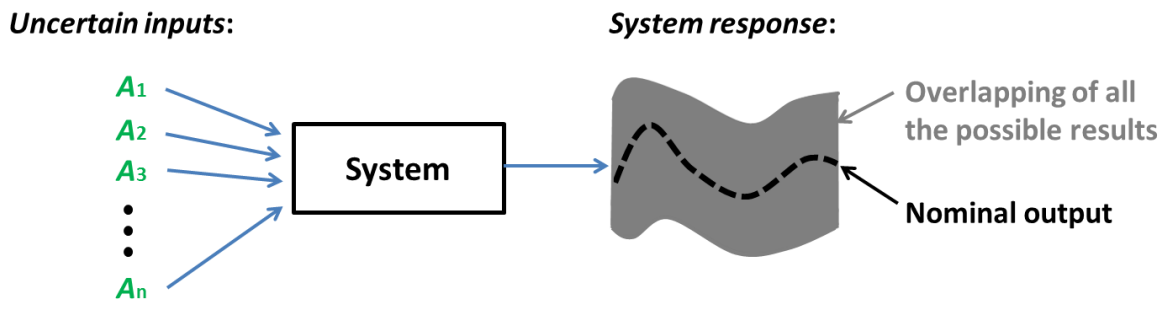

Fig. 1-9. Effect of uncertain input parameters on the system response: causing the output to randomly vary. The dashed black line denotes the nominal system response produced by the nominal values of *n* input variables (i.e., A_1, A_2, …, A_n). The grey shaded area shows the variation range consisting of all the possible system responses due to uncertain inputs.

Before propagating the uncertainty from the input variable to the system response, one needs to first describe the variability of an observed variable. Here, the observed variable can either refer to a random input variable or the system response. Typically, the randomness of the observed variable can be described using the CDF, mean value, standard deviation, etc. Therefore, the uncertainty propagation is essentially the process of deriving the CDF, mean value, and standard deviation of the system response from those of the random input.

To perform uncertainty quantification, statistical methods are needed to deal with the parametric uncertainty. Traditionally, the Monte-Carlo (MC) method [28] is used to take into account the parametric uncertainty inherently existing in the system, and quantify the spread effect of uncertain inputs on the system response.

To perform the MC analysis, a deterministic solver is needed to generate the samples of the system response based on the samples of random input variables. Here, any possible value of an observed variable is referred to as its sample. In addition to the deterministic solver, the randomness feature of input variables is required to be known before starting the MC analysis.

To obtain the accurate statistical properties of the system response, the deterministic solver has to be run for a sufficiently large number of realisations. Here, a realisation is essentially a simulation of one possible configuration of the system. In every realisation, each random input variable characterising the system is represented by a sample randomly selected from its uncertain region based on its statistical properties. Finally, after all the MC realisations, a

large number of samples for the system response are obtained to produce the statistical property of the system response.

For statistical analysis, the number of uncertain input variables in the system is referred to as the randomness dimension. If the random dimension is small (e.g. one or two random variables), the randomness dimension of the stochastic problem is considered to be low. The MC method is competent to propagate uncertainty for problems with a small randomness dimension. This is because the computational cost is directly related to the number of MC simulations required to produce the converged statistics of the system response. For stochastic problems with small randomness dimension, the required number of simulations is usually reasonable. Therefore, the required computational cost would typically stay within the affordable range in this case.

However, the number of variables in a complex system can be very large. This is in line with the aforementioned multiple uncertainty sources in Section 1.3. In this case, a large number of variables are needed to represent various attributes of the complex system. As mentioned in Section 1.3 for the cable interconnecting system, uncertainty is inevitably introduced artificially or naturally to the variables characterising the system. Here, the uncertainty of a variable can be interpreted as the potential variation of the variable. As a result, the prediction analysis is confronted by a large number of random variables. Accordingly, the stochastic problem under investigation is considered now to have a large randomness dimension.

Let us focus on the computational cost of the MC method. In order to produce the convincing result, the MC method needs to consider nearly all the possible scenarios of the uncertain system. As the computational cost is proportional to the number of simulations, the required computational cost of the MC method also increases exponentially with the number of random variables increasing. Due to this exponentially increasing rate, the MC computational cost for high-dimensional stochastic problems is very likely to be overwhelming, and may even exceed the available computational resource. This phenomenon is referred to as the curse of dimensionality. This limitation is especially true when investigating an extremely complicated system. For example, one simulation on the aircraft scale (such as simulating the response of the cable in the aircraft to lightning strikes) could take up to three months even using a massively parallel high-performance computer. Therefore, when the randomness dimension is high, the uncertainty propagation in complex stochastic systems may require prohibitive computational cost and reach the bottleneck.

Clearly, due to the curse of dimensionality, proceeding with the MC method is unsuitable to resolve a complex uncertainty-embedded EMC problem. If possible, it is desirable to propagate uncertainty in an efficient way from multiple random variables to the system response. This motivation gives rise to the main objective of this PhD work: to efficiently quantify the variability of the cable interference affected by multivariate parametric uncertainties.

The first cornerstone/objective of the PhD objective is the "statistical analysis". This objective will achieve a significant breakthrough to provide an insightful understanding of the stochastic feature of the cable interference. Traditionally, the deterministic analysis was used to take into account a single definition of the system and ignores the potential variability of the system. The single-valued result from the deterministic analysis was unable to reflect the random variability of the system response. As the cable interference phenomenon is actually a multivariate stochastic process due to the uncertainty in a range of properties, the stochastic feature of the cable interference problem is the desired outcome. This is the first significant breakthrough of this PhD work.

The second cornerstone/objective of the PhD objective is the "efficiency". Unlike the MC method, this PhD work aims to derive the statistics of cable interference using an innovative and efficient stochastic approach. In other words, by using the chosen method, the uncertainty of multiple random variables needs to be accurately propagated to the cable interference (i.e., the system response), whilst keeping the computational cost as small as possible.

In addition to the aforementioned two objectives, the chosen stochastic method is required to be non-intrusive. For a non-intrusive stochastic method, the coding of the deterministic solver for executing simulations is not subject to any change. Typically, the coding of the deterministic solver is uniquely bundled with the investigated problem. If the implementation of the stochastic method does not require changing the coding of the deterministic solver, this stochastic method can be applied straightforwardly to various uncertainty-embedded EMC problems. Therefore, the non-intrusive feature makes the stochastic method general and versatile. Now it is clear that the non-intrusive feature is an appreciated feature of the chosen stochastic method. More information about non-intrusive stochastic approaches will be given in Chapter 2.

1.5 Organisation of the Thesis

Having emphasised the challenges and motivations of this PhD work, the main objective now becomes clear: to efficiently predict the stochastic feature of the cable interference affected by the uncertainty in the wire-to-wire and field-to-wire coupling scenarios. This aim requires the applied statistical method to be able to accurately propagate the uncertainty from random multivariate inputs to the system response, whilst keeping the computational cost as small as possible.

In addition to developing the statistical analysis framework of cable interference, other research work regarding the cable coupling phenomenon is also conducted. First, it is necessary to validate the necessity of considering the parametric uncertainty. A parametric study is performed to show the variation of cable interference when the configuration of the cable varies. As the variation of the investigated variable leading to high coupling levels is identified, the parametric study is very useful for engineers to diagnose possible causes for strong interference in the cable system, and resolve the EMC issues accordingly.

Second, it is also important to identify the critical contributing and the least contributing variables in the cable interference prediction. As a result, the uncertainty of these weak cable variables can be ignored due to the negligible influence on the variation of interference. Thus, the statistical analysis of cable interference can be simplified by considering a smaller number of random input variables. This is called the reduction of randomness dimension, for the purpose of reducing the computational cost to the practical range. Clearly, the sensitivity analysis of cable interference to different cable variables is of paramount significance and also an important task of this project. However, the knowledge of the influential power of different cable variables is still missing. Due to this incentive, the sensitivity analysis of cable interference is also an important task to be performed in this thesis.

By nature, the sensitivities of cable interference to different cable variables are not the same. The typical aspects to perform the sensitivity analysis against could be from the cable geometry, cable routing in the system, cable materials, and termination loads. In fact, the sensitivity analysis with respect to a cable variable is a process of solely propagating the uncertainty of this cable variable to interference, whilst keeping other variables deterministic. Therefore, the sensitivity analysis is essentially an uncertainty propagation process, and expected to be performed efficiently using the developed statistical analysis framework.

Based on the background, objective, and the contribution of the PhD work, this thesis is composed of eight chapters. The detailed organisation of the thesis is listed below:

- Chapter 1 presents a brief introduction to the EMC field, with an emphasis on cable EMC problems. The challenges remaining in cable coupling problems are explicitly explained. Based on this, the objectives of this PhD work are also set.
- In Chapter 2, a comprehensive overview of the deterministic analysis of cable coupling problems and the family of stochastic methods are presented. Specifically, in the first section of Chapter 2, the theoretical foundation of the deterministic analysis of cable coupling problems is introduced. In the second section of Chapter 2, the principles of the conventional and state-of-the-art statistical methods, namely the MC, polynomial chaos expansion (PCE) [29], and stochastic collocation (SC) [30] methods, are introduced, together with a discussion on their advantages and drawbacks. On this basis, the evolution of the statistical analysis of cable coupling to account for increasingly complex problems with reduced computational cost is outlined. In the final section of Chapter 2, the principle of a novel non-intrusive statistical method referred to as the *stochastic reduced order model* (SROM) method [27] is introduced in detail. The SROM method is able to efficiently predict the statistics of the system response raised by the random inputs, without the drawbacks seen in other statistical methods. Therefore, the SROM method is used as the framework to undertake the efficient uncertainty quantification in various statistical EMC problems in the scope of this thesis.
- Chapter 3 presents a parametric study to investigate how the cable coupling level varies due to certain configurational changes. Different aspects of the cable configuration, such as the cable geometry and its position from the ground plane, are tested to meet the practical scenario. The noticeable variation of the coupling level due to cable configurational changes confirms the need for statistical analysis in Chapter 4. From the result of the parametric study, the variation (i.e., increasing or decreasing) trend of the crosstalk level due to cable configurational changes is identified. It is also found that the cable interference shows different sensitivities against various variables, yielding the motivation for the sensitivity analysis in Chapter 5.
- In Chapter 4, under the assumption of a random cable configuration, the variability of interference in the wire-to-wire coupling scenario is efficiently quantified using the

SROM method. This is the first application of the SROM method in uncertainty quantification in the EMC field, and broadens the family of suitable stochastic approaches for EMC analysis. To validate the efficacy of the SROM method, the traditional MC method and the standard SC method are also applied. The comparison result shows that to obtain the statistics of the cable interference, the SROM method is much more efficient than the MC method, and shows similar efficiency as the SC method in the investigated case. On this basis, the objective of predicting the variation range of the interference level is successfully accomplished.

- Chapter 5 is dedicated to exploring the feasibility of reducing the random dimension of stochastic cable crosstalk problems. To this end, the sensitivity analysis of crosstalk to different cable variables is performed to rank the cable variable based on its impact on affecting the crosstalk. As the sensitivity analysis regarding a cable variable is to solely propagate its uncertainty to the crosstalk, the SROM method is applied to increase the efficiency of the sensitivity analysis. The performance of the SROM method is evaluated by comparing to that of the MC method, and is found to be more efficient by at least two orders of magnitude. Having differentiated the impacts of different cable variables, the feasibility of reducing the computational cost of the statistical cable EMC problem by ignoring the uncertainty of weak variables is investigated.
- In Chapter 6, the scenario of interest is switched from the wire-to-wire coupling to field-to-wire coupling. This is because the cable interference induced by the illuminating electromagnetic field may lead to the degradation of the electronic system function. This investigation is especially important to the aerospace industry as any malfunction caused by the impinging electromagnetic field is fatal in this circumstance. This chapter provides a contribution to solving statistical field-to-wire coupling problems by applying innovative methodologies. Specifically, an in-depth statistical analysis of the induced effect in the transmission line excited by a random incident wave is conducted using SROM, MC, and the improved SC methods. Two demonstrations are presented in this chapter, and the complexity of the stochastic problem is increased by increasing the number of random variables to represent the chaotic scenario as close as possible. Compared with the competing techniques, the SROM method shows a better efficiency to obtain the statistics of the induced effect. On this basis, the worst-case boundary of the induced current is accurately produced. The result of this chapter demonstrates the competent efficacy of the SROM method

to quantify the variability of the system response caused by the random illuminating field. At the end of Chapter 6, an in-depth discussion on the current limitations of the SROM method is also provided, thus to suggest future research directions.

- Chapter 7 is dedicated to experimentally performing the statistical analysis of multipath field-to-wire coupling problems using a reverberation chamber (RC) [31]. Specifically, the applicability of using the RC to take into account the effect of the random multipath illuminations is clearly explained. On this basis, the experiment setup in the RC at the University of Liverpool to statistically study the cable coupling due to random multipath illuminations is introduced. Finally, experimental results are shown to validate the efficiency of using the RC to measure the statistics of the cable interference caused by the random multipath illuminations.
- Finally, Chapter 8 presents a summary of each chapter, and highlights the key contributions of this PhD work as the development of a framework for statistical analysis not only for the cable EMC problems in this thesis, and also potentially applicable to other stochastic EMC problems. The future research directions are also pointed out at the end of Chapter 8.

Chapter 2 Overview of the Deterministic and Stochastic Analyses of Cable Interference

In Chapter 1, a comprehensive background of this PhD work is given. Specifically, the importance of electromagnetic compatibility (EMC) in the life cycle of the electronic system is clearly explained. As the EMC performance validation comes across all the categories of the electronic devices, this thesis is focused on the EMC performance of the cable interconnecting system. The inevitable uncertainty in the cable system is explained and emphasised, in order to give a better understanding of the cable EMC problem in reality. Therefore, it is necessary to predict the cable interference using statistical methods to account for uncertainty. Based on this background, the novelty of this PhD work is to build a framework for conducting efficient statistical analysis of cable interference.

This chapter gives a comprehensive overview of the framework for deterministically calculating cable interference, as well as the family of stochastic approaches. Specifically, in the first section of Chapter 2, the theory of the deterministic calculation of the interference in the cable interconnecting system is outlined in detail. It is important to understand the theory of deterministic analysis at this beginning stage, as this knowledge lays a solid foundation to understand the cable coupling mechanism in depth. Also, the deterministic analysis is the basis on which the stochastic analysis of cable interference is performed. In the second section of Chapter 2, the popular stochastic approaches, such as the Monte-Carlo (MC), polynomial chaos expansion (PCE), and stochastic collocation (SC) methods, are introduced and evaluated in detail. The impact of these methods on the development of solving stochastic cable EMC problems is also reviewed. Due to the drawbacks of the existing statistical methods, the motivation for applying the *stochastic reduced order model* (SROM) method to propagate uncertainty in this thesis is clarified in the last section of Chapter 2, together with a detailed introduction of the SROM method.

First, let us focus on the deterministic analysis of the cable coupling problem. In this thesis, the deterministic analysis is a process of calculating the value of cable interference from the values of the variables characterising the cable system. Under the framework of the deterministic solver, it is assumed that the nominal value of an input variable is the same as its exact physical quantity. As only a certain scenario is investigated in the deterministic analysis, the obtained cable interference level from the deterministic analysis is unique. Clearly, the deterministic analysis is very useful to predict the accurate cable coupling if the precise value of each cable variable is known.

Terminologically, conducting a deterministic analysis can be referred to as performing a numerical simulation. The numerical simulation is of great significance to the industry, as engineers can forecast the system response before investing in the actual fabrication. The numerical simulation can also be used to diagnose the potential malfunction of the system without the need of real measurements. If the result of the numerical simulation is alarming, the redesign of the system can be suggested in the early stage of the product development, thus to avoid the request of the costly redesign in the final stage. The deterministic simulation is also the foundation of the stochastic analysis of the system response, i.e., the cable interference in this thesis. This is because the methodology of performing the deterministic simulation plays the role of the deterministic solver in the statistical analysis. More details about this aspect will be given in Section 2.2.

Due to the significance of the deterministic analysis, it is necessary to understand the theory for calculating the cable interference level. In the following sections, the transmission-line theory is introduced as the theoretical foundation on which the deterministic analysis of cable interference is built.

2.1 Deterministic Analysis of Cable Interference

As introduced in Chapter 1, cables are used to transmit power and signals between different components in the system. In practice, cables can consist of different types of individual wires bundled together. To analyse the cable structure using the theory of electronics, the multiconductor transmission line (MTL) is used to model the cable. This is because a MTL refers to a set of conductors used to transmit signals between the source and load, serving a good analogy to the cable. Therefore, the cable structure is typically modelled as the MTL, in

order to apply the theory of electronics to study the cable coupling phenomenon. It is worth noting that other interconnecting structures with different scales of length, such as printed circuit boards (PCB) in high-speed digital systems, can also be modelled using the MTL, in order to investigate the coupling phenomenon and then remove the potential degradation in the early design stage. However, this thesis is focused on the prediction of the inference in the cable structure due to the scope of the PhD work.

Numerous research work, such as [32] and [33] based on the MTL analysis, as well as [34] and [35] using unstructured transmission line modelling (UTLM), has been dedicated to the deterministic prediction of the cable interference. Section 2.1 aims to provide a systemic theoretical description of the deterministic prediction of cable interference and its development based on the MTL theory.

2.1.1 Per-Unit-Length Parameters

Let us start the MTL analysis by introducing the per-unit-length parameters. This is because the per-unit-length parameters are heavily involved in the calculation of the cable interference level. This section is intended to provide a detailed introduction of the per-unit-length parameters.

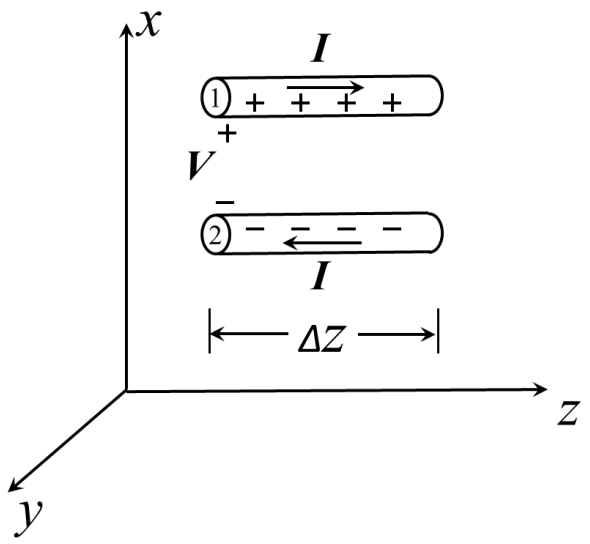

Fig. 2-1. A short segment of a two-conductor transmission line placed along *z*-axis direction in the Cartesian coordinate system.

As shown in Fig. 2-1, a segment of a two-conductor transmission line is used to straightforwardly demonstrate the concept of the per-unit-length parameters. By assumption, the segment in Fig. 2-1 is uniform, namely that the cross-section of the two-conductor transmission line is invariant in the z-axis direction. Also, the length Δz of the segment is assumed to be electrically short (typically smaller than a tenth of the wavelength of the signal transmitted in the line). In the two-conductor transmission line, the conductor ② is called the reference conductor to benchmark the voltage at any point along the conductor ①. Given this configuration, we assume that the current I flows in the conductor ① in the z-axis direction to the termination load, and returns in the opposite direction to the source through the conductor ②.

Let us start the introduction of per-unit-length parameters with the per-unit-length conductance g. Due to the positive charge in the upper conductor ① and the negative charge in the lower conductor ②, the transverse electric field is induced from the conductor ① to the conductor ②. One effect of the transverse electric field is the induced transverse conduction current flowing between the conductors ① and ②. To reflect such an effect, this segment of the two-conductor line is regarded having a conductance G. For this segment with the length Δz, the per-unit-length conductance g can be defined as:

$$g = \lim_{\Delta z \to 0} \frac{G}{\Delta z} \quad (S/m) \tag{2.1}$$

The role of the per-unit-length conductance g is to relate the per-unit-length transverse conduction current to the voltage V between the conductors ① and ②. The value of g is the ratio of the aforementioned two physical quantities.

Also, there is a capacitance between the conductors ① and ② due to the positive charge in conductor ① and the negative charge in conductor ②. If the capacitance of the segment in Fig. 2-1 is denoted by C, the per-unit-length capacitance c can be defined as:

$$c = \lim_{\Delta z \to 0} \frac{C}{\Delta z} \quad (F/m) \tag{2.2}$$

From the circuit point of view, the per-unit-length capacitance c in (2.2) can be seen as the ratio of the per-unit-length charge to the voltage V between the conductors ① and ②.

In addition to the conductance G and capacitance C, this segment of the two-conductor transmission line can also be considered having the inductance L. The reason is that due to the current flowing in the conductors ① and ②, the magnetic field is produced and penetrates the transverse plane formed with the two conductors, giving rise to the magnetic flux through the transverse area formed by the conductors ① and ②. Given the length of the segment as Δz, the per-unit-length inductance l can be defined as:

$$l = \lim_{\Delta z \to 0} \frac{L}{\Delta z} \quad (H/m) \tag{2.3}$$

Apart from the mathematical definition of the per-unit-length inductance l in (2.3), it can also be interpreted as the ratio of the per-unit-length magnetic flux through the area between the two conductors to the current I flowing in each conductor.

Finally, if the conductor of the transmission line is considered imperfect and has resistance, then the per-unit-length resistance denoted by r may also need to be included as a property of the transmission line. In this case, the transmission line is claimed to be lossy.

Typically, the per-unit-length parameters g, c, and l are dependent on the cross-section geometry of the transmission line. In a uniform transmission line, as the cross-section characteristic is the same at any position along the line, the per-unit-length parameter is also invariant regardless of the position along the z-axis. On the contrary, if the transmission line is non-uniform due to the varying cross-section along the line, the per-unit-length parameter now also becomes dependent on the position along the line axis.

To deterministically predict the coupling in a given MTL, the first step is to obtain the per-unit-length parameters for this MTL. To this end, one needs to know the characteristics of the cross-section geometry, such as the separation between the conductors in the line. The analytical formulas for calculating the per-unit-length parameters for the two-conductor transmission line and the MTL are given in Section 2.1.2 and Section 2.1.3, respectively.

2.1.2 Transmission-Line Equations for Two-Conductor Lines

Having understood the concepts of the per-unit-length parameters, Let us focus on the transmission-line equation governing the deterministic analysis of cable interference. Before introducing the transmission-line equation, the concept of the transverse electromagnetic (TEM) field needs to be clarified. This is because in the derivation of the transmission-line

equation, the wave propagated along the line is usually assumed to be in the TEM mode. If a TEM wave is transmitted in the line, it is assumed that the electric and magnetic fields only exist in the plane perpendicular to the wave propagation direction (i.e., the line axis in this thesis). In other words, the electric and magnetic fields of the TEM wave have no projection along the line axis in the cable coupling problem.

However, in practice, the perfect TEM wave may not exist due to the materials used to make the conductors in the cable. This is because the wires in the cable are typically made of lossy conductors. The resistance of the conductor creates the electric field component along the line axis. As a result, this longitudinal electric field component violates the definition of the TEM wave. However, as long as the line loss is reasonably small, the transmission-line equation can still be used to describe the cable system. In this scenario, the wave propagation is considered to be in the *quasi-TEM* mode.

Now let us look at the assumptions used to derive the transmission-line equation governing the voltage and current along the line. First, the transmission line is assumed to be immersed in a homogenous medium. In other words, there is only one medium surrounding the conductor of the transmission line. For a cable in the free space, this assumption implies that there is no insulation layer around the conductor. Second, the sum of the currents at any cross-section along the line axis is assumed to be zero. Taking the two-conductor line in Fig. 2-2 for example, the currents in the upper and lower conductors at the position z are of the same amplitude $I(z, t)$, but flow in different directions.

In this section, the transmission-line equations are derived for the two-conductor line. This is because this simplest configuration provides a straightforward foundation to the general MTL configuration in Section 2.1.3. Here, the term *transmission line* means the collection of conductors in proximity serving to transmit signals. Fig. 2-2 shows an electrically short segment of length Δz to derive the transmission-line equations for the two-conductor transmission line. The entire line can be seen as many cascades of the segment in Fig. 2-2. As introduced in Section 2.1.1, the notations l, g, c, and r in Fig. 2-2 denote the per-unit-length inductance, conductance, capacitance, and resistance (if the conductor is lossy), respectively. Multiplying the per-unit-length parameters by the segment length Δz gives the lumped inductance, conductance, capacitance, and resistance of this segment as $l\Delta z$, $g\Delta z$, $c\Delta z$, and $r\Delta z$, respectively. On this basis, the equivalent circuit of this segment is shown in Fig. 2-2.

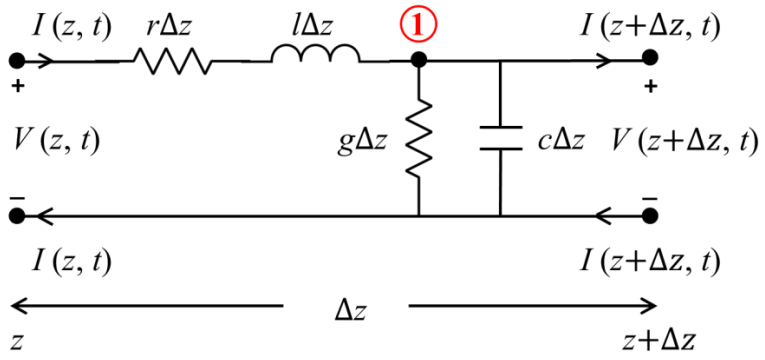

Fig. 2-2. Per-unit-length equivalent circuit of a short segment (with length Δz) of a two-conductor transmission line.

Let us first focus on the transmission-line equations in the time domain. The counterpart in the frequency domain will be addressed in Section 2.1.4. With the equivalent circuit in Fig. 2-2, one can apply the Kirchhoff's voltage law (KVL) around the segment loop to yield:

$$V(z,t) = V(z+\Delta z,t) + r\Delta z\, I(z,t) + l\Delta z\, \frac{\partial I(z,t)}{\partial t} \tag{2.4}$$

After simple transposition, the form of (2.4) can be changed to:

$$V(z+\Delta z,t) - V(z,t) = -r\Delta z\, I(z,t) - l\Delta z\, \frac{\partial I(z,t)}{\partial t} \tag{2.5}$$

Dividing both sides of (2.5) by Δz and making Δz approach zero yields the following transmission-line equation:

$$\frac{\partial V(z,t)}{\partial z} = -rI(z,t) - l\frac{\partial I(z,t)}{\partial t} \tag{2.6}$$

On the other hand, one can apply the Kirchhoff's current law (KCL) at node ① in Fig. 2-2 to obtain:

$$I(z,t) = I(z+\Delta z,t) + g\Delta z\, V(z+\Delta z,t) + c\Delta z\frac{\partial V(z+\Delta z,t)}{\partial t} \tag{2.7}$$

By applying the mathematical transformation in (2.5) and (2.6), one can rewrite (2.7) in the following form:

$$\frac{\partial I(z,t)}{\partial z} = -gV(z,t) - c\frac{\partial V(z,t)}{\partial t} \tag{2.8}$$

Equations (2.6) and (2.8) are referred to as the transmission-line equations for the two-conductor line. The solution of (2.6) and (2.8) tells the voltage and current along the transmission line. To solve the transmission-line equations, the per-unit-length parameters in the equations need to be known first. As mentioned in Section 2.1.1, the per-unit-length parameters are dependent on the structure of the transmission line. In this chapter, we assume that the transmission line takes the structure of wire-type conductors placed above a metallic ground plane. This is because this transmission line structure is widely used in industry. Under this assumption, the investigated two-conductor transmission line consists of a wire-type conductor placed above a ground plane. The solution of the per-unit-length parameters for the two-conductor transmission line is given in (2.9)-(2.11). Specifically, the per-unit-length inductance l can be calculated using [18]:

$$l = \frac{\mu}{2\pi} \ln(\frac{2h}{r_w}) \tag{2.9}$$

where μ is the permeability of the surrounding environment, h is the height of the wire above the ground plane, and r_w is the radius of the wire.

Having calculated the per-unit-length inductance l in (2.9), the per-unit-length capacitance c and conductance g can be obtained from the value of l using the following forms, after the mathematical derivation presented in [18]:

$$c = \frac{\mu\varepsilon}{l} \tag{2.10}$$

$$g = \frac{\mu\sigma}{l} \tag{2.11}$$

where ε and σ are the permittivity and conductivity of the homogeneous medium immersing the transmission line, respectively.

The two-conductor transmission-line equations in (2.6) and (2.8) serve as a good foundation to understand the equations for the MTL with (n+1) conductors, where $n \geq 2$. This is because the form of the MTL equations using matrix notation is the same as in the two-conductor case. The only difference is that for the two-conductor transmission-line, each symbol in the equations is a single-valued scalar. On the other hand, each symbol in the MTL equations is a matrix containing the values of a physical quantity for all the n conductors above the ground

plane. The MTL equations are clearly introduced in the next section. The solution of the transmission-line equations will be discussed in Section 2.1.5.

2.1.3 Transmission-Line Equations for Multiconductor Lines

It is of great importance to derive the transmission-line equations for the MTL. This is because the MTL is a common structure of the cable in reality, due to the increase in the signal transmission rate. As a MTL is a collection of (n+1) conductors, where $n \geq 2$, the minimum number of conductors in the MTL is three. Therefore, taking one of the (n+1) conductors as the reference conductor, there are at least two circuit loops in the MTL, resulting in the coupling between conductors. For the MTL, the per-unit-length parameter can be categorised into the per-unit-length self-parameter and the per-unit-length mutual-parameter.

Let us start the analysis of the MTL from the simplest case: a three-conductor transmission line. In the typical configuration of the three-conductor transmission line, two conductors are used to transmit signals, and the third conductor acts as the ground plane to form circuit loops. There were many assumptions applied in the analysis of the three-conductor transmission line, in order to reduce the complexity of the coupling analysis. The two most widely applied assumptions were the low-frequency and weak-coupling assumptions. Under the low-frequency assumption, the length of the three-conductor transmission line must be much smaller compared to the wavelength of the transmission signal [36]. However, the low-frequency model proposed in [36] was useful, as the cable interference was found to be contributed by the inductive and capacitive coupling due to the mutual inductance and capacitance between conductors. Under the weak-coupling assumption, the effect of the victim conductor on the emitting conductor was usually ignored [37]. The conditions to justify if the weak-coupling assumption is valid were clearly explained in [38].

Apparently, the aforementioned assumptions fail to meet the need of real-world applications. Efforts were made in [15] to derive the exact closed-form formula of the cable interference in the three-conductor transmission line. The solution in [15] removed the low-frequency and weak-coupling assumptions, and only required the medium surrounding the transmission line to be homogeneous and lossless. Finally, it is worth noting that the interference may be contributed by the lossy reference conductor (i.e., with resistance). This mechanism was

called the common impedance coupling and explained in [39]. The main effect of the common impedance coupling is to increase the interference at low frequencies.

The analysis of the coupling in the three-conductor transmission line is very useful, as it provides an intuitive understanding of the coupling mechanisms. However, it is very difficult to derive the closed-form solution of the interference in a MTL with more than three conductors. To obtain the inference in a MTL with an arbitrary number of conductors, a general methodology is needed, and therefore presented hereafter.

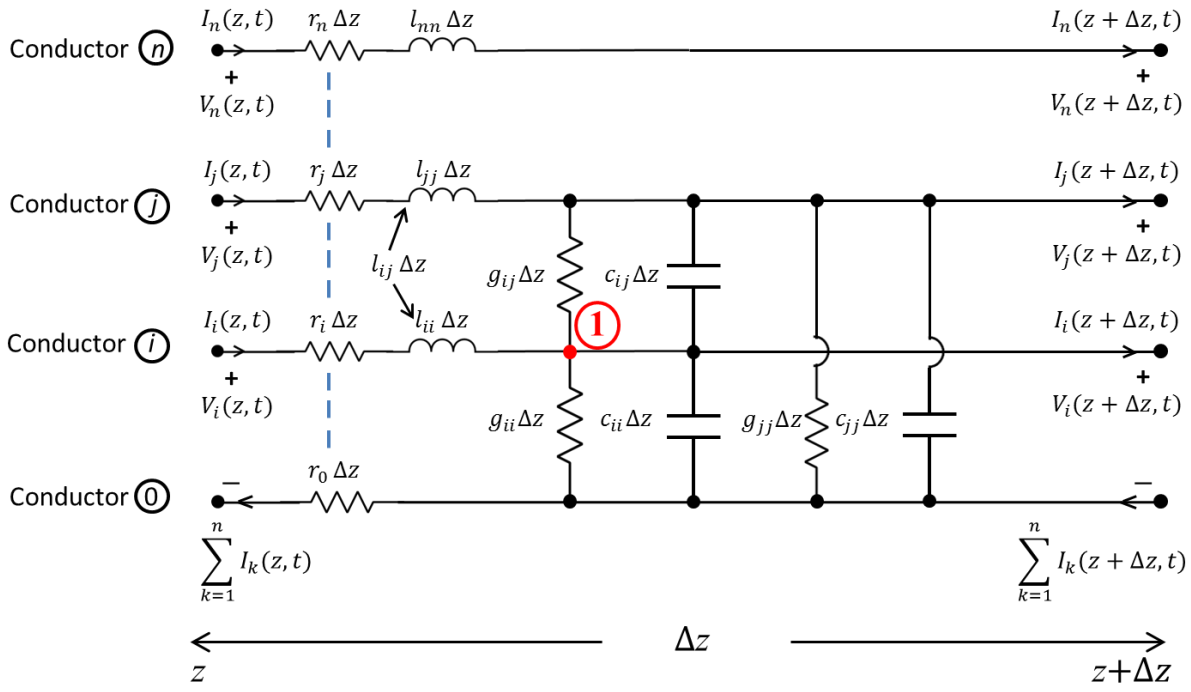

Fig. 2-3. Per-unit-length equivalent circuit of a short segment (with length Δz) of a MTL.

Before deriving the transmission-line equations for the MTL, the characteristics of the cable system need to be clarified. Let us assume that the MTL is placed in a homogeneous medium with the permeability μ, the conductivity σ, and the permittivity ε. The MTL with the length L is assumed to consist of $(n+1)$ uniform conductors with circular cross-sections. Fig. 2-3 shows the equivalent circuit characterised by per-unit-length parameters for an electrically short segment (with length Δz) of a general MTL. In Fig. 2-3, the 0th conductor is used as the reference conductor for the currents to flow back to the source, and the ith conductor ($1 \leq i \leq n$) is designated to transmit signals to the termination network.

The symbols l_{ii} and l_{ij} in Fig. 2-3 denote the per-unit-length self-inductance of the ith circuit (formed by the ith conductor and the reference conductor), and the per-unit-length mutual-inductance between the ith and jth circuits, respectively. Similarly, the notations c_{ii} and g_{ii} represent the per-unit-length self-capacitance and self-conductance between the ith conductor and the reference conductor, respectively. Also, the symbols c_{ij} and g_{ij} are the per-unit-length mutual-capacitance and mutual-conductance between the ith and jth conductors, respectively. Finally, the per-unit-length resistance of the ith conductor ($0 \leq i \leq n$) is denoted by r_i. The definition of the voltage and current along the conductor in the MTL is analogous to that in the case of the two-conductor transmission line. Comparing Fig. 2-3 to Fig. 2-2, it is clear that the circuit schematic of the MTL is a straightforward extension of the two-conductor scenario.

Now let us derive the transmission-line equations in the time domain for the ith ($1 \leq i \leq n$) conductor in the MTL. Applying the KVL around the ith circuit loop consisting of the ith conductor and the 0th conductor gives the following equation:

$$V_i(z+\Delta z,t) - V_i(z,t) = -r_i \Delta z I_i(z,t) - r_0 \Delta z \sum_{k=1}^{n} I_k(z,t) - \sum_{k=1}^{n} l_{ik} \Delta z \frac{\partial I_k(z,t)}{\partial t} \quad (2.12)$$

Dividing both sides of (2.12) by Δz and calculating the limit of each side as Δz approaches zero gives the first equation for the ith circuit as follows:

$$\frac{\partial V_i(z,t)}{\partial t} = -\sum_{k=1;\, k\neq i}^{n} r_0 I_k(z,t) - (r_0 + r_i) I_i(z,t) - \sum_{k=1}^{n} l_{ik} \frac{\partial I_k(z,t)}{\partial t} \quad (2.13)$$

By applying the KCL at node ① in the ith conductor in Fig. 2-3, the following equation can be obtained:

$$\begin{aligned} I_i(z+\Delta z,t) - I_i(z,t) = &-\textstyle\sum_{k=1;\, k\neq i}^{n} g_{ik} \Delta z \left[V_i(z+\Delta z,t) - V_j(z+\Delta z,t)\right] - g_{ii} \Delta z\, V_i(z+ \\ &\Delta z,t) - \textstyle\sum_{k=1;\, k\neq i}^{n} c_{ik} \Delta z \frac{\partial}{\partial t} \left[V_i(z+\Delta z,t) - V_j(z+\Delta z,t)\right] - \\ &c_{ii} \Delta z \frac{\partial}{\partial t} V_i(z+\Delta z,t) \end{aligned} \quad (2.14)$$

After applying the mathematical transformation to (2.14), the second equation for the ith circuit can be obtained in the following form:

$$\frac{\partial I_i(z,t)}{\partial z} =$$

$$\sum_{k=1;k\neq i}^{n} g_{ik}V_k(z,t) - \sum_{k=1}^{n} g_{ik}V_i(z,t) + \sum_{k=1;k\neq i}^{n} c_{ik}\frac{\partial}{\partial t}V_k(z,t) - \sum_{k=1}^{n} c_{ik}\frac{\partial}{\partial t}V_i(z,t) \quad (2.15)$$

Now the derivation of the equations in (2.13) and (2.15) for the *i*th circuit is clearly demonstrated. By applying the KVL and KCL to each circuit in the MTL, we can obtain a collection of the first equation and a collection of the second equation for all the circuits. These two collections of equations combined are referred to as the MTL equations. By using matrix notations, the MTL equations can be concisely represented as shown below:

$$\frac{\partial}{\partial z}\boldsymbol{V}(z,t) = -\boldsymbol{R}\,\boldsymbol{I}(z,t) - \boldsymbol{L}\frac{\partial}{\partial t}\boldsymbol{I}(z,t) \quad (2.16)$$

$$\frac{\partial}{\partial z}\boldsymbol{I}(z,t) = -\boldsymbol{G}\,\boldsymbol{V}(z,t) - \boldsymbol{C}\frac{\partial}{\partial t}\boldsymbol{V}(z,t) \quad (2.17)$$

where the matrix symbols in (2.16) and (2.17) take the following forms:

$$\boldsymbol{V}(z,t) = \begin{bmatrix} V_1(z,t) \\ V_2(z,t) \\ \vdots \\ V_n(z,t) \end{bmatrix} \quad (2.18)$$

$$\boldsymbol{I}(z,t) = \begin{bmatrix} I_1(z,t) \\ I_2(z,t) \\ \vdots \\ I_n(z,t) \end{bmatrix} \quad (2.19)$$

$$\boldsymbol{L} = \begin{bmatrix} l_{11} & l_{12} & \cdots & l_{1n} \\ l_{12} & l_{22} & \cdots & l_{2n} \\ \vdots & \vdots & \ddots & \vdots \\ l_{1n} & l_{2n} & \cdots & l_{nn} \end{bmatrix} \quad (2.20)$$

$$\boldsymbol{G} = \begin{bmatrix} \sum_{k=1}^{n} g_{1k} & -g_{12} & \cdots & -g_{1n} \\ -g_{12} & \sum_{k=1}^{n} g_{2k} & \cdots & -g_{2n} \\ \vdots & \vdots & \ddots & \vdots \\ -g_{1n} & -g_{2n} & \cdots & \sum_{k=1}^{n} g_{nk} \end{bmatrix} \quad (2.21)$$

$$\boldsymbol{R} = \begin{bmatrix} (r_1 + r_0) & r_0 & \cdots & r_0 \\ r_0 & (r_2 + r_0) & \cdots & r_0 \\ \vdots & \vdots & \ddots & \vdots \\ r_0 & r_0 & \cdots & (r_n + r_0) \end{bmatrix} \tag{2.22}$$

$$\boldsymbol{C} = \begin{bmatrix} \sum_{k=1}^{n} c_{1k} & -c_{12} & \cdots & -c_{1n} \\ -c_{12} & \sum_{k=1}^{n} c_{2k} & \cdots & -c_{2n} \\ \vdots & \vdots & \ddots & \vdots \\ -c_{1n} & -c_{2n} & \cdots & \sum_{k=1}^{n} c_{nk} \end{bmatrix} \tag{2.23}$$

Clearly, by using matrix symbols, the form of the MTL equations is essentially the same as (2.6) and (2.8) for the two-conductor transmission line. The vector $\boldsymbol{V}(z, t)$ in (2.18) contains the voltage along each signal conductor, and the vector $\boldsymbol{I}(z, t)$ in (2.19) collects the currents flowing in these conductors. The notations $\boldsymbol{L}$, $\boldsymbol{G}$, $\boldsymbol{C}$, and $\boldsymbol{R}$ represent the per-unit-length inductance, conductance, capacitance, and resistance matrices, respectively. The entries in $\boldsymbol{L}$, $\boldsymbol{G}$, $\boldsymbol{C}$, and $\boldsymbol{R}$ need to be known in order to solve the transmission-line equations in (2.16) and (2.17). The calculation of the entries in the per-unit-length parameter matrices is dependent on the configuration of the MTL. In practice, a MTL typically consists of many signal conductors with circular cross-sections and a reference conductor as the ground plane. In this MTL structure, the per-unit-length parameter matrices can be obtained using closed-form expressions. For example, the entries in the per-unit-length inductance matrix $\boldsymbol{L}$ can be obtained by:

$$l_{ii} = \frac{\mu}{2\pi} \ln\left(\frac{2h_i}{r_i}\right) \tag{2.24}$$

$$l_{ij} = \frac{\mu}{4\pi} \ln\left(1 + \frac{4h_i h_j}{d_{ij}^2}\right) \tag{2.25}$$

where h_i and h_j represent the heights of the ith and jth conductors above the ground plane, respectively. The notation d_{ij} refers to the distance between the centres in the cross-sections of the ith and jth conductors, and the symbol r_i is the radius of the ith conductor. The permeability of the medium immersing the MTL is represented by μ.

Having obtained the per-unit-length inductance matrix $\boldsymbol{L}$, the entries in the per-unit-length capacitance and conductance matrices can be obtained from $\boldsymbol{L}$ using the following expressions:

$$\boldsymbol{C} = \mu\varepsilon\, \boldsymbol{L}^{-1} \tag{2.26}$$

$$\boldsymbol{G} = \mu\sigma\, \boldsymbol{L}^{-1} \tag{2.27}$$

where ε and σ are the permittivity and conductivity of the surrounding medium, respectively. The per-unit-length resistance matrix $\boldsymbol{R}$ can be obtained using numerical approaches, such as the method of moments used in [40]. It is worth noting that if the conductors are perfect and the homogenous medium is lossless, we have $\boldsymbol{R} = \boldsymbol{0}$ and $\boldsymbol{G} = \boldsymbol{0}$, where $\boldsymbol{0}$ is an n-dimensional zero matrix.

Now it is clear that the cross-sectional feature of the MTL uniquely determines the entries in the per-unit-length parameter matrices. Therefore, the matrices $\boldsymbol{L}$, $\boldsymbol{C}$, $\boldsymbol{G}$, and $\boldsymbol{R}$ are the unique characteristics of the MTL. Please note that the complex numerical calculation is usually required to obtain the matrices $\boldsymbol{L}$, $\boldsymbol{C}$, $\boldsymbol{G}$, and $\boldsymbol{R}$. However, novel algorithms can be used to expedite the calculation process of these matrices. For example, the neural network method was used in [41] to implement this task. This is because the neural network method is able to construct the relationship between the input variables and the output response. By training the neural network with different cross-sections and the corresponding per-unit-length parameter matrices, the neural network method was shown in [41] to be able to calculate the matrices $\boldsymbol{L}$, $\boldsymbol{C}$, $\boldsymbol{G}$, and $\boldsymbol{R}$ for an unseen cross-section with less time.

2.1.4 Frequency Analysis of Multiconductor Transmission Lines

Section 2.1.3 gives a comprehensive introduction of the MTL equations in the time domain. However, there is a significant need to perform the MTL analysis in the frequency domain. This is because the entries in the per-unit-length parameter matrices $\boldsymbol{L}$, $\boldsymbol{C}$, $\boldsymbol{G}$, and $\boldsymbol{R}$ are actually dependent on the frequency to some extent. Taking the per-unit-length resistance matrix $\boldsymbol{R}$ for example, if the conductors are imperfect, the current distribution in the cross-section is densified in an annulus towards the conductor surface at high frequencies, due to the *skin effect*. As the thickness of the annulus is affected by the frequency of the signal source, the per-unit-length resistance of the conductor also varies due to the changing

frequency. The detailed explanation for the dependency of other matrices (i.e., $\boldsymbol{L}$, $\boldsymbol{C}$, and $\boldsymbol{G}$) on the frequency can be found in [18].

Clearly, the frequency-domain analysis of the MTL equations is more straightforward to take into account the dependency of per-unit-length parameter matrices on the frequency. To reflect the dependency on the frequency, it is more appropriate to denote the per-unit-length inductance, capacitance, conductance, and resistance matrices as $\boldsymbol{L}(\omega)$, $\boldsymbol{C}(\omega)$, $\boldsymbol{G}(\omega)$, and $\boldsymbol{R}(\omega)$, respectively, where $\omega = 2\pi f$ is the angular frequency of the signal source.

To transform the time-domain MTL equations into the frequency-domain counterparts, one needs to replace the time derivative $\frac{\partial}{\partial t}$ in (2.16) and (2.17) with $j\omega$. Now the frequency-domain MTL equations can be written in the following forms:

$$\frac{d}{dz}\widehat{\boldsymbol{V}}(z,\omega) = -\widehat{\boldsymbol{Z}}(\omega)\widehat{\boldsymbol{I}}(z,\omega) \tag{2.28}$$

$$\frac{d}{dz}\widehat{\boldsymbol{I}}(z,\omega) = -\widehat{\boldsymbol{Y}}(\omega)\widehat{\boldsymbol{V}}(z,\omega) \tag{2.29}$$

where the per-unit-length impedance matrix $\widehat{\boldsymbol{Z}}(\omega)$ and admittance matrix $\widehat{\boldsymbol{Y}}(\omega)$ are given as:

$$\widehat{\boldsymbol{Z}}(\omega) = \boldsymbol{R}(\omega) + j\omega\boldsymbol{L}(\omega) \tag{2.30}$$

$$\widehat{\boldsymbol{Y}}(\omega) = \boldsymbol{G}(\omega) + j\omega\boldsymbol{C}(\omega) \tag{2.31}$$

It is worth noting that the entries in $\widehat{\boldsymbol{Z}}(\omega)$ and $\widehat{\boldsymbol{Y}}(\omega)$ are related to the frequency of interest. The calculation of these entries is very complex and usually requires the use of numerical methods.

Having yielded the frequency-domain MTL equations in (2.28) and (2.29), the only remaining task is to obtain the solutions $\widehat{\boldsymbol{V}}(z,\omega)$ and $\widehat{\boldsymbol{I}}(z,\omega)$ to reveal the voltage and current along each conductor. A brief description of solving the frequency-domain MTL equations is presented in the next section.

2.1.5 Solution of the Frequency-Domain MTL Equations

This section presents a concise introduction to the final step of the deterministic analysis, namely, solving the transmission-line equations in (2.28) and (2.29). The solutions $\widehat{\boldsymbol{V}}(z,\omega)$ and $\widehat{\boldsymbol{I}}(z,\omega)$ of (2.28) and (2.29) tell the voltage and current along each conductor at the

frequency of interest. On this basis, the unintended coupling effect (typically represented by the induced voltage or current) to one specific conductor can be quantified. It is worth noting that the solutions $\widehat{\boldsymbol{V}}(z,\omega)$ and $\widehat{\boldsymbol{I}}(z,\omega)$ are dependent on the frequency of interest. In other words, if the coupling level in a frequency band needs to be analysed, then the deterministic analysis needs to be performed at each frequency in the frequency band of interest.

The technique referred to as *a change of variables* is usually used to calculate the solution to the MTL equation. A detailed description of this technique can be found in [42]. By applying this technique at the interested frequency ω, the general forms of the solutions $\widehat{\boldsymbol{V}}(z)$ and $\widehat{\boldsymbol{I}}(z)$ can be given in the following forms:

$$\widehat{\boldsymbol{V}}(z) = \widehat{\boldsymbol{Z}}_C\, \widehat{\boldsymbol{T}}_I\, (\boldsymbol{e}^{-\hat{\gamma} z}\, \widehat{\boldsymbol{I}}_m^{+} + \boldsymbol{e}^{\hat{\gamma} z}\, \widehat{\boldsymbol{I}}_m^{-}) \tag{2.32}$$

$$\widehat{\boldsymbol{I}}(z) = \widehat{\boldsymbol{T}}_I\, (\boldsymbol{e}^{-\hat{\gamma} z}\, \widehat{\boldsymbol{I}}_m^{+} - \boldsymbol{e}^{\hat{\gamma} z}\, \widehat{\boldsymbol{I}}_m^{-}) \tag{2.33}$$

where $\widehat{\boldsymbol{Z}}_C$ is the characteristic impedance matrix, $\widehat{\boldsymbol{T}}_I$ is the transformation matrix, $\hat{\gamma}$ denotes the propagation constant matrix, $\boldsymbol{e}^{\pm\hat{\gamma} z}$ represent the exponential of the matrices $\pm\hat{\gamma} z$, and $\widehat{\boldsymbol{I}}_m^{+}$ and $\widehat{\boldsymbol{I}}_m^{-}$ are the undetermined vectors of the forward and backward *mode* currents, respectively. Please note that the symbol ω representing the frequency is omitted for the brevity of the solution expressions in (2.32) and (2.33). This is because the dependency on the frequency is already taken into account in the calculation process of $\widehat{\boldsymbol{Z}}_C$, $\widehat{\boldsymbol{T}}_I$, $\boldsymbol{e}^{\pm\hat{\gamma} z}$, and $\widehat{\boldsymbol{I}}_m^{\pm}$.

The matrices $\widehat{\boldsymbol{Z}}_C$, $\widehat{\boldsymbol{T}}_I$, and $\boldsymbol{e}^{\pm\hat{\gamma} z}$ can be straightforwardly obtained from the per-unit-length parameter matrices $\boldsymbol{L}$, $\boldsymbol{C}$, $\boldsymbol{G}$, and $\boldsymbol{R}$ using the closed-form relationships detailed in [18]. Now the only terms to be determined in (2.32) and (2.33) are the vectors $\widehat{\boldsymbol{I}}_m^{+}$ and $\widehat{\boldsymbol{I}}_m^{-}$, in order to obtain the solutions $\widehat{\boldsymbol{V}}(z)$ and $\widehat{\boldsymbol{I}}(z)$. However, extra constraint equations are required to determine $\widehat{\boldsymbol{I}}_m^{+}$ and $\widehat{\boldsymbol{I}}_m^{-}$.

To construct the constraint equations, one need to model the two ends of the MTL (i.e., at z = 0 and $z = L$, where L is the length of the MTL) using Thevenin equivalent circuits. The constraint equations can be obtained from the Thevenin equivalent circuits to associate the voltage $\widehat{\boldsymbol{V}}(0)$ with the current $\widehat{\boldsymbol{I}}(0)$ at the left end of the MTL, and relate the voltage $\widehat{\boldsymbol{V}}(L)$ to the current $\widehat{\boldsymbol{I}}(L)$ at the right end of the MTL. Replacing the terms $\widehat{\boldsymbol{V}}(0)$, $\widehat{\boldsymbol{I}}(0)$, $\widehat{\boldsymbol{V}}(L)$, and $\widehat{\boldsymbol{I}}(L)$ in the constraint equations with the evaluations of (2.32) and (2.33) at z = 0 and $z = L$ yields a set of equations where only $\widehat{\boldsymbol{I}}_m^{+}$ and $\widehat{\boldsymbol{I}}_m^{-}$ are unknown.

Finally, once the vectors $\hat{\boldsymbol{I}}_m^+$ and $\hat{\boldsymbol{I}}_m^-$ are solved from this set of equations, the solutions $\hat{\boldsymbol{V}}(z)$ and $\hat{\boldsymbol{I}}(z)$ can now be calculated using (2.32) and (2.33). The numerical calculation is typically required to solve the MTL equations. However, efforts were made to accelerate the calculation process. For example, the interference level was directly predicted in [43] using the neural network method trained with many sets of existing cable configurations and the corresponding coupling levels.

Although the solutions of (2.32) and (2.33) tell the voltage and current at any position along the cable, the interference at two terminals is generally of more significance. This is because the interference at these positions directly determines the failure risk of the cable system.

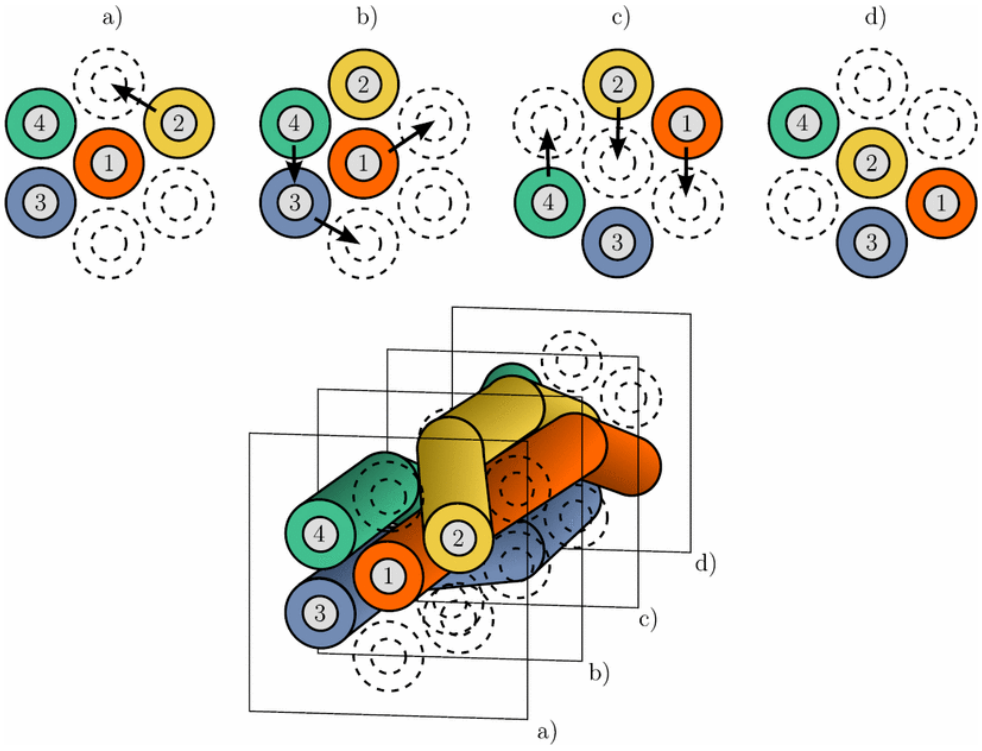

Fig. 2-4. An example of the non-uniform MTL [44].

Now the deterministic analysis of the interference in the uniform MTL is clearly addressed. Another category of the MTL commonly seen in reality is the non-uniform MTL. For the non-uniform MTL, each conductor meanders from one end to the other end, and therefore, the cross-section varies along the line. An example of the non-uniform MTL is shown in Fig. 2-4 [44]. As can be seen in Fig. 2-4, at different longitudinal positions (a), (b), (c), and (d), the cross-sections of the cable are also different, resulting in the non-uniformity of the cable.

The analysis of the non-uniform MTL is well addressed in [18]. The technique for analysing the non-uniform MTL is also based on the MTL theory presented in this chapter. However, due to the variation of the cross-section along the line, the dependency of the per-unit-length parameter matrices on the cable-axis position needs to be taken into account. For the non-uniform cable such as the twisted wire pair, illustrative applications of the MTL theory in the interference prediction can be found in [45] and [46]. Due to the unlimited arbitrary forms that a non-uniform MTL could take, the analysis of the non-uniform MTL is beyond the scope of this thesis.

Please note that the deterministic analysis of the MTL presented in this chapter is based on the wire-to-wire coupling model. This is because the main scope of this thesis is concerned with the coupling amongst the wires in the cable. On the other hand, a concise introduction to the deterministic analysis of the field-to-wire coupling model is given in Section 6.2, where the response of the transmission line to a random illuminating field becomes the observable of interest.

Now a comprehensive introduction to the deterministic analysis of the wire-to-wire coupling problems has been clearly presented. In the next section, the popular stochastic methods for uncertainty propagation will be introduced in detail. The applications of these methods in the statistical analysis of EMC problems will also be presented.

2.2 Popular Stochastic Methods

The deterministic analysis of the MTL presented in Section 2.1 is very useful to calculate the exact interference level, given that the value of each cable variable is accurately known. However, as emphasised in Section 1.3, during the cable fabrication and installation processes, randomness (i.e., potential variation) is inevitably introduced to the variables characterising the cable system. As a result, the accurate information about the cable configuration, such as the geometric characteristics of the cable cross-section, is typically unavailable in the real-world scenario. On the other hand, as pointed out in [47], the cable interference is sensitive to the variation of the cable configuration. Therefore, as the deterministic analysis fails to include the effect of the potential configurational variation, the nominal result is very likely to deviate from the actual interference level. Clearly, it is more

sensible to aim at quantifying the potential variability of the cable interference using statistics.

In fact, the statistical analysis of the cable interference has been intensively researched in the last three decades. For statistical analysis, the variability of each random input variable (e.g. the conductor height above the ground plane) is described using statistical terms, such as the mean value, standard deviation, and probability density function (PDF). Before commencing the statistical analysis, it is assumed that the statistics of random variables are already known.

The most intuitive and straightforward statistical approach is to use the mathematical transformation based on the probability theory [26], if the closed-form relationship between the random input variables and the output is available. Such an idea was first applied in [48] to calculate the statistics of the interference in the three-conductor transmission line at low frequencies. However, one drawback of this technique is that the mathematical transformation process is customised according to the assumed statistics of the random variables. In other words, if the cable variables were modelled using different probability distributions other than those assumed in [48], the mathematical transformation requires to be performed again accordingly. Also, this technique is feasible only when the analytical relationship between the input variable and the system response is available, such as in [49]. This feature limits the application of this technique for complex EMC problems where the relationship between the input and output cannot be expressed in analytical forms.

Efforts were also made to obtain the statistics of the interference in the non-uniform cable in [50] and [51]. However, the methodologies applied in [50] and [51] were applicable only under the customised assumptions made for the simplicity of the analysis, such as the weak-coupling and low-frequency assumptions. As a result, these methodologies were inapplicable to other cable EMC problems due to the lack of versatility.

The worst-case prediction is a special category of the statistical analysis. In this scenario, engineers may not be concerned with the statistics of the cable interference, but only desire to know the maximum interference level that may occur. The motivation was to bypass the need of statistical analysis, and directly predict the potential maximum interference level raised by the parametric uncertainty. Now the EMC performance of the design can be directly evaluated by comparing the predicted maximum of interference to the critical threshold. This is because the systematic failure becomes no concern if the maximum interference level is

below the critical threshold. At this point, the variability of the interference level within the safe margin is of little interest.

Due to this motivation, the worst-case method was used in [52], [53], [54] to provide an envelope holding underneath all the possible values of the cable interference. Specifically, the function of the maximum interference level was derived for the lossless transmission line immersed in the homogeneous medium [53]. The result was later generalised in [54] with no request of the transmission line being lossless and the surrounding medium being homogeneous. Finally, the worst-case prediction of the cable interference in the non-uniform transmission line was addressed in [52].

The worst-case method shows a superior efficiency to predict the interference envelope. This is because the maximum coupling level is described using a closed-form formula regarding cable variables, and thus only requires one evaluation of this formula. Also, the association of the maximum coupling level with the cable variables helps identify the causes of excessive coupling.

However, the worst-case method may lead to overly conservative design, as this method overestimated the coupling level at non-resonant frequencies. Also, similar to the mathematical transformation technique in [48], the worst-case method calls for the closed-form expression of the output. This drawback implies the difficulty of applying the worst-case method to real-world cable EMC problems. For evidence, the investigated cases in [53] and [54] were simplified using a simple cable model under the weak-coupling assumption, in order to apply the worst-case method.

Now it is clear that all the aforementioned techniques relied on certain assumptions for the ease of analysis, and a systematic and general methodology to deal with the cable parametric uncertainty was totally lacking.

In fact, it is desired to apply general stochastic methods to quantify the uncertainty of the cable coupling. This is because the workflow of a general uncertainty quantification method follows systematic procedures. As a result, one can straightforwardly transplant the workflow in different problems of interest. The family of stochastic approaches is typically considered to comprise the Monte-Carlo (MC) method [28], the polynomial chaos expansion (PCE) method [29], and the stochastic collocation (SC) method [30], [55]. In addition to these well-established statistical methods, the *stochastic reduced order model* (SROM) method was

recently proposed in [27] as a potential new member of the family of the stochastic approaches. In this thesis, the SROM method is chosen as the main tool to solve uncertainty-embedded cable coupling problems, and is separately introduced in Section 2.3 in detail. From Section 2.2.1 to Section 2.2.3, the MC, PCE, and SC methods are introduced, together with the applications in the uncertainty quantification of the cable interference.

Before introducing these stochastic methods, it is important at this stage to know that uncertainty quantification methods are categorised into the intrusive and non-intrusive types. Before understanding the features of the intrusive and non-intrusive statistical methods, let us first define the concept of simulation as: a calculation process taking in the values of input variables and then producing the value of the output response. Taking the cable coupling model for example, the input variables can be selected from any characteristics of the cable configuration (such as the conductor height above the ground plane), and the output response is the cable interference level. The calculation process of the cable interference is based on the MTL principle described in Section 2.1. In this thesis, the deterministic solver can be seen as the customised coding to execute the calculation process of the simulation.

Now let us focus on the clear definition of intrusive and non-intrusive statistical methods. The intrusive statistical method requires the software coding of the deterministic solver to be modified, in order to propagate uncertainty. Clearly, the complexity of such an implementation may become unaffordable, if the problem under investigation is governed by complex equations. On the other hand, the non-intrusive statistical method does not require any modification of the software coding of the deterministic solver. In other words, the deterministic solver is directly used during the uncertainty propagation process in this case. As a result, the non-intrusive statistical method is general and usually more practical to apply. This is because its implementation is completely separated from the problem of interest, thus not being affected by the complexity of the problem. Therefore, the non-intrusive statistical method should always be preferred for practical engineering problems.

2.2.1 Monte-Carlo Method

The Monte-Carlo (MC) method is a traditional non-intrusive statistical approach. The idea of the MC method is to take into account the potential variability of the random input using many deterministic simulations with slightly different input values. For the MC method, the deterministic solver is necessary to generate the sample of the output response given the

samples of random input variables. Clearly, the deterministic solver is used without modification during the implementation of the MC method.

Before performing uncertainty propagation using the MC method, one first needs to know the statistics of random input variables. To obtain the accurate statistics of the output, a sufficient number of possible cases must be simulated using the deterministic solver. In each simulation, input samples are randomly generated according to the predefined statistics, and the output sample is produced using the deterministic solver. Now let the notation y denote the output response from the deterministic solver. After evaluating a sufficient number (denoted by N) of possible cases, a large output sample set $\{y_i, i = 1, \ldots, N\}$ can be obtained to calculate the statistics of the output. Specifically, according to [26], the mean value $E(y)$ and standard deviation σ_y of the output y are given by:

$$E(y) = \frac{1}{N} \sum_{i=1}^{N} y_i \tag{2.34}$$

$$\sigma_y = \sqrt{\frac{1}{N} \sum_{i=1}^{N} [y_i - E(y)]^2} \tag{2.35}$$

respectively.

The MC method is especially useful to deal with complex scenarios where the deterministic solver is regarded as a black box. In such complex scenarios, the aforementioned mathematical transformation technique and the worst-case method are inapplicable, due to the lack of the analytical form of the deterministic solver.

Efforts were made to investigate the effect of random non-uniform cable configurations on interference using the MC method. In this scenario, it is assumed that the number and type of the wires are already known, but the information about the exact cable configuration is obscure. This is because the routing of the wire meandering within the cable is typically random. To take into account the randomness of the non-uniform cable configuration, a large number of slightly different cable configurations needs to be generated for simulation.

Clearly, to this end, one first needs to develop techniques to generate the geometric model of the cable with meandering wires. Different techniques were proposed in [44], [56], [57] to construct the geometry of the wires in the non-uniform cable. The basic idea of these

techniques was the same: to partition the cable length into many segments, then define the positions of the wires in each segment, and finally cascade all the segments together to form the cable model. Specifically, the primitive "wire-hole" (WH) method was introduced in [44] to generate the geometry of the cable structure. In [56], the random midpoint displacement (RMD) method was proposed to model the meandering wire using fractal curves, and was shown to be able to tune the twisting degree of the wires in the cable. However, the remaining problem was the large discontinuity of the wire position between any two consecutive segments. To solve this problem, the random displacement spline interpolation (RDSI) method was developed in [57] to vary the wire position more smoothly along the cable axis, thus to produce a more practical cable structure.

After generating many different cable configurations using the aforementioned techniques, the deterministic analysis is performed to obtain the interference level in each configuration. The statistics given by the collection of all the interference samples can reveal the influence of the random cable structure on the coupling variability.

However, although the implementation of the MC method is with ease due to the non-intrusive feature, the required computational cost could be excessively large, causing the analysis to be overly time-consuming. This is because an extremely large number of possible cases needs to be checked to produce the accurate statistics, especially when the number of random variables is large. This is referred to as the curse of dimensionality, and limits the application of the MC method in multivariate stochastic EMC problems. For this reason, efficient statistical methods are urgently desired.

Before introducing the efficient statistical methods in the following sections, please note that the MC method is used in this thesis to demonstrate the efficiency of the advocated approach to solve the uncertainty-embedded cable EMC problems presented from Chapter 4 to Chapter 6.

2.2.2 Polynomial Chaos Expansion Method

As emphasised in the end of Section 2.2.1, the implementation of the MC method needs a very large number of simulations. This is because the MC method blindly and exhaustively evaluates all the possible cases to produce the converged result. Therefore, the computational cost of the MC method is typically heavy, and could become unaffordable in the presence of a large number of random variables. The reason is that the computational cost required by the

MC method grows exponentially with the increasing number of random variables. On the other hand, for large platforms, even one simulation could be time-consuming, making the MC method inapplicable to such problems. Therefore, efficient statistical methods are desired to reduce the computational cost of the statistical analysis.

The polynomial chaos expansion (PCE) method was proposed in [29] as an efficient uncertainty quantification method, and was applied intensively in the last decade. This method can express the deterministic solver as an analytical formula regarding uncertain input variables. This analytical formula is regarded as an equivalent replacement of the deterministic solver. Now the statistics of the output can be obtained by evaluating all the possible cases using this analytical formula.

It is worth noting that at this stage, it is efficient to perform a large number of simulations. The reason is that the calculation of the output sample using the analytical formula barely requires any computational cost. Alternatively, as the analytical form of the deterministic solver is available, the mathematical transformation based on the probability theory in [26] can be used to obtain the statistics of the output.

Before introducing the PCE method in detail, let us first define the N-dimensional random variable $\boldsymbol{x} = [x_1, x_2, .., x_N]$ as the input of the system affected by N random variables, and denote y as the system output. Here, each dimension in $\boldsymbol{x}$ characterises a random variable. The aim of the PCE method is to derive an analytic formula relating the system input $\boldsymbol{x}$ to the output y. This analytic formula is the sum of a series of polynomial basis functions $\{\phi_k(\boldsymbol{x})\}$ with proper coefficients $\{c_k\}$, as shown below:

$$y \approx \sum_{k=0}^{P} c_k \phi_k(\boldsymbol{x}) \tag{2.36}$$

The total number of terms in (2.36) is $(P+1)$, and is determined by the number of random variables (denoted by N) and the order r of the expansion in the following form:

$$P + 1 = \frac{(r+N)!}{r!\,N!} \tag{2.37}$$

Clearly, the accuracy of the PCE result is dependent on how precisely the analytical formula in (2.36) represents the deterministic solver. In order to improve the accuracy of the approximation of y in (2.36), one needs to increase the order r of the expansion [58].

The forms of the polynomial basis functions $\{\phi_k(\boldsymbol{x})\}$ are dependent on the probability distribution of the *N*-dimensional random variable $\boldsymbol{x}$ and its dimension *N*. To clarify this point, let us first assume that $\boldsymbol{x}$ is univariate (i.e., $N = 1$), and is represented by the 1-dimensional random variable *x*. The polynomial type for the common probability distributions is listed in Table 2-1 [59].

It is worth noting that the Hermite polynomial was first developed for the Gaussian random variable in [60]. However, in reality, as the random variable may not necessarily follow the Gaussian distribution, efforts were made in [29] to develop the polynomials for different types of probability distributions.

Taking the univariate *x* following the Gaussian distribution for example, the three polynomial basis functions $\{\phi_0(x),\ \phi_1(x),\ \phi_2(x)\}$ for (2.36) at the order $r = 3$ are given in Table 2-2.

Table 2-1. Askey-Scheme Polynomials

Probability distribution of the random variable *x*	Type of polynomials
Gaussian	Hermite
Gamma	Laguerre
Beta	Jacobi
Uniform	Legendre

Table 2-2. Hermite Polynomials

Index *k*	Hermite polynomials
0	$\phi_0(x)$=1
1	$\phi_1(x) = x$
2	$\phi_2(x) = x^2 - 1$

If the random variable $\boldsymbol{x}$ is multivariate (i.e., $\boldsymbol{x} = [x_1, x_2, .., x_N]$, $N > 1$), the multivariate polynomial basis functions $\{\phi_k(\boldsymbol{x})\}$ are given by the products of the polynomial for each dimension x_i $(1 \leq i \leq N)$, as shown below:

$$\phi_k(\boldsymbol{x}) = \prod_{i=1}^{N} \phi_{k_i}(x_i) \tag{2.38}$$

where the index k of the multivariate polynomial basis functions is denoted by an N-dimensional vector $k = [k_1, \ldots, k_N]$. The elements $\{k_i, 1 \le i \le N\}$ in the vector k need to satisfy the following condition:

$$\sum_{i=1}^{N} k_i \le r \tag{2.39}$$

Let us demonstrate the meaning of (2.38) and (2.39) using a bivariate Gaussian example. In this case, the dimension of the bivariate $\boldsymbol{x} = [x_1, x_2]$ is $N = 2$. At the expansion order $r = 2$, the legitimate forms of the vector k under the condition in (2.39) are: [0, 0], [1, 0], [0, 1], [2, 0], [1, 1], and [0, 2]. Based on the univariate Hermite polynomials in Table 2-2, the multivariate polynomial basis functions $\{\phi_k(\boldsymbol{x})\}$ are obtained using (2.38) as:

$$\begin{aligned}
\phi_{[0,0]}(\boldsymbol{x}) &= \phi_{[0,0]}(x_1, x_2) = \phi_0(x_1)\,\phi_0(x_2) = 1 \\
\phi_{[1,0]}(\boldsymbol{x}) &= \phi_{[1,0]}(x_1, x_2) = \phi_1(x_1)\,\phi_0(x_2) = x_1 \\
\phi_{[0,1]}(\boldsymbol{x}) &= \phi_{[0,1]}(x_1, x_2) = \phi_0(x_1)\,\phi_1(x_2) = x_2 \\
\phi_{[2,0]}(\boldsymbol{x}) &= \phi_{[2,0]}(x_1, x_2) = \phi_2(x_1)\,\phi_0(x_2) = x_1^2 - 1 \\
\phi_{[1,1]}(\boldsymbol{x}) &= \phi_{[1,1]}(x_1, x_2) = \phi_1(x_1)\,\phi_1(x_2) = x_1 x_2 \\
\phi_{[0,2]}(\boldsymbol{x}) &= \phi_{[0,2]}(x_1, x_2) = \phi_0(x_1)\,\phi_2(x_2) = x_2^2 - 1
\end{aligned} \tag{2.40}$$

Now it becomes clear that the polynomial basis functions $\{\phi_k(\boldsymbol{x})\}$ in (2.36) are determined by the number of random variables (i.e., the randomness dimension N), the probability distribution of each variable, and the expansion order r.

The only remaining task is to determine the unknown coefficients $\{c_k\}$ for the polynomial basis functions $\{\phi_k(\boldsymbol{x})\}$ in (2.36). The typical approach to obtain the coefficients $\{c_k\}$ is via the stochastic Galerkin (SG) method in [61]. Specifically, the SG method transforms the governing equation of the deterministic solver into a large set of equations. The solutions of this equation set are the desired coefficients $\{c_k\}$ in (2.36). Now it is clear that the implementation of the PCE method demonstrated herein is intrusive, as the coding of the

deterministic solver is modified. This is considered as a drawback, and may result in overwhelmingly difficult implementation if the governing equation of the deterministic solver takes complex forms.

Once both the coefficients $\{c_k\}$ and polynomial basis functions $\{\phi_k(\boldsymbol{x})\}$ in (2.36) are determined, the output y can be described with the derived analytical formula regarding random input variables. On this basis, the statistics of the output y can be obtained using either the mathematical transformation or running sufficient simulations with the derived analytical formula. At this stage, simulating via the analytical formula uses much less computational cost compared to actually running the deterministic solver.

Please note that the workflow of the PCE method introduced herein is on a standard basis. However, intensive development was made to improve the applicability of the PCE method. For example, apart from the common distribution types listed in Table 2-1, several techniques such as in [62] and [63] were proposed to deal with systems affected by random variables with arbitrary distributions. Also, efforts were made in [64] and [65] to implement the PCE method in a non-intrusive manner, thus to reduce the complexity of implementation. Finally, the computation process for the coefficients of the polynomial basis functions was considered a limitation of the PCE method, especially for the large randomness dimension case. However, the decoupled PCE technique developed in [66] can be used to greatly reduce the impact of this limitation.

The PCE framework presented in this chapter was successfully applied to obtain the statistics of the interference in cables [67], [68], and at the chip interconnecting level in [69].

2.2.3 Stochastic Collocation Method

Unlike the intrusive PCE method presented in Section 2.2.2, the stochastic collocation (SC) method proposed in [30] and [70] is non-intrusive, and therefore, applicable to complex EMC problems affected by parametric uncertainty. The aim of the SC method is the same as that of the PCE method: to express the deterministic solver as an analytical formula. After deriving this analytical formula, the statistics of the output response can be obtained using the same procedure as described for the PCE implementation in Section 2.2.2.

Now let us start the detailed introduction of the standard SC method with the univariate case. By default, the Lagrange polynomial [71] is used as the interpolating function for the SC

method. In this univariate case, the system output y is related to the input x using the deterministic solver $f(x)$, i.e., $y = f(x)$. If the n collocation points $[x_1, \ldots, x_n]$ for x and the corresponding output samples $[f(x_1), \ldots, f(x_n)]$ are known, the deterministic solver $f(x)$ can be approximated using an analytical formula $F(x)$ as shown below:

$$f(x) \approx F(x) = \sum_{j=1}^{n} f(x_j) L_j(x) \tag{2.41}$$

where $L_j(x)$ is the Lagrange interpolating function taking the following form:

$$L_j(x) = \prod_{k=1, k\neq j}^{n} \frac{x - x_k}{x_j - x_k}, \qquad j = 1, \ldots, n. \tag{2.42}$$

Clearly, in (2.42), we have $L_j(x)$=1 at $x = x_j$, and $L_j(x)$=0 at $x = x_k$ $(1 \leq k \leq n, k \neq j)$. As a result, the approximated analytical formula $F(x)$ produces the exact output samples at the n collocation points $[x_1, \ldots, x_n]$, i.e., $F(x_j) = f(x_j)$ for $1 \leq j \leq n$.

However, dealing with the univariate random process is not enough, as the multivariate random processes are mostly seen in reality. Now let us extent to the multivariate Lagrange interpolation by defining the N-dimensional variable $\boldsymbol{X} = [X_1, \ldots, X_N]$ to contain all the N random variables. Also, let the collection $\{X_{j(i)}, i = 1, \ldots, m_j\}$ represent the m_j collocation points for the jth-dimension X_j $(1 \leq j \leq N)$ in $\boldsymbol{X}$. If the samples of the output y at each collocation point in the uncertain input space of $\boldsymbol{X}$ are known, the deterministic solver $f(\boldsymbol{X})$ can be approximated using the analytical formula $F(\boldsymbol{X})$ in the following form:

$$f(\boldsymbol{X}) \approx F(\boldsymbol{X}) = \sum_{j_1=1}^{m_1} \cdots \sum_{j_N=1}^{m_N} f(X_{1(j_1)}, \cdots, X_{N(j_N)}) \prod_{i=1}^{N} L_{j_i}(X_i) \tag{2.43}$$

where Lagrange interpolating function $L_{j_i}(X_i)$ takes the form below:

$$L_{j_i}(X_i) = \prod_{k=1, k\neq j}^{m_{j_i}} \frac{X_i - X_{j_i(k)}}{X_{j_i(j_i)} - X_{j_i(k)}} \tag{2.44}$$

At this stage, it is clear that the workflow of the SC method involves three main steps. First, one needs to select a set of collocation points in the uncertain input space. The technique based on Chebyshev polynomials was introduced in [71] to select collocation points in the

uncertain input space. Second, the output samples at these collocation points are to be obtained using the deterministic solver. Finally, the Lagrange interpolating function is used to construct the approximated analytical formula passing through all the output samples at the collocation points. This analytical formula will be used as the equivalent replacement of the deterministic solver to run simulations. Having obtained this analytical formula, the statistics of the output can be efficiently obtained via either the mathematical transformation in [26] or running a sufficient number of simulations using the derived analytical formula. The primitive statistical analysis of cable crosstalk using the standard SC method was presented in [72]. However, it is worth noting that the cable configuration was assumed to be partially random in [72], not satisfying the need of the real-world scenario.

Clearly, the existing deterministic solver is used without any modification in the implementation of the SC method, demonstrating its non-intrusive feature. However, despite being non-intrusive, the weakness of the SC method needs to be pointed out. First, the result of the SC method is sensitive to the choice of the interpolating function. This is because apart from the Lagrange interpolating function demonstrated herein, other interpolating functions are possible, and may result in different forms of the approximated analytical formula. Second, as pointed out in [73], the selection of collocation points in the uncertain input space is regardless of the probability distribution of the random variable, and therefore, is not optimal.

In addition to the aforementioned drawbacks, the standard SC method presented in this section was unsuitable for stochastic problems with large randomness dimension. This is because the construction of the approximated analytical formula in (2.43) is based on the multivariate tensor-product interpolation. The drawback of the tensor-product interpolation is that the computational cost grows exponentially with the increasing number of random variables. To demonstrate this point, the deterministic solver needs to be executed for $\prod_{j=1}^{N} m_j$ times to construct the approximated analytical formula in (2.43). As a result, the applicability of the standard SC method may be greatly limited by the curse of dimensionality.

However, the sparse-grid sampling technique in [71] and [74] based on the Smolyak's algorithm [75] can be used to reduce the impact of this limitation. Compared to the tensor-product sampling technique applied in (2.43), the sparse-grid sampling technique can significantly reduce the number of collocation points, especially in the case of the large

randomness dimension, thus to reduce the computational cost of running the deterministic solver.

For the sparse-grid sampling technique, the number of collocation points is determined by the randomness dimension N and the Smolyak construction level k. If the randomness dimension N is fixed, the number of collocation points is increased by increasing the Smolyak construction level k, so are the accuracy and computational cost. As the SC method based on the sparse-grid sampling technique is not the advocated approach in this thesis, only a concise description is provided herein. The customised software tool to implement this technique is available in [76]. Further theoretical details can be found in [30] and [74].

In this thesis, the SC method is used as the reference method to benchmark the performance of the advocated SROM method introduced in Section 2.3. Specifically, the standard SC method based on the tensor-product sampling technique is applied in Chapter 4 to quantify the variability of the cable interference in the wire-to-wire coupling model affected by cable configurational uncertainty. In Chapter 6, the SC method based on the sparse-grid sampling technique is used to obtain the statistics of the cable interference introduced by the random illuminating field.

Finally, before introducing the SROM method, it is worth noting that the efficient statistical analysis of EMC problems via the unscented transformation technique [77] is also possible, as demonstrated in [78]. This technique is beyond the scope of this thesis.

2.3 Stochastic Reduced Order Model Method

It is clear from Section 2.2 that in order to implement the PCE method, an explicit form of the governing equation relating the input to output is required. Therefore, the PCE method is unsuitable for complex EMC problems where the deterministic solver is regarded as a black box. On the other hand, the SC method is non-intrusive, but its results are sensitive to the choice of the interpolating function, as different interpolating functions produce slightly different forms of the deterministic solver. Also, the selection of collocation points is regardless of the statistics of the uncertain input variable, and therefore is not optimal.

To overcome the drawbacks of the PCE and SC methods, the *stochastic reduced order model* (SROM) method was proposed very recently in [27] to efficiently quantify the uncertainty of

the system response. This method is non-intrusive and very efficient compared with the traditional MC method. The idea of the SROM method is conceptually simple, and essentially different from the PCE and SC methods, but to approximate the statistics of random input variables using a very small number of selected samples assigned with probabilities. Therefore, unlike the MC method blindly and exhaustively checking all the possible cases, the SROM method only needs to examine these selected samples without sacrificing accuracy. Clearly, the SROM method can be regarded as a small but smart version of the MC method, and therefore is general for a wide range of stochastic problems. An in-depth comparison between the PCE, SC, and SROM methods is given in [79].

The SROM method has been used to solve uncertainty-embedded mechanical and materials engineering problems in [73], [80], [81], and [82], but had not been applied in the EMC domain before the research work presented in this thesis. The pioneering applications of the SROM method in the uncertainty quantification of cable interference are presented from Chapter 4 to Chapter 6 in this thesis.

Now let us focus on the technical introduction of the SROM method. First, the definition of a random variable is needed. Let $\boldsymbol{X}$ be a N-dimensional random variable ($N \geq 1$) if $\boldsymbol{X}$ is jointly described by N variables. Each dimension X_i ($1 \leq i \leq N$) is used to describe the variation of a random variable, and can be correlated or uncorrelated with other dimensions. For example, if $\boldsymbol{X}$ is a bivariate random variable, i.e., $\boldsymbol{X} = [X_1, X_2]$, then $N = 2$. The values of X_1 and X_2 tell the coordinates of $\boldsymbol{X}$ on the two-dimensional X_1-X_2 plane. It is assumed that the statistical properties of $\boldsymbol{X}$ are fully known beforehand, which are the marginal distribution, q-th order moment, and the correlation matrix as shown in (2.45), (2.46), and (2.47), respectively [83]:

$$F_i(\theta) = P(X_i \leq \theta) \tag{2.45}$$

$$\mu_i(q) = E\left(X_i^q\right) \tag{2.46}$$

$$\boldsymbol{r} = E[\boldsymbol{X}\boldsymbol{X}^T] \tag{2.47}$$

where $i = 1, \ldots, N$. Here, $F_i(\theta)$ is the probability of X_i taking a value smaller than or equal to θ, i.e., the cumulative distribution function (CDF) value of X_i at $X_i = \theta$. The operator $E(\cdot)$ means calculating the expectation value. Please note that the first order moment is equivalent to the mean value.

2.3.1 Definition of SROM

A SROM $\tilde{\boldsymbol{X}}$ is an approximation of the random variable $\boldsymbol{X}$ in the sense that $\tilde{\boldsymbol{X}}$ and $\boldsymbol{X}$ have similar statistical properties quantified in (2.45)-(2.47). The SROM $\tilde{\boldsymbol{X}}$ consists of a sample set $\tilde{\boldsymbol{x}} = \{\tilde{\boldsymbol{x}}^{(1)}, \dots, \tilde{\boldsymbol{x}}^{(m)}\}$ with the corresponding probabilities $\boldsymbol{p} = (p^{(1)}, \dots, p^{(m)})$ for each sample in $\tilde{\boldsymbol{x}}$. Any sample $\tilde{\boldsymbol{x}}^{(k)}$, $1 \leq k \leq m$, contains one or multiple values depending on the dimension N of $\boldsymbol{X}$, as $\tilde{\boldsymbol{x}}^{(k)} = (\tilde{x}_1^{(k)}, \dots, \tilde{x}_N^{(k)})$, with $\tilde{x}_1^{(k)}$ being the coordinate of $\boldsymbol{X}$ in the dimension X_1. The elements in $\boldsymbol{p}$ are required to meet the constraints $\sum_{k=1}^{m} p^{(k)} = 1$ and $p^{(k)} \geq 0$. Once the sample set $\tilde{\boldsymbol{x}}$ and probabilities $\boldsymbol{p}$ are selected, the SROM $\tilde{\boldsymbol{X}}$ is completely defined. The model size m is determined by the trade-off between accuracy and computational cost. A large value of m usually gives very accurate statistical approximation of a random variable, but makes the implementation very computationally intensive [27]. Similar to $\boldsymbol{X}$, the statistics of the SROM $\tilde{\boldsymbol{X}}$ are defined as:

$$\tilde{F}_i(\theta) = P\left(\tilde{X}_i \leq \theta\right) = \sum_{k=1}^{m} p^{(k)} \boldsymbol{I}\left(\tilde{x}_i^{(k)} \leq \theta\right) \tag{2.48}$$

$$\tilde{\mu}_i(q) = E\left(\tilde{X}_i^q\right) = \sum_{k=1}^{m} p^{(k)} \left(\tilde{x}_i^{(k)}\right)^q \tag{2.49}$$

$$\tilde{r}_{ij} = E\left[\tilde{X}_i \tilde{X}_j\right] = \sum_{k=1}^{m} p^{(k)} \tilde{x}_i^{(k)} \tilde{x}_j^{(k)} \tag{2.50}$$

where $\boldsymbol{I}(A) = 1$ if A is true and $\boldsymbol{I}(A) = 0$ if A is false. Any sample set $\tilde{\boldsymbol{x}}$ and probabilities $\boldsymbol{p}$ can construct a SROM for $\boldsymbol{X}$. However, some SROMs produce a more accurate approximation of the statistics of $\boldsymbol{X}$. For this reason, a measure of the discrepancy between the statistics of $\tilde{\boldsymbol{X}}$ and $\boldsymbol{X}$ is needed. The next section describes how to construct an optimal SROM $\tilde{\boldsymbol{X}}$ for $\boldsymbol{X}$ so that the discrepancy is minimised.

2.3.2 Construction of SROM

There exist many SROMs for the random variable $\boldsymbol{X}$ as long as the sample-probability pair $\{\tilde{\boldsymbol{x}}, \boldsymbol{p}\}$ meets the constraints in the previous section. However, to implement the SROM method, an optimal SROM $\tilde{\boldsymbol{X}}$ for the input variable $\boldsymbol{X}$ is required so that the discrepancy between the statistics of $\tilde{\boldsymbol{X}}$ and $\boldsymbol{X}$ is minimised. The discrepancy is measured with an

objective function containing three error metrics. These error metrics represent the errors between marginal distributions, moments up to order of $\bar{q}$, and correlation matrices of $\tilde{\boldsymbol{X}}$ and $\boldsymbol{X}$, respectively, and are defined as:

$$e_1(\tilde{\boldsymbol{x}}, \boldsymbol{p}) = \sum_{i=1}^{N} \sum_{k=1}^{m} (\tilde{F}_i\left(\tilde{x}_i^{(k)}\right) - F_i\left(\tilde{x}_i^{(k)}\right))^2 \tag{2.51}$$

$$e_2(\tilde{\boldsymbol{x}}, \boldsymbol{p}) = \sum_{i=1}^{N} \sum_{q=1}^{\bar{q}} (\tilde{\mu}_i(q) - \mu_i(q))^2 \tag{2.52}$$

$$e_3(\tilde{\boldsymbol{x}}, \boldsymbol{p}) = \sum_{i,j=1,\dots,N; j>i} (\tilde{r}_{ij} - r_{ij})^2 \tag{2.53}$$

With each error metric being defined, the objective function measuring the total discrepancy of the statistics between $\tilde{\boldsymbol{X}}$ and $\boldsymbol{X}$ can be expressed as:

$$e(\tilde{\boldsymbol{x}}, \boldsymbol{p}) = \alpha_1 e_1(\tilde{\boldsymbol{x}}, \boldsymbol{p}) + \alpha_2 e_2(\tilde{\boldsymbol{x}}, \boldsymbol{p}) + \alpha_3 e_3(\tilde{\boldsymbol{x}}, \boldsymbol{p}) \tag{2.54}$$

where α_1, α_2, $\alpha_3 \geq 0$ are weighting factors to make each error metric have a similar order of magnitude, or to emphasise which statistical property of $\boldsymbol{X}$ to be approximated more accurately. For example, we can set $\alpha_1 \gg \alpha_2$ and α_3 if the marginal distribution of $\boldsymbol{X}$ needs to be approximated more precisely by $\tilde{\boldsymbol{X}}$. The optimal SROM $\tilde{\boldsymbol{X}}$ is defined by the sample-probability pair $\{\tilde{\boldsymbol{x}}_{(\text{opt})}, \boldsymbol{p}_{(\text{opt})}\}$ that minimises the objective function in (2.54). As a result, this $\tilde{\boldsymbol{X}}$ is the closest to $\boldsymbol{X}$ in the statistical sense. If $\boldsymbol{X}$ is a one-dimensional random variable, i.e., $N = 1$, the approximation error of correlation matrices in (2.53) can be ignored when constructing the optimal SROM $\tilde{\boldsymbol{X}}$. In practice, finding the optimal $\tilde{\boldsymbol{X}}$ can be too exhaustive or even impossible. This is because strictly speaking, the optimal $\tilde{\boldsymbol{X}}$ can only be credited after examining every possible combination of the legitimate $\tilde{\boldsymbol{x}}$ and $\boldsymbol{p}$.

To solve this problem, three sampling techniques (i.e., *Dependent thinning*, *Integer optimisation*, and *Pattern classification*) were suggested in [27] as guidelines on choosing the sample set $\tilde{\boldsymbol{x}}$ of $\tilde{\boldsymbol{X}}$. Which technique to use can be chosen heuristically, as all three techniques have the same aim: to select m samples scattered as far from each other as possible, thus to explore the entire uncertain space of $\boldsymbol{X}$. The *pattern classification* is chosen in this thesis to find the optimal SROM $\tilde{\boldsymbol{X}}$, and is outlined in eight steps as follows:

Step 1): Generate n independent samples ($\boldsymbol{\xi}_1, \dots, \boldsymbol{\xi}_n$) based on the statistics of $\boldsymbol{X}$. The sample

size n should be sufficiently large, so that the sample set ($\boldsymbol{\xi}_1$, …, $\boldsymbol{\xi}_n$) produces accurate statistics of $\boldsymbol{X}$.

Step 2): Randomly select m samples ($\tilde{\boldsymbol{x}}^{(1)}$, … , $\tilde{\boldsymbol{x}}^{(m)}$) from ($\boldsymbol{\xi}_1$, …, $\boldsymbol{\xi}_n$) to form a candidate for $\tilde{\boldsymbol{x}}_{(\mathrm{opt})}$, $m \ll n$.

Step 3): Partition the uncertain space of $\boldsymbol{X}$ into m Voronoi regions (Γ_1, …, Γ_m) [84] centred at ($\tilde{\boldsymbol{x}}^{(1)}$, …, $\tilde{\boldsymbol{x}}^{(m)}$), respectively. This means that the region Γ_k centred at $\tilde{\boldsymbol{x}}^{(k)}$ ($1 \le k \le m$) only contains the samples from ($\boldsymbol{\xi}_1$, …, $\boldsymbol{\xi}_n$) which are closer to $\tilde{\boldsymbol{x}}^{(k)}$ than to $\tilde{\boldsymbol{x}}^{(l)}$ ($l \ne k$, $1 \le l \le m$). Here, the Euclidean distance is used.

Step 4): Let $d^{(k)} = \sum_{\boldsymbol{\xi}_i \in \Gamma_k} d(\tilde{\boldsymbol{x}}^k, \boldsymbol{\xi}_i)$ denote the intra-cluster distance of Γ_k ($1 \le k \le m$). Here, $\boldsymbol{\xi}_i$ can be any sample located in Γ_k, and $d(\tilde{\boldsymbol{x}}^k, \boldsymbol{\xi}_i)$ means the distance between the sample $\boldsymbol{\xi}_i$ and the centre $\tilde{\boldsymbol{x}}^k$.

Step 5): Let d be the summation of the intra-cluster distance of all the Voronoi regions, i.e., $d = \sum_{k=1}^{m} d^{(k)}$.

Step 6): Select other candidates for $\tilde{\boldsymbol{x}}_{(\mathrm{opt})}$ and calculate the value of d for each candidate.

Step 7): Choose the candidate with the minimum value of d as $\tilde{\boldsymbol{x}}_{(\mathrm{opt})}$, as the samples in this subset explore the entire range of $\boldsymbol{X}$. After this selection process, the obtained samples in $\tilde{\boldsymbol{x}}_{(\mathrm{opt})}$ should be most widely scattered in the uncertain space of $\boldsymbol{X}$.

Having obtained $\tilde{\boldsymbol{x}}_{(\mathrm{opt})}$, the probability set $\boldsymbol{p}_{(\mathrm{opt})}$ can be determined as follows:

Step 8): If the number of samples in the region Γ_k is n_k ($1 \le k \le m$), the probability $p^{(k)}$ assigned to the sample $\tilde{\boldsymbol{x}}^{(k)}$ in $\tilde{\boldsymbol{x}}_{(\mathrm{opt})}$ can be obtained as: $p^{(k)} = n_k \ / \ n$. Performing this calculation for each Voronoi region can give the probability set $\boldsymbol{p}_{(\mathrm{opt})}$. Now the optimal $\widetilde{\boldsymbol{X}}$ is fully constructed.

Please note that the resulting sample-probability pair $\{\tilde{\boldsymbol{x}}_{(\mathrm{opt})}, \boldsymbol{p}_{(\mathrm{opt})}\}$ may not be strictly optimal, but it generally provides a more accurate statistical approximation of $\boldsymbol{X}$, compared with other candidates obtained using random selection.

2.3.3 Uncertainty Propagation by SROM

This section describes how to propagate uncertainty from the multivariate random variable $\boldsymbol{X} = (X_1, X_2, \ldots, X_N)$ to the output $\boldsymbol{Y}$ using the SROM method. Here, $\boldsymbol{X}$ can be interpreted as a collection of N random variables. A workflow illustrating the uncertainty quantification with the SROM method is outlined in Fig. 2-5. The statistics of the actual output $\boldsymbol{Y}$ are approximated by those of the SROM-based output $\widetilde{\boldsymbol{Y}}$. The construction of $\widetilde{\boldsymbol{Y}}$ requires an optimal SROM $\widetilde{\boldsymbol{X}} = \{\tilde{\boldsymbol{x}}, \boldsymbol{p}\}$ for $\boldsymbol{X}$ and a deterministic solver M. The deterministic solver is used to produce the samples of the output $\boldsymbol{Y}$ given the samples of the input $\boldsymbol{X}$. Similar to $\widetilde{\boldsymbol{X}}$, $\widetilde{\boldsymbol{Y}}$ is also defined by a sample set $\tilde{\boldsymbol{y}} = \{\tilde{\boldsymbol{y}}^{(1)}, \ldots, \tilde{\boldsymbol{y}}^{(m)}\}$ together with the corresponding probabilities $\boldsymbol{p}_y = (p_y{}^{(1)}, \ldots, p_y{}^{(m)})$. With the samples $\{\widetilde{\boldsymbol{x}}^{(i)}\}_{i=1}^{m}$ for $\widetilde{\boldsymbol{X}}$ being known, the samples $\{\widetilde{\boldsymbol{y}}^{(i)}\}_{i=1}^{m}$ for $\widetilde{\boldsymbol{Y}}$ can be obtained by performing m deterministic calculations with the variable $\boldsymbol{X}$ set equal to $\tilde{\boldsymbol{x}}^{(1)}, \ldots, \tilde{\boldsymbol{x}}^{(m)}$:

$$M: \widetilde{\boldsymbol{x}}^{(k)} \rightarrow \widetilde{\boldsymbol{y}}^{(k)}, k = 1, \ldots, m \tag{2.55}$$

The probabilities $\boldsymbol{p}_y$ of $\widetilde{\boldsymbol{Y}}$ are the same as the probabilities $\boldsymbol{p}$ of $\widetilde{\boldsymbol{X}}$, i.e., $p_y{}^{(k)} = p^{(k)}$, $k = 1, \ldots, m$. The reason is that $\tilde{\boldsymbol{y}}^{(k)}$ only occurs when the input is $\tilde{\boldsymbol{x}}^{(k)}$. Having obtained the sample set $\tilde{\boldsymbol{y}}$ and probabilities $\boldsymbol{p}_y$, the SROM-based solution $\widetilde{\boldsymbol{Y}}$ is completely defined. The calculation of the statistics of $\widetilde{\boldsymbol{Y}}$, such as the CDF and the moment of order q, becomes an easy task as shown below:

$$P\left(\tilde{Y} \leq \xi\right) = \sum_{k=1}^{m} p^{(k)} \boldsymbol{I}\left(\tilde{y}^{(k)} \leq \xi\right) \tag{2.56}$$

$$E\left(\tilde{Y}^{q}\right) = \sum_{k=1}^{m} p^{(k)} \left(\tilde{y}^{(k)}\right)^{q} \tag{2.57}$$

The standard deviation σ for $\widetilde{\boldsymbol{Y}}$ can be obtained using:

$$\sigma\left(\tilde{Y}\right) = \sum_{k=1}^{m} p^{(k)} \left(\tilde{y}^{(k)} - E\left(\tilde{Y}^{1}\right)\right)^{2} \tag{2.58}$$

The statistics of $\boldsymbol{Y}$ are approximated by those of $\widetilde{\boldsymbol{Y}}$ in (2.56)-(2.58).

Now let us detail how to implement the SROM method in this thesis. In the context of this thesis, the statistical EMC analysis via the SROM method is implemented in the commercial

software: the matrix laboratory (MATLAB) [85] environment. First, the relationship between system variables (i.e., inputs) and cable coupling (i.e., the output) is constructed to form the deterministic solver. After this stage, the cable coupling level can be obtained given a certain configuration of the cable system. Second, the SROM stochastic framework is constructed to interface with the deterministic solver. Specifically, for an uncertainty-embedded cable EMC problem, the *pattern classification* technique presented in Section 2.3.2 is implemented in MATLAB to produce optimal SROM-based input samples and the associated probabilities. Then, these optimal SROM-based input samples are fed into the deterministic solver to generate SROM-based output samples of cable coupling. Finally, combined with the associated probabilities, the statistics of the cable coupling level can be straightforwardly obtained according to the SROM principle in (2.56)-(2.58). It is worth noting that linking the SROM algorithm implementation to the commercial software MATLAB is a significant contribution of this thesis.

It is clear that the SROM method has the non-intrusive feature and is therefore very convenient to implement. This method is also very efficient compared to the traditional MC simulation, as the effect of the uncertain input space on the output variation is taken into account using only m samples and the corresponding probabilities. In contrast, the MC method exhaustively examines almost every input sample until the converged result is obtained. The only overhead is to construct the optimal $\widetilde{\boldsymbol{X}}$ to ensure that the statistics of the input variable $\boldsymbol{X}$ are accurately approximated. Obviously, this overhead is negligible compared with the computational cost of the MC method.

There are some points worth mentioning regarding the SROM method. Specifically, the SROM method can be an *a-priori* evaluation by developing the error bound of the SROM solution for different model sizes as demonstrated in [80], [81], which is beyond the scope of this thesis. Increasing the model size m is an effective way to reduce the error of the result, but the selection of the value of m mainly depends on the consideration of computation time. In principle, the SROM solution is guaranteed to converge to the theoretical statistics of $\boldsymbol{Y}$ when the model size m approaches infinity [73]. Despite this, the SROM method has been shown to be able to produce very accurate statistics, even with a small m to reduce the computational cost [73], [83].

In summary, to propagate the uncertainty from the input variable $\boldsymbol{X}$ to the output $\boldsymbol{Y}$ using the SROM method, only three steps are needed. First, an optimal SROM $\widetilde{\boldsymbol{X}}$ for $\boldsymbol{X}$ is constructed

to minimise the approximation error in (2.54). This step is the nucleus of the SROM method, and can be implemented using the *pattern classification* method introduced in this section. Second, the SROM-based output $\widetilde{\boldsymbol{Y}}$ for $\boldsymbol{Y}$ is constructed using $\widetilde{\boldsymbol{X}}$ and the deterministic solver. Finally, the statistics of $\widetilde{\boldsymbol{Y}}$ are calculated to approximate those of the actual output $\boldsymbol{Y}$.

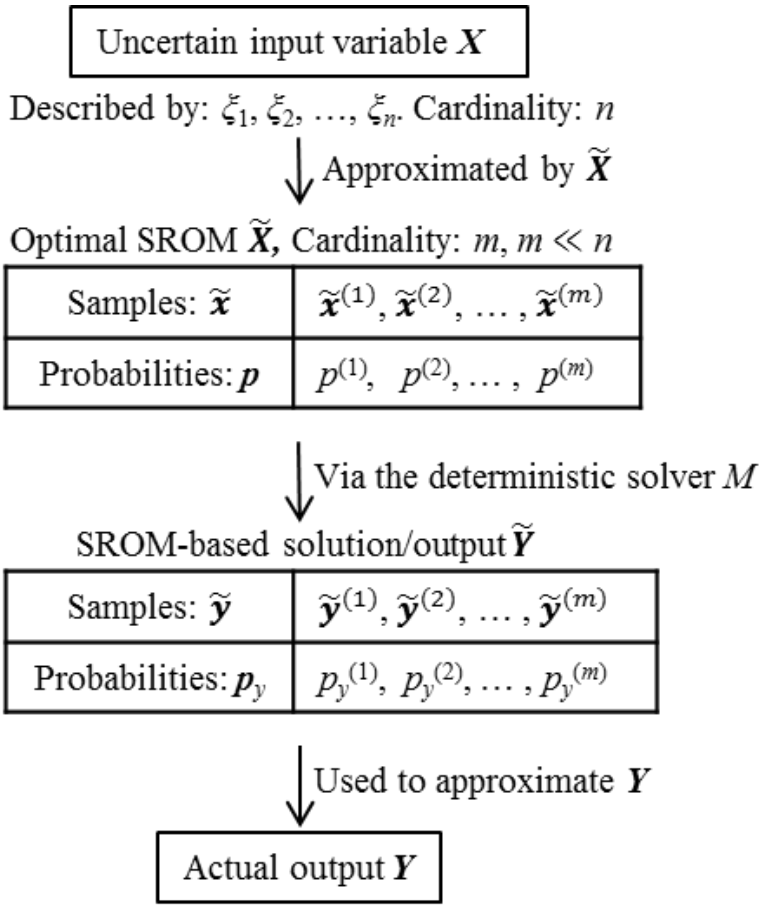

Fig. 2-5. Workflow of propagating uncertainty from the input variable X to the output Y with the SROM method.

Table 2-3. Comparison of the Various Statistical Methods

Method	Intrusive / Non-intrusive	Form of deterministic solver	Recovery of output statistics	Computational cost	Repeatability of result
Probabilistic mathematical transformation	Intrusive	Closed-form formula	Every statistic	Low	Repeatable
Worst-case method	Intrusive	Closed-form formula	Only the upper boundary	Low	Repeatable
MC	Non-intrusive	Any form	Every statistic	High	Repeatable only for converged result
PCE	Intrusive	Governing equation	Every statistic	Low	Repeatable
SC	Non-intrusive	Any form	Every statistic	Low	Repeatable only when using the same interpolating function
SROM (advocated in this thesis)	Non-intrusive	Any form	Every statistic	Low	Repeatable

2.4 Summary

The contribution of this chapter is twofold. First, a detailed introduction of the deterministic analysis of cable coupling has been presented. The workflow of the deterministic analysis has been shown to comprise the modelling of the cable structure using the MTL, the construction of the MTL equations governing the coupling phenomenon, and the solution of the interference in the cable. Second, a comprehensive overview of popular statistical methods has been presented. The principle, as well as the advantage and disadvantage of the MC, PCE, and SC methods, have been explained in detail. The development of the statistical analysis of cable interference using these statistical methods has been clearly outlined. On this basis, the motivation of using the SROM method in this PhD work and its principle has been explained. Therefore, this chapter has laid a solid foundation to perform the insightful investigation of the cable EMC problems affected by parametric uncertainty in the following chapters. Finally, a summary table showing the comparison of the various statistical methods introduced in this chapter is presented in Table 2-3.

Chapter 3 Crosstalk Variations Caused by Uncertainties in Three-Conductor Transmission Lines

In Chapter 1, the significance of predicting the cable interference in the design stage of the cable interconnecting system is emphasised. Also, the necessity of performing the prediction as a statistical analysis is pointed out, due to the inevitable uncertainty introduced to the cable configuration during the fabrication, installation, operation, and ageing processes.

Having identified the objective of this PhD work in Chapter 1, Chapter 2 presents the typical workflow of the deterministic analysis of the cable coupling problem, and introduces the popular statistical methods (including the advocated approach in this thesis), together with their applications in the stochastic cable EMC problem.

This chapter acts as the starting point of the cable coupling analysis to accomplish two aims. First, the necessity of considering the parametric uncertainty is proved by showing the significant influence of the cable configurational variation on the interference level. Second, how the cable interference responds to the common variations of the cable configuration is investigated. In other words, we are interested to see if the coupling level is increased or reduced as a response to the typical configurational variation. The result of this investigation can produce a better understanding to identify factors causing the excessive interference level in the cable interconnecting system. It is worth noting that the analysis presented in this chapter is on the deterministic basis, as no statistical information regarding the cable interference is extracted from the analysis.

3.1 Introduction

As introduced in Chapter 1, cables are used to transmit power and signals from one place to another. Due to the close proximity of the wires corded in the cable, interference is coupled amongst wires due to the interaction of the surrounding electromagnetic fields. In the wire-to-wire coupling scenario, the cable interference is terminologically referred to as crosstalk. The crosstalk may disturb the original signals at the ends of the cable and cause transmission errors. Therefore, it is of great significance to predict the crosstalk at the early design stage to evaluate the cable EMC performance.

By applying the deterministic analysis to different cable structures, it was found in [47] that the crosstalk was sensitive to the configurational variation of the cable. In reality, the configuration of the cable could be vaguely known due to uncertainty. Due to this reason, research work was intensively dedicated to dealing with the uncertainty of the cable configuration in the last three decades. For example, pioneering statistical analyses of cable crosstalk were presented in [52], [86], [87]. Due to the rapid development of the efficient statistical analysis, now the uncertainty-embedded EMC problems can be potentially solved using various efficient uncertainty quantification methods summarised in [88].

The uncertainties could arise from different aspects as explained in Section 1.3. For example, during the fabrication process, the wires in the cable are twisted randomly, making the information of the exact cross-section difficult to be obtained. Also, in the installation process, the distance of the cable from/to the ambient metallic structure is largely dependent on the installer's personal preference. The cable configurational variation investigated in this chapter mainly rises from the aforementioned sources of uncertainty.

It is clear the uncertainties of the cable configuration cause the crosstalk to vary. However, how different variations of the cable configuration could affect crosstalk is still unclear, and therefore investigated in this chapter. Herein, the configurational variation is mainly reflected by the variations in (1) the layout of the wires in the cable, (2) the relative position of the cable to the ground plane, (3) the format of the wire, and (4) the termination load at the end of the wire.

In this chapter, the cable is modelled as a three-conductor transmission line. The remaining part of this chapter is organised as follows: Section 3.2 describes the three-conductor transmission line as the model of the cable. In Section 3.3, the crosstalk variations due to the

changes of the cable configuration are presented, which shows the factors of influencing the certain behaviours of the crosstalk. The summary of this chapter is given in Section 3.4.

3.2 Three-Conductor Transmission-Line Model

In this section, the model of a three-conductor transmission line is introduced. It can be seen as a specific case of the multi-conductor transmission line (MTL) introduced in Section 2.1.3.

Here, the three-conductor transmission line is used because this model describes the integrity of cable configurational features without redundancy. For example, the typical geometric and electrical features of the cable system are included in the model of the three-conductor transmission line. The investigation result based on this model is believed to address common queries regarding the cable EMC performance to some extent. More realistic cables such as co-axial cables which minimise the interference can be seen as extensions of the three-conductor line model, which is beyond the scope of this study.

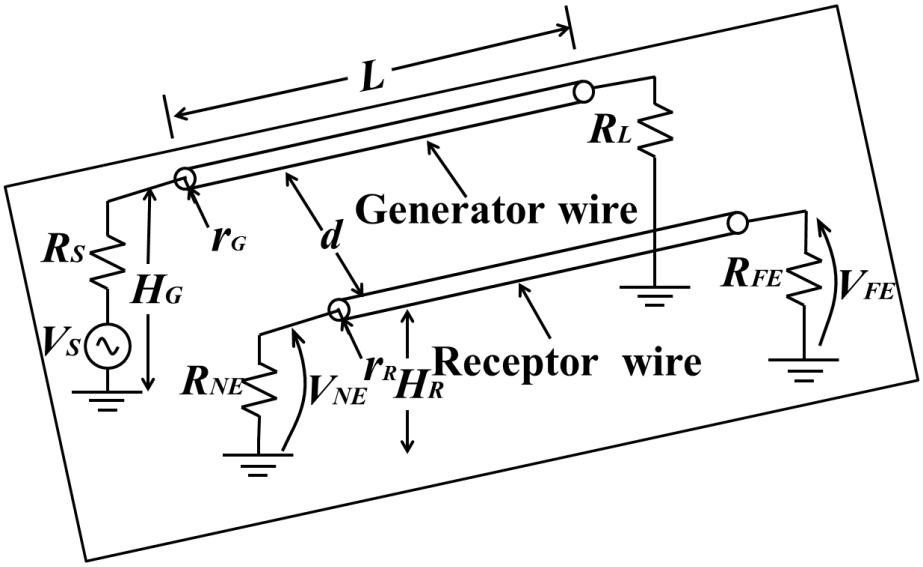

Fig. 3-1. The model of the three-conductor transmission line.

In Fig. 3-1, the two parallel conductors are referred to as the generator wire and the receptor wire, respectively. It means that the generator wire could introduce crosstalk to the receptor wire. The third conductor is the ground plane to which the voltage is referenced. In the generator circuit, the voltage source V_S with source impedance R_S is connected to the load impedance R_L by the generator wire. In the receptor circuit, the loads at the two ends, referred to as the *near-end* load R_{NE} and the *far-end* load R_{FE}, are connected using the receptor wire.

The subscripts *NE* and *FE* show if the load in the receptor circuit is at the *near-end* or *far-end*. The ground plane acts as the return path in the generator and receptor circuits. This return conductor can take different forms depending on the application scenario. For example, the metallic chassis of a vehicle or the fuselage of an airplane can be seen as the return conductor of the cable interconnecting system.

In this chapter, the model uses the following assumptions: 1) the two wires and the ground plane are perfect electric conductors; 2) the cross-sections of the two wires are uniform along the wire axis; and 3) the medium around the wires is lossless and homogeneous.

When the voltage source V_S in the generator circuit is on, the unintended voltage V_{NE} is introduced to the *near-end* load R_{NE} in the receptor circuit. The crosstalk can be quantified using the ratio of the induced voltage to the source voltage as follows [48]:

$$NEXT = \frac{V_{NE}}{V_S} \tag{3.1}$$

where *NEXT* is the *near-end* crosstalk. Once the values of all the termination impedances are chosen, the crosstalk is solely determined by the cable configuration. In the model of Fig. 3-1, the cable configuration is described by the following parameters: the wire length L, the radius r_G and the height H_G of the generator wire (the height is measured from the ground), the radius r_R and the height H_R of the receptor wire, the distance d between the generator and receptor wires, and the four termination loads R_S, R_L, R_{NE}, and R_{FE}.

3.3 Effects of Uncertainties on Crosstalk

In this section, uncertainties are introduced to the selected cable variables, in other words, the cable configuration varies in different ways. Each of the following sections describes a type of variation of the cable configuration, and discusses how the crosstalk is affected accordingly. In each variation, the crosstalk level is given by the simulation using the CST Cable Studio [19]. In this software, the simulation of the cable system can be performed by modelling the characteristics of the cable configuration.

The results from Section 3.3.1 to Section 3.3.4 below can be validated using the analytical solution of the crosstalk in the three-conductor transmission line derived in [89]. The

simulation for the following cases was performed under the assumption that L = 2 m and R_S = R_L = R_{NE} = R_{FE} = 50 Ω, if not specially stated.

3.3.1 Generator Rotating Anti-clockwise around Receptor

Fig. 3-2 shows how the *near-end* crosstalk varies when the generator wire rotates around the receptor wire in anti-clockwise direction. As can be seen in Fig. 3-2, the variation of the *near-end* crosstalk is very small. As we will see from Section 3.3.3, this is mainly due to the fact that the generator wire is well above the ground.

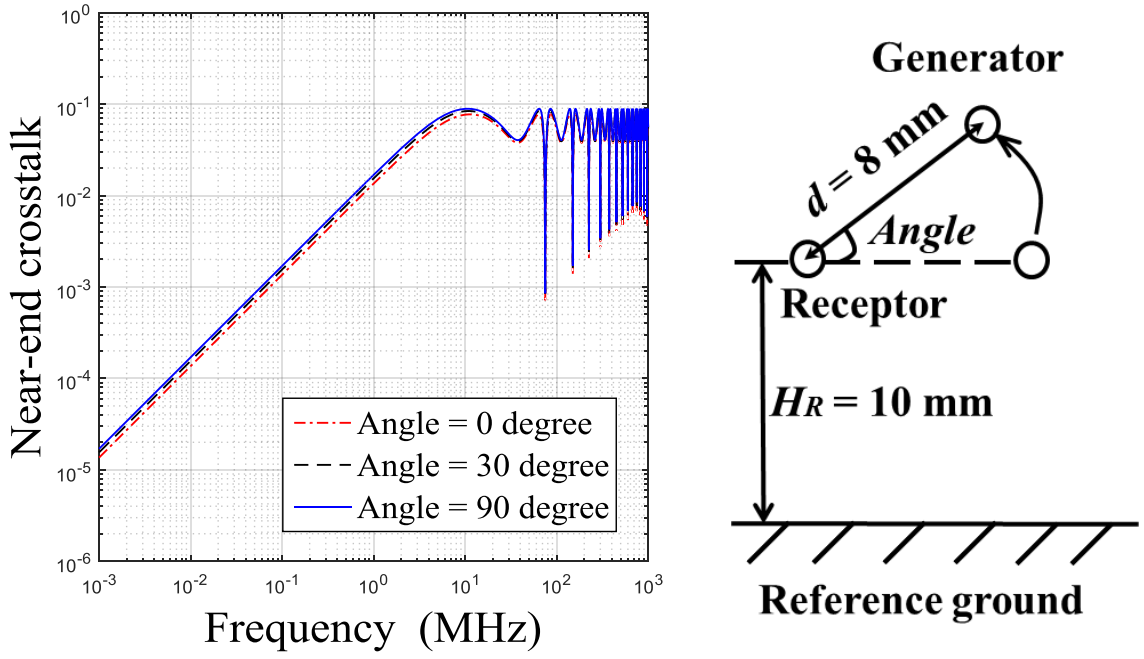

Fig. 3-2. Variation of crosstalk when the generator wire rotates anticlockwise around the receptor wire, for r_G = r_R = 0.69 mm. (a) Crosstalk as a function of frequency. (b) Illustration of the rotation of the generator wire. The *Angle* is selected as the uncertain variable.

Now let us focus on the underlying physical mechanism derived in [89] to explain the behaviour of the *near-end* crosstalk in Fig. 3-2 (a). Specifically, four different behaviours of the crosstalk will be validated using the theory in [89] as follows. First, as proved in [89], the frequency period of the crosstalk in the three-conductor transmission line is given by the frequency at which the wire length is half the wavelength. Given the wire length L = 2 m in

this section, the period of the crosstalk variation is calculated to be 75 MHz. Meanwhile, the variation pattern of the crosstalk shown in Fig. 3-2 (a) is replicated every 75 MHz. Therefore, the theoretical period of the crosstalk variation shows a good agreement with the observed period shown in Fig. 3-2 (a). Second, according to [89], the variation pattern of the crosstalk should be symmetrical about the frequency at which the wire length is a quarter of the wavelength. Again, as shown in Fig. 3-2 (a), the symmetrical axis at the frequency of 35 MHz is in line with this theory. Third, as revealed in [89], the frequency of the first maximum crosstalk is dependent on the electrical and geometric features of the cable system, such as the termination load, the height of each wire above the ground plane, and the separation between wires. Applying the theory in [89] to the case of *Angle* = 0 degree (i.e., the red curve) in Fig. 3-2 (a) yields the frequency of the first maximum crosstalk to be 11 MHz, conforming with the real observation shown in Fig. 3-2 (a). Frequencies for other peaks of the crosstalk can be estimated using the aforementioned symmetrical feature of the crosstalk variation. Finally, the theory in [89] shows that in the three-conductor line, the crosstalk should be increased by a factor of 10 with a 10-times increase in frequency before reaching the first maximum crosstalk. Again, the increasing slope of the crosstalk before reaching 11 MHz (i.e., the frequency of the first maximum crosstalk) shown in Fig. 3-2 (a) conforms with this theory.

3.3.2 Generator Rotating Clockwise around Receptor

How the *near-end* crosstalk varies when the generator wire rotates clockwise around the receptor wire is plotted in Fig. 3-3. In this case, the *near-end* crosstalk is reduced when increasing the rotation angle. Unlike in Section 3.3.1, this time, an obvious variation of the *near-end* crosstalk due to rotation angle changes is shown. As we will see from Section 3.3.3, this is mainly due to the generator wire is getting closer to the ground. Noting that when the cable configuration changes, it is the variations of cable variables that change the crosstalk. In the case of changing the rotation angle, the variation of the crosstalk is in fact caused by the variation of the height H_G of the generator wire.

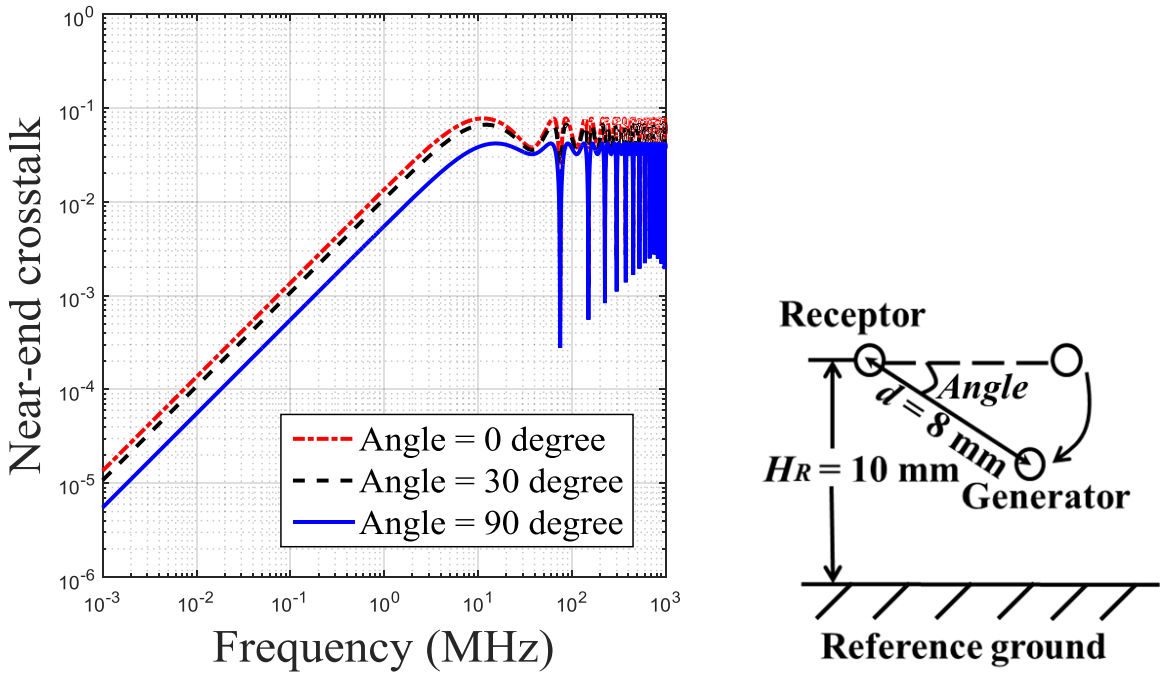

(a) **(b)**

Fig. 3-3. Variation of crosstalk when the generator wire rotates clockwise around the receptor wire, for r_G = r_R = 0.69 mm. (a) Crosstalk as a function of frequency. (b) Illustration of the rotation of the generator wire. The *Angle* is selected as the uncertain variable.

3.3.3 Effect of the Heights of the Generator and Receptor

How the heights H_G and H_R of the generator and receptor wires may affect the crosstalk is studied in this section. Herein, H_G is set equal to H_R. It is shown in Fig. 3-4(a) that the *near-end* crosstalk increases when the height of the wires increases. Therefore, for cable installations, placing wires close to the ground plane is able to reduce crosstalk.

Fig. 3-4(b) shows the *near-end* crosstalk for different heights at the frequency of 300 MHz. At the low-height range, the crosstalk is sensitive to the variation of the height. However, when the height goes beyond 40 mm, increasing the height does not significantly increase the crosstalk further. The reason is that the heights H_G and H_R are logarithmically related to the crosstalk [15].

For Section 3.3.1 and Section 3.3.2, although the separation between the two wires is fixed at 8 mm, H_G is increased from 10 mm in Section 3.3.1, while H_G is decreased from 10 mm in Section 3.3.2, as we can see from Fig. 3-4(b), the crosstalk is much more sensitive to the latter variation, which yields larger variation of crosstalk seen in Section 3.3.2.

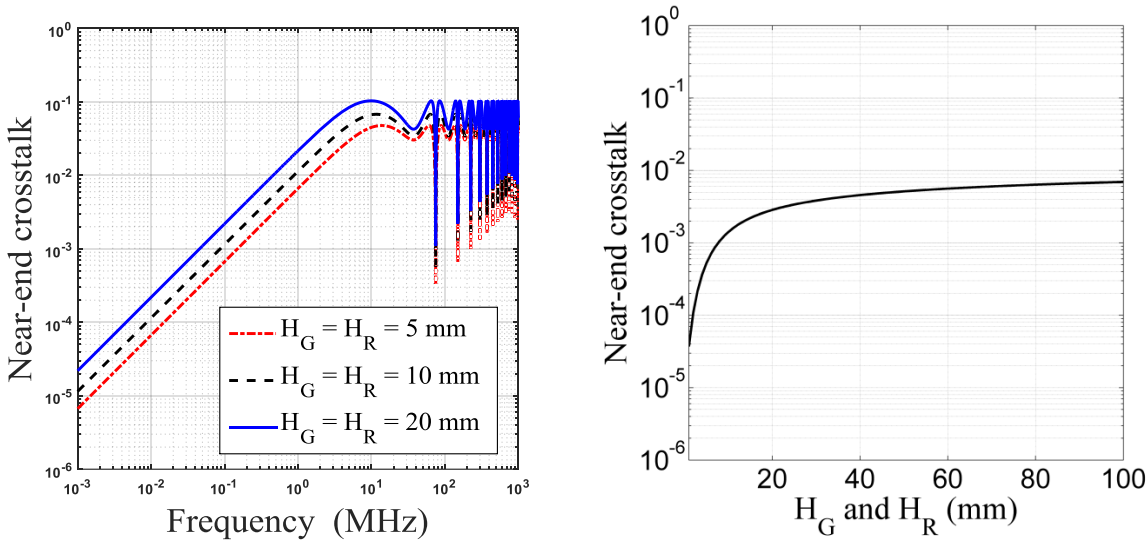

(a) **(b)**

Fig. 3-4. Variation of crosstalk when the heights of the generator and receptor wires increase, for distance d = 8 mm and $r_G = r_R$ = 0.69 mm. (a) Crosstalk as a function of frequency. The heights H_G and H_R are selected as the uncertain variables. (b) Crosstalk as a function of height at frequency of 300 MHz when $H_G = H_R$.

3.3.4 Effect of the Radii of the Generator and Receptor

In this section, how different radii of the generator and receptor wires might affect the crosstalk is shown. The two wires are placed at the same height above the ground, and the distance d between the two wires is fixed as shown in Fig. 3-5. The only uncertain variables in this cable configuration are the radii r_G and r_R of the two wires.

Herein, we set $r_G = r_R$. As shown in Fig. 3-5, increasing the radii of the wires increases the *near-end* crosstalk at high frequencies (i.e., from 10 MHz onwards), but has little impact on the crosstalk at low frequencies.

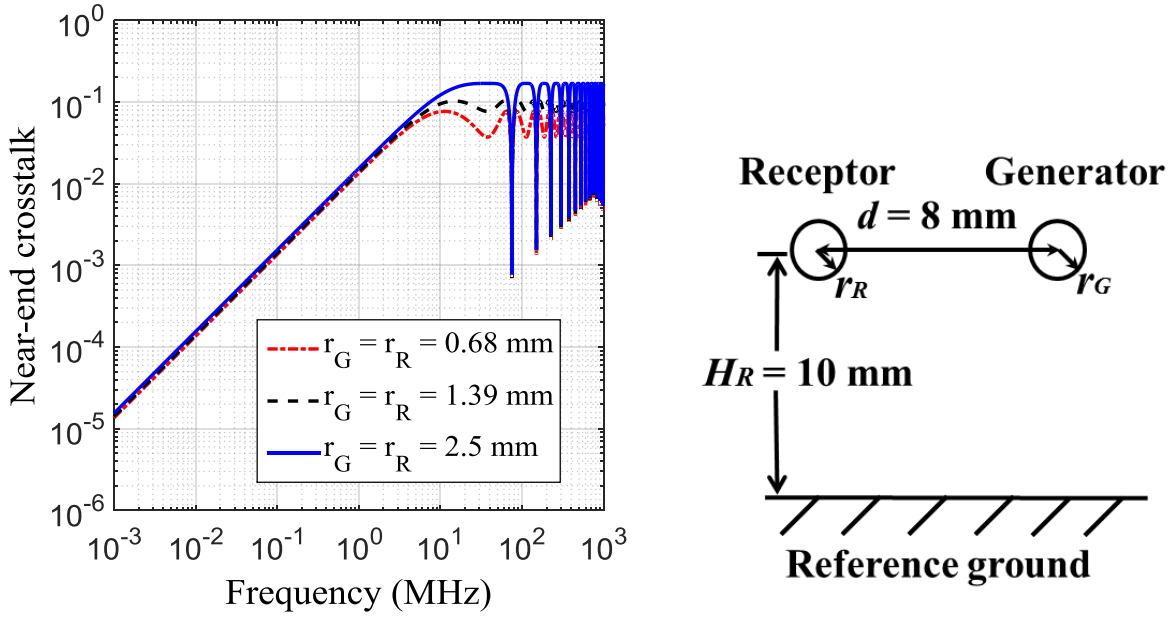

(a) **(b)**

Fig. 3-5. Variation of crosstalk due to different radii of the generator and receptor wires, for $H_G = H_R = 10$ mm and $d = 8$ mm. (a) Crosstalk as a function of frequency. (b) Cross-section view of the cable configuration. The radii r_G and r_R are selected as the uncertain variables.

3.3.5 Effect of the Coating Layers around the Wires

As coating layers are widely used in a cable to insulate wires from each other, understanding how coating layers might affect crosstalk is also of interest. Therefore, in this section, coating layers made of polyvinyl chloride (PVC) are added to the two wires.

The details of the configurations for the uncoated and coated wires are given in Fig. 3-6(b) and Fig. 3-6(c), respectively. As shown in Fig. 3-6(a), the presence of the coating layers mainly increases the crosstalk at the high frequency range, and shifts the resonant frequencies noticeably.

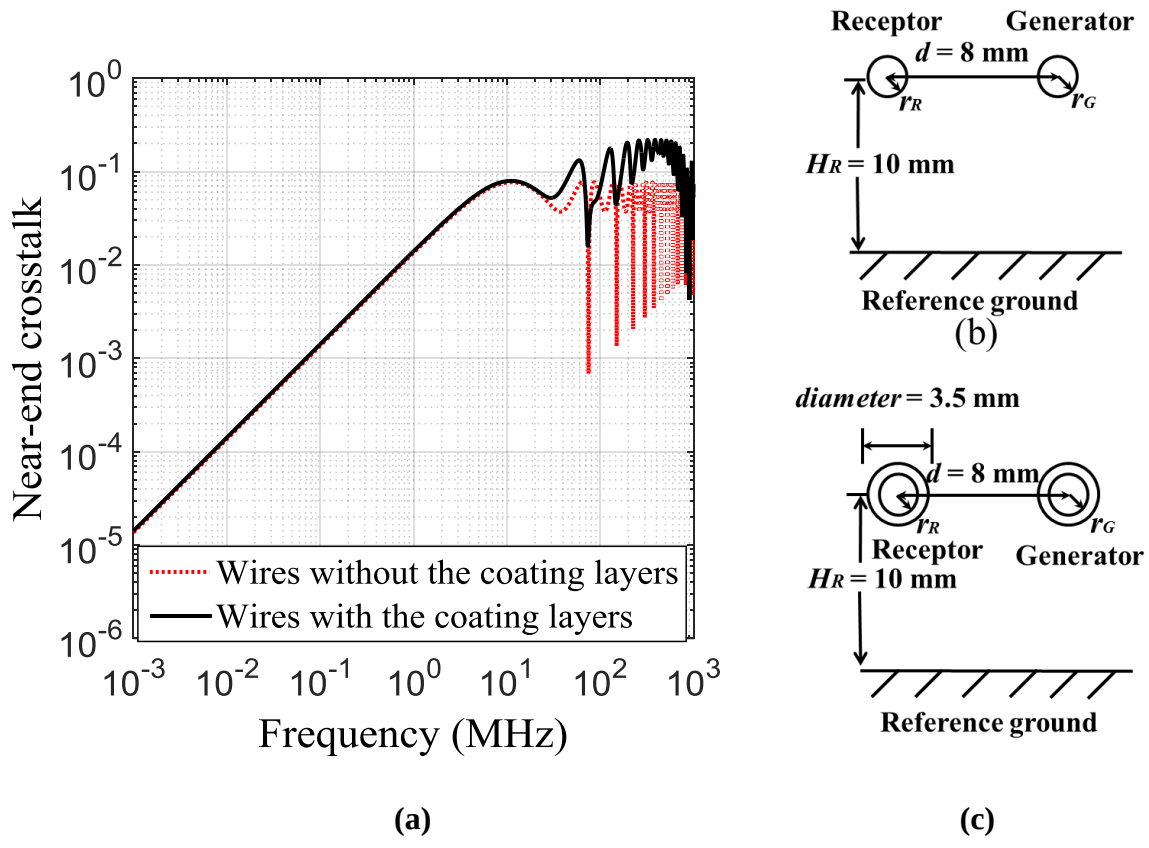

Fig. 3-6. Variation of crosstalk due to the coating layers, for $r_G = r_R = 0.69$ mm, $H_G = H_R = 10$ mm, and $d = 8$ mm. (a) Crosstalk as a function of frequency. (b) Configuration of the uncoated wires. (c) Configuration of the coated wires. The diameter of the coated wires is 3.5 mm.

3.3.6 Effect of the Impedance on Standing Waves

It is widely accepted that the frequency of the maximum crosstalk in the cable is determined by the wire length L shown in Fig. 3-1 [89]. However, looking at the line length to define a resonance is not completely correct as this section shall demonstrate. As shown in Fig. 3-7, the two cases have the same geometric configuration but different termination loads, and the frequencies of the first maximum crosstalk for the two cases are 2 MHz and 10 MHz, respectively. The reason for this difference is that apart from the wire length, the frequency of the maximum crosstalk is also affected by other variables such as the termination impedance. More details of how to estimate the frequency of the maximum crosstalk can be found in [89]. The wire length only uniquely determines the period of crosstalk. Specifically, the period of the crosstalk variation is given as the frequency at which the line length is half the wavelength. Therefore, due to the same wire length L = 2 m in the two cases (i.e., with the

termination loads of 10 Ω and 50 Ω, respectively), the period of the crosstalk is 75 MHz for the both cases as shown in Fig. 3-7.

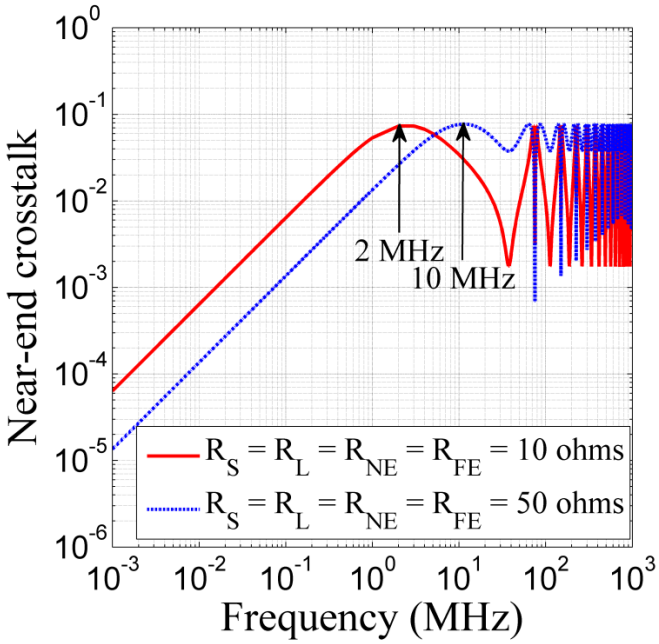

Fig. 3-7. Shift of resonant frequencies due to the variation of termination loads, for L = 2 m, $r_G = r_R$ = 0.69 mm, $H_G = H_R$ = 10 mm, and d = 8 mm. No insulation layers are added to the wires.

3.4 Summary

As uncertainties always exist in cable variables, estimating the crosstalk of cable has become a stochastic process. However, how the variations of cable configurations might affect crosstalk was still missing. Due to this incentive, the contributions of this chapter are threefold.

Firstly, by demonstrating the noticeable influence of the cable configurational variation on the crosstalk in this chapter, the necessity of considering the parametric uncertainty in the prediction of crosstalk has been validated, hatching the plan of the uncertainty quantification of cable crosstalk in Chapter 4.

Secondly, this chapter has presented how different configurational (such as the cross-section, height, conductor radius, insulation layer, and termination load of the cable) variations in the

three-conductor transmission line might affect crosstalk. The result has provided a useful understanding of the causes for excessive crosstalk in applications.

Finally, the result given by the CST simulation has shown that the crosstalk in the three-conductor transmission line has different sensitivities to the variations of different cable variables. Even for the same variable, the sensitivity of crosstalk could be different at various ranges of this variable. Therefore, it has suggested that the sensitivity analysis of cable crosstalk is to be performed as a future work, in order to rank the cable variables based on their isolated effects on the uncertainty degree of crosstalk. The result of the sensitivity analysis can be used to reduce the randomness dimension, thus to simplify the statistical analysis of cable crosstalk. This motivation gives rise to the sensitivity analysis of crosstalk to different cable variables presented in Chapter 5.

Chapter 4 Uncertainty Quantification of Crosstalk Using Stochastic Reduced Order Models

Chapter 3 has given a clear demonstration of the significant impact of the cable configurational variation on the crosstalk. Therefore, the deterministic prediction of crosstalk is not a suitable estimation of the cable EMC performance, as it fails to include the effect of the potential variation of the cable interconnecting system. Ideally, the uncertainty of the cable configuration needs to be taken into account in the prediction of cable crosstalk, and is successfully addressed in this Chapter.

Specifically, this chapter is focused on the prediction of the variability of cable crosstalk subject to a range of parametric uncertainties in the three-conductor transmission line. Unlike the deterministic analysis presented in Chapter 3, the advocated statistical method referred to as the *stochastic reduced order model* (SROM) method is used in this chapter to account for the effect of the cable configurational uncertainty. As introduced in Section 2.3, The SROM method is a new member of the family of stochastic approaches designated to quantify propagated uncertainty in the presence of multiple uncertainty sources. It is non-intrusive, accurate, efficient, and stable, thus could be a promising alternative to some well-established methods such as the polynomial chaos expansion (PCE) and stochastic collocation (SC) methods.

To briefly outline the implementation of the SROM method in this chapter, the statistics of uncertain cable variables are first accurately approximated by the SROM-based input, i.e., pairs of very few samples with known probabilities, such that the uncertain input space is well represented. Then, a deterministic solver is used to produce the samples of cable crosstalk with the corresponding probabilities, and finally the uncertainty propagated to the crosstalk is quantified with good accuracy. As shown in Section 4.3, the statistics of crosstalk obtained by the SROM method converge much faster, by orders of magnitude, compared to

the conventional Monte Carlo (MC) simulation. Also, the computational cost of the SROM method is shown to be small and can be tuned flexibly depending on the accuracy requirement.

To validate the competency of the SROM method as an alternative to the popular efficient statistical approaches, the standard SC method based on the tensor-product sampling strategy introduced in Section 2.2.3 is also implemented for comparison. Herein, the SC method is chosen as its implementation is also on the non-intrusive basis, thus to present a fair comparison with the SROM method. Now let us focus on the detailed application of the SROM method in the uncertainty quantification of cable crosstalk.

4.1 Introduction

It is known from Chapter 1 that the quality of the signal transmitted in a wire is often degraded by the crosstalk from other wires in the cable or nearby cables. The crosstalk is a response to the interaction of electromagnetic fields generated by the currents along the wires or cables. This crosstalk may cause the malfunction of the cable interconnecting system if the crosstalk exceeds the threshold. Therefore, the prediction of crosstalk is an important task to guarantee the cable performance from an early stage.

The theory of the deterministic analysis of crosstalk was systematically addressed in [18], [32], [33], and concisely summarised in Section 2.1. The deterministic analysis is presented in Chapter 3 to investigate the effect of the cable configurational variation on crosstalk. In each deterministic analysis, the cable input variables were assumed to take deterministic values, i.e., these values truly represented input variables, and the deterministic solver is used to obtain the exact crosstalk level. In such a case, the crosstalk level is unique.

However, as pointed out in Section 1.3, the deterministic prediction of crosstalk is not enough, due to the significant effect of the potential parametric variation of the cable interconnecting system demonstrated in Section 3.3. In reality, these potential parametric variations are raised by the uncertainties from many aspects described in Section 1.3, such as cable materials and routing [21], [25]. These uncertainties cause input variables to deviate from the nominal value. Therefore, the deterministic result obtained using the nominal input values may be unconvincing. As a result, rather than having a specific crosstalk level, the

output becomes a variation range consisting of all the possible crosstalk values caused by the uncertainties of input variables.

Due to the input uncertainties, statistical analyses need to be performed to predict the variation range and probability distribution of crosstalk [25], [37], [48], [87]. A comprehensive overview of the traditional and state-of-the-art statistical approaches is presented in Chapter 2. Based on Chapter 2, the traditional Monte-Carlo (MC) method [28] requires a large number of simulations to obtain the converged result, and therefore is time-consuming. However, the MC method is non-intrusive as the existing deterministic solver is used without modifications. It is also general to all the uncertainty-embedded problems.

Thanks to the breakthrough in the efficiency of uncertainty quantification methods, the polynomial chaos expansion (PCE) [29] and stochastic collocation (SC) methods [30] have been intensively applied to obtain the statistics of crosstalk in the presence of input variability. In the implementation of the PCE method, the crosstalk can be described using an analytic formula with respect to uncertain input variables [67], [68], [69]. If the probability distributions of each uncertain variable were known, the statistics of crosstalk could be obtained by propagating input uncertainties to crosstalk using the probability theory in [26]. However, it is worth noting that in [67], [68], and [69], the PCE method was intrusive as modifications to the existing deterministic solver were needed, making the implementation very complex in terms of the involved algebraic calculation and customised software coding.

On the other hand, the SC method was non-intrusive and only required a selection of collocation points for each uncertain variable [79]. At collocation points, samples of crosstalk were obtained deterministically, and then interpolating functions were used to construct an analytical approximation of crosstalk, thus to recover statistics. However, the result of the SC method is sensitive to the choice of interpolating functions, as different interpolating functions produce slightly different output samples at the interpolated points adjacent to collocation points. As introduced in Chapter 2, the SC method can be performed with the tensor-product or sparse-grid sampling technique.

The *stochastic reduced order model* (SROM) method recently proposed in [27] is a potential alternative to the PCE and SC methods to quantify propagated uncertainties in stochastic systems. Chapter 2 describes the merits of the SROM method as conceptually simple, non-intrusive and efficient, compared with the traditional MC method. The SROM method can be regarded as a small but smart version of the MC method, and therefore can be a general

approach. It can be applied to uncertain variables with any types of distributions, and select input samples with regard to input distributions. An in-depth comparison between the PCE, SC, and SROM methods was given in [79].

A SROM is an approximation of a random variable in the statistical sense, and has a small number of samples. Each sample is given a certain probability, such that the SROM and the random variable have similar statistics. To guarantee the performance, an objective function measuring the discrepancy between the statistics of the SROM and the random variable can be used. Once the SROM of uncertain input variables is constructed, the deterministic solver is used to obtain the SROM-based output response. Then, the statistics of the SROM-based output can be obtained with elementary calculations, and are used to approximate the statistics of the actual output.

The aim of this chapter is to present the first application of the SROM method to uncertainty-embedded EMC problems, in particular the uncertainty quantification of cable crosstalk. Given uncertain geometric variables of a cable, the statistics of crosstalk are obtained using the SROM method with a small computational cost, and the variation range is successfully bounded. The SC method implemented via tensor-product sampling strategy is used as a reference to evaluate the performance of the SROM method. However, it is worth noting that more efficient SC implementations based on sparse-grid sampling computed via the Smolyak algorithm are possible [74], and used to evaluate the SROM performance in Chapter 6. The remainder of this chapter is organised as follows: Section 4.2 describes the three-conductor transmission line as the cable model, and defines uncertain cable variables and crosstalk. Section 4.3 presents the implementation of the SROM method to predict the statistics of crosstalk, and the result is compared to those of the SC and MC methods. Finally, the summary of this chapter is given in Section 4.4. Please note that due to the detailed description of the SROM method in Chapter 2, the introduction of the SROM method is not repeated in this chapter for brevity.

4.2 Cable Model

In this study, the cable bundle is modelled as a three-conductor transmission line. Due to the well-established deterministic solver of this model, it has been used to validate the efficacy of the PCE and SC methods for predicting the statistics of crosstalk in [67], [90]. Therefore, the

three-conductor transmission line is also chosen to verify the efficacy of the SROM method for quantifying the uncertainty propagated from input variables to crosstalk.

Although the cable modelled using the three-conductor transmission line is described in Section 3.2, the introduction of the three-conductor transmission line model in this chapter is rearranged into three aspects: the input variables, output responses, and deterministic solver, as these three aspects need to be defined in the implementation of the SROM method.

4.2.1 Input Variables

Fig. 4-1 shows the schematic of a three-conductor transmission line. The two parallel generator and receptor wires are placed above the ground plane to which voltages and the heights of wires are referenced. The three-conductor transmission line is characterised by the following electrical variables: the voltage source V_S with the source impedance R_S and the load impedance R_L in the generator circuit, as well as the termination loads R_{NE} and R_{FE} at two ends of the receptor wire.

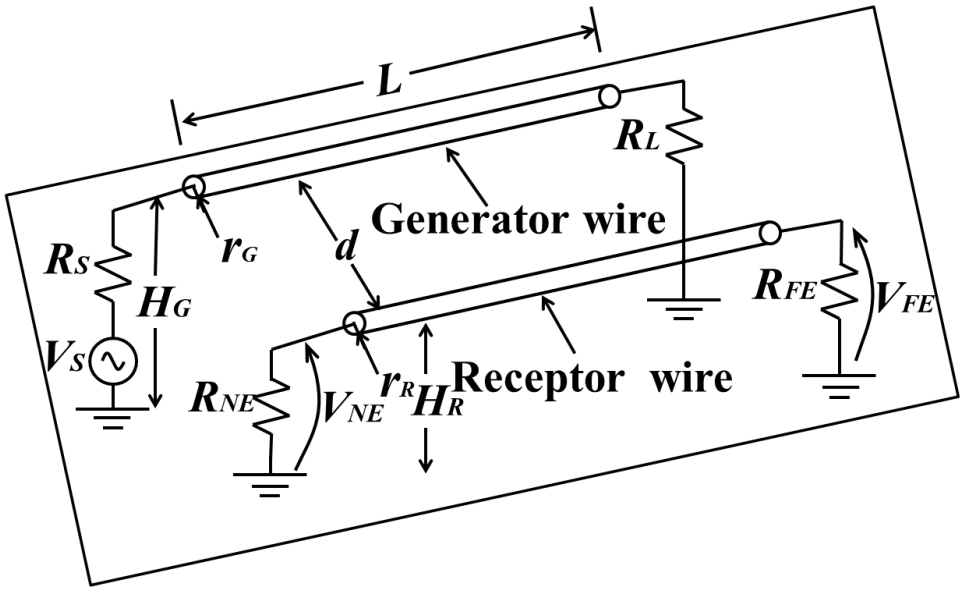

Fig. 4-1. The model of a three-conductor transmission line.

Apart from the electrical variables mentioned above, the crosstalk is also determined by the following geometric variables: the wire length L, the radius r_G and height H_G of the generator wire, the radius r_R and height H_R of the receptor wire, and the distance d between the generator and receptor wires. The following assumptions are used: $r_G = r_R = r$, $H_G = H_R = H$, and $R_S = R_L = R_{NE} = R_{FE} = T$.

4.2.2 Output Responses

The *near-end* crosstalk (*NEXT*) and *far-end* crosstalk (*FEXT*) are selected as the output responses of the cable model, and are defined as the ratio of the induced voltage to the source voltage in the following form:

$$NEXT = \frac{V_{NE}}{V_S}\ , FEXT = \frac{V_{FE}}{V_S} \tag{4.1}$$

4.2.3 Deterministic Solver

The traditional deterministic calculation of crosstalk is to solve the MTL equations described in Section 2.1. However, an analytical solution of crosstalk in the three-conductor transmission line was derived to directly calculate crosstalk based on the values of input variables [89], thus to bypass solving the MTL equations. Therefore, this analytical solution is used as the deterministic solver with the following assumptions: 1) the two wires and ground are made of perfect electric conductors; 2) the cross-sections of two wires are invariant along the cable length; and 3) the medium around wires is lossless and homogeneous.

4.3 Applications of SROMs

In this section, the SROM method is applied to obtain the statistics of crosstalk in the presence of single or multiple uncertain variables. To propagate uncertainty with the SROM method, the first step is to construct a SROM for uncertain cable variables. Then, the SROM-based output $\widetilde{NEXT}$ and $\widetilde{FEXT}$ for the actual output *NEXT* and *FEXT* can be constructed with the deterministic solver. Finally, the statistics of *NEXT* and *FEXT* are approximated by those of $\widetilde{NEXT}$ and $\widetilde{FEXT}$ using (2.56)-(2.58) in Section 2.3. In subsequent sections, the *NEXT* is considered as the output in one example, and then the *FEXT* is used in the other example. For the demonstration purpose, uncertain cable variables are assumed to have Gaussian distributions. However, it is worth noting that the SROM method is applicable for any types of probability distributions, and switching from one type of probability distributions to another is straightforward. The SROM method is demonstrated with four examples where the number of random variables gradually increases. The frequency at which the simulation was run is set to 400 MHz. To validate the SROM method, the SROM-based result is compared to

those of the MC method and the SC implementation based on tensor-product sampling strategy. The statistics from 1,000,000 MC simulations are used as reference results to set benchmarks.

4.3.1 Single Uncertainty Source: Height *H*

The aim of this section is to demonstrate the implementation of the SROM method for a single uncertainty variable: the wire height H with a Gaussian distribution of mean $E(H) = 10$ mm and standard deviation $\sigma(H) = 1$ mm. Other variables are regarded to take the deterministic values shown in Table 4-1.

The listed values in Table 4-1 are chosen for the following reasons: 1) the wire length $L = 7$ m is used as a typical length of the cable in large platforms such as vehicles and airplanes; 2) the conductor radius $r = 1.024$ mm is for the single-core conductor of the 12 gauge typically used to transmit signals in aerial systems; 3) the terminating resistance $T = 50\ \Omega$ is one of the common choices to terminate cables in industry; 4) the frequency $f = 400$ MHz is the maximum frequency of interest to aerial EMC engineers; and 5) the inter-wire distance $d = 6$ mm and the cable height $H = 10$ mm above the ground plane are commonly seen in practical scenarios.

Table 4-1. Deterministic Values of Input Variables

Input variable	Deterministic value
L (m)	7
r (mm)	1.024
d (mm)	6
T (Ω)	50
f (MHz)	400
H (mm)	10

The construction of the optimal $\widetilde{H}$ for H follows the guideline described in Section 2.3. As H is a 1-dimensional random variable, there is no need to consider the discrepancy in correlation matrices in (2.53) when constructing $\widetilde{H}$. Three optimal SROMs $\widetilde{H}$ are constructed

with 5, 10, and 20 samples, respectively, and are used to approximate the cumulative distribution function (CDF) of H denoted by F(H) in Fig. 4-2(a). It is clear that as the sample size of $\widetilde{H}$ increases, the approximated probability distribution of H becomes closer to the reference distribution. When the sample size is 20, the difference between the reference and SROM-based distributions is very small.

Fig. 4-2(b) shows the absolute error of moments up to the order of 4 for $\widetilde{H}$ constructed with 5, 10, and 20 samples. Generally speaking, the error at each moment order is reduced by increasing the sample size of $\widetilde{H}$. It is seen that the model size of 10 can provide an accurate approximation for each moment order, and increasing the size from 10 to 20 does not further reduce the error significantly. This nice feature means that the SROM method does not need a very large sample size to achieve good accuracy. In the case of uncertain H, a sample size of 10 is reasonable as the approximated CDF and moment orders match the reference counterparts in good agreement, and the computational cost is kept low.

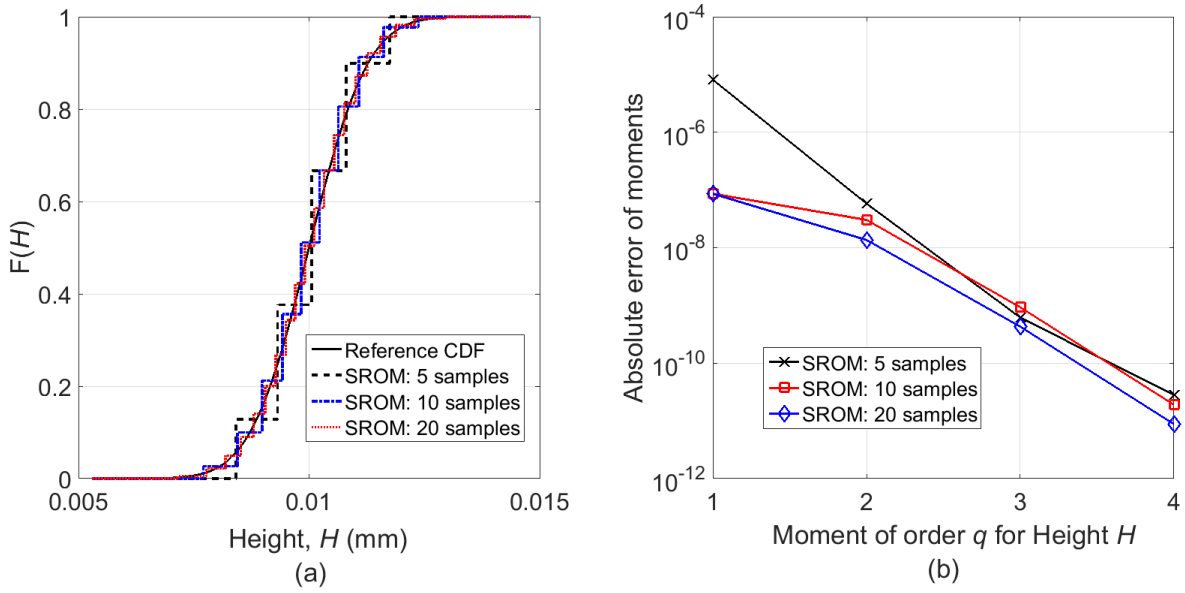

Fig. 4-2. (a) The reference CDF of the uncertain variable H and the CDFs approximated by the SROMs $\widetilde{H}$ formed with 5, 10, and 20 samples. (b) Absolute errors of moments approximated by SROMs $\widetilde{H}$ with sizes of 5, 10, and 20.

After the SROMs $\widetilde{H}$ with sizes of 5, 10, and 20 samples are constructed, the deterministic solver is used to produce the samples of the SROM-based output $\widetilde{NEXT}$. Due to the one-to-one relationship between the input and output samples, the sample sizes of the three corresponding $\widetilde{NEXT}$ are also 5, 10, and 20, respectively. The probabilities of the samples in

$\widetilde{NEXT}$ are the same as those in $\widetilde{H}$. With the samples and probabilities obtained, the SROM-based solution $\widetilde{NEXT}$ can be constructed.

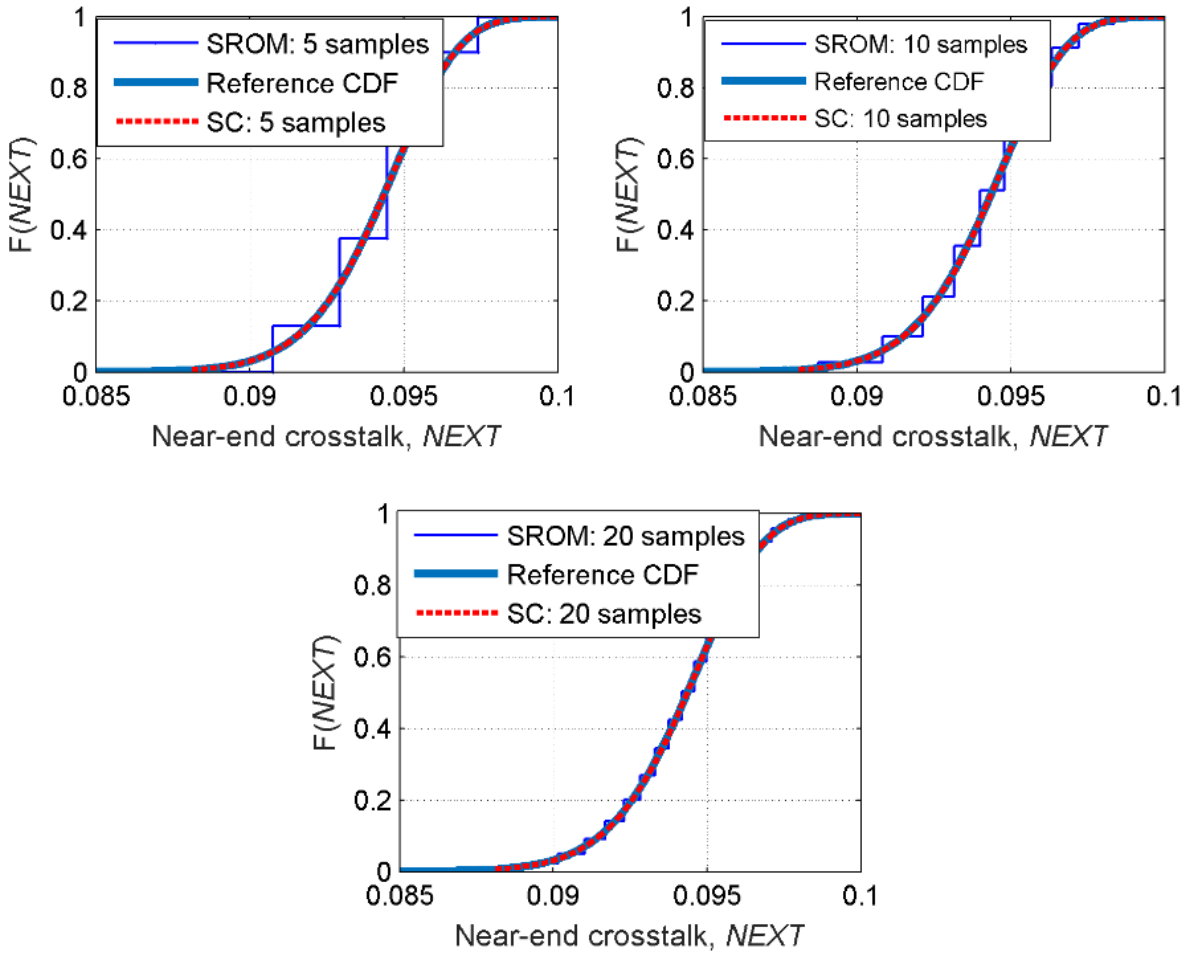

Fig. 4-3. The reference CDF of *NEXT*, the CDFs approximated by the SC method with 5, 10, and 20 collocation points, and the CDFs approximated by the SROMs $\widetilde{NEXT}$ with sample sizes of 5, 10, and 20.

In Fig. 4-3, the CDFs of $\widetilde{NEXT}$ are plotted to approximate the reference CDF of the actual *NEXT*. It is seen that all three $\widetilde{NEXT}$ are able to recover the general shape of the reference distribution, and the $\widetilde{NEXT}$ with 20 samples gives the closest distribution for *NEXT*. This is because the corresponding input $\widetilde{H}$ with size of 20 provides the most accurate statistics for *H*. Therefore, the performance of the SROM method is highly dependent on the quality of the input SROM. On the other hand, the SC method using Lagrange polynomials as the interpolating function is also implemented to compare with the SROM method. For the SC method of this study, the number of collocation points is chosen the same as the sample size of the SROM method, such that the deterministic solver is run for the same number of times

by the two methods. As can be seen in Fig. 4-3, unlike the step-shaped CDFs given by the SROM method, the SC method can produce faultless and continuous CDFs for *NEXT* using 5, 10, and 20 collocation points.

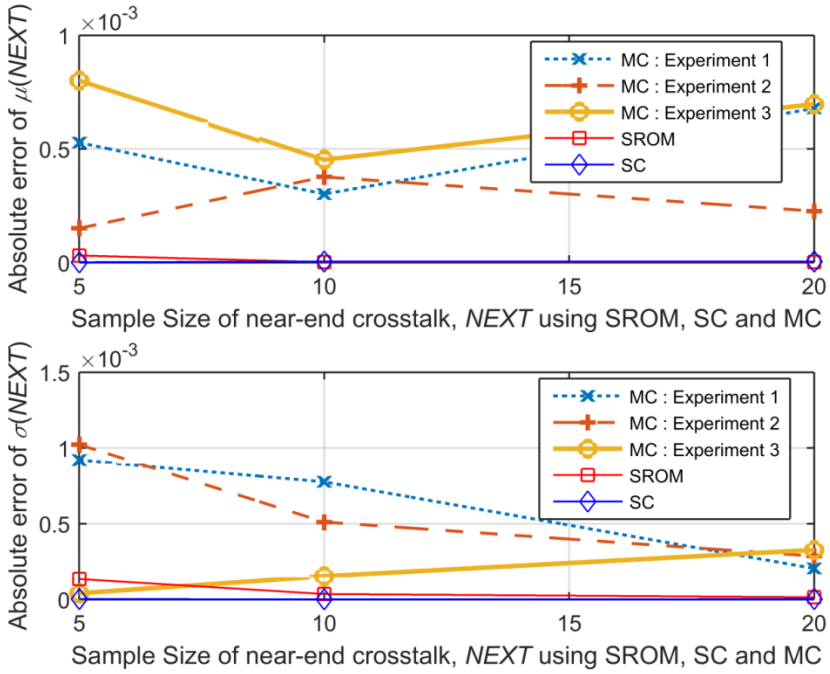

Fig. 4-4. Absolute errors of the statistics of *NEXT* obtained by the SROM, SC, and MC methods using small sample sizes.

In addition to providing the distribution information, the SROM method is also able to predict the mean and standard deviation of *NEXT* with great accuracy. As Fig. 4-4 shows, the mean value μ (*NEXT*) and standard deviation σ (*NEXT*) given by $\widetilde{NEXT}$ with different sizes are very accurate, and the accuracy is improved by increasing the sample size of $\widetilde{NEXT}$, but not dramatically. This is because in this case the approximated statistics by the SROM method converge to the reference values very fast. At the sample size of 10, the mean value and standard deviation given by the SROM method are almost identical to the reference counterparts. In contrast to the SROM method, three MC experiments are performed, and each MC experiment is performed with 5, 10, and 20 samples. As shown in Fig. 4-4, from size of 5 to 20, the variation of the statistics given by the MC method is different from one experiment to another. At the size of 20, the mean and standard deviation by the MC method fail to converge to the reference results as close as the SROM method. We note that in the MC experiment 3 with the size of 5, an accurate standard deviation could be produced because of the stochastic nature of the process, but the accuracy is unrepeatable. Therefore, at

small sample sizes, the MC method is inaccurate and gives different results when repeating numerical experiments. It is worth noting that the corresponding confidence interval for each moment can be estimated based on the sample size of the MC simulation. Also, the MC performance can be evaluated using error-bar. These aspects are beyond the scope of this study. By contrast, the SROM method is stable as long as the uncertain input space is well approximated by SROMs, and is able to provide a very accurate mean using small sample sizes. On the other hand, the SC method can produce almost error-free statistics using only 5 collocation points, but the difference between the accuracies of the SROM and SC methods is very small in this example.

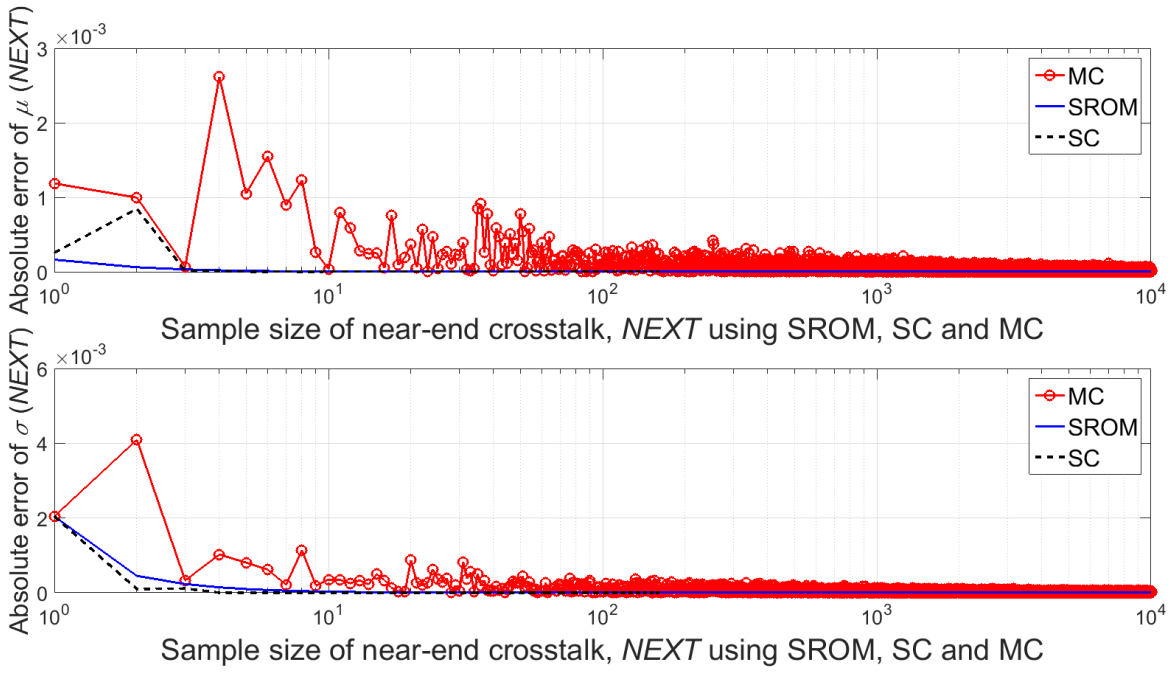

Fig. 4-5. Convergence rates of the SROM, SC and MC methods to the reference statistics of *NEXT*.

Fig. 4-5 demonstrates the convergence rates of the SROM, SC and MC methods to produce accurate statistics of *NEXT*. As can be seen, both the SROM and SC methods converge to the reference result faster than the MC method. Specifically, the MC method needs at least 10^4 samples to converge to the accuracy of the SROM method at sample size of 10. Therefore, comparing with MC, the SROM method reduces the computational cost by a factor of $10^4/10 = 10^3$ in this case, which is a sizable acceleration for stochastic analysis. On the other hand, only 4 collocation points are needed by the SC method to give the same performance of the SROM method with size of 10. However, the performances of the SC and SROM methods cannot be purely evaluated using the sample size needed for certain accuracy. This is because

for the SC method, after obtaining the output samples at collocation points, the overhead is to derive the analytical approximation of the output response using the interpolating function, and then the statistics of the output can be recovered. By contrast, for the SROM method, after the SROM-based output is obtained, only the elementary calculation given by equations (2.56) – (2.58) in Chapter 2 is needed to recover the statistics of the output. It is clear that in the presence of a single uncertain source, both the SROM and SC methods are efficient to produce the accurate statistics of crosstalk, as only a small fraction of the computational cost of the MC method is required.

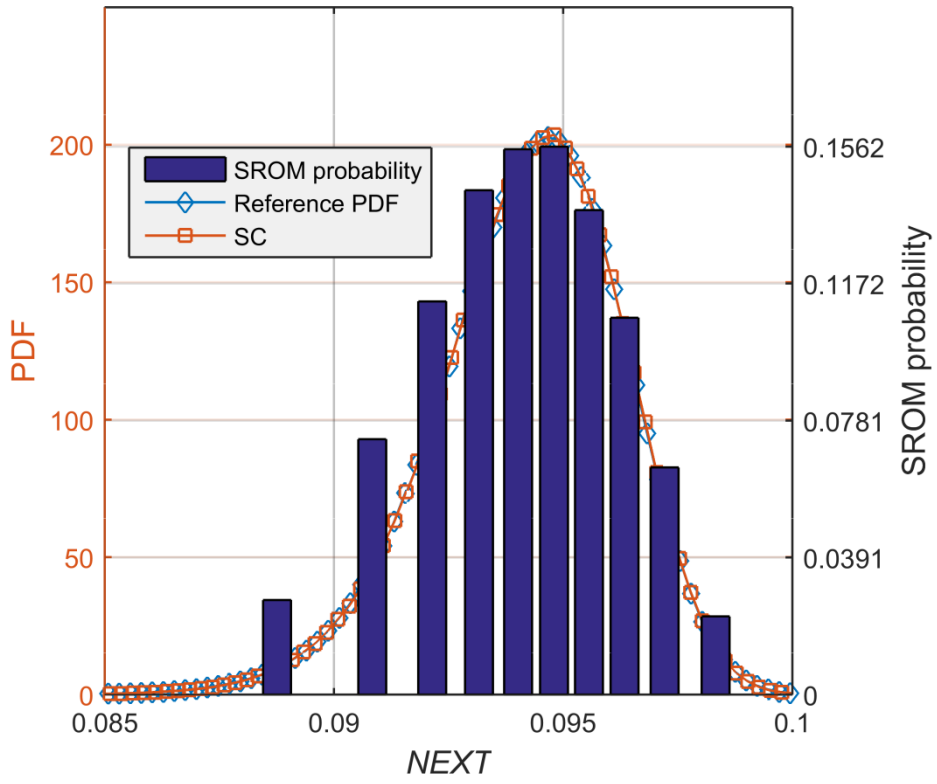

Fig. 4-6. The reference PDF of the output *NEXT*, the PDF obtained by the SC method with 10 collocation points, and the probabilities of the samples in the SROM-based $\widetilde{NEXT}$ with sample size of 10.

In Fig. 4-6, the reference probability distribution function (PDF) of *NEXT* is plotted as the blue diamond-shaped curve to compare with the probabilities of the samples in $\widetilde{NEXT}$ with sample size of 10 (plotted as the blue histogram). It is clear that the discrete probabilities of $\widetilde{NEXT}$ are in good agreement with the shape of the reference PDF. Therefore, the probability of each sample in $\widetilde{NEXT}$ can reflect the possibility of the actual *NEXT* taking values in the

vicinity of this sample. On the other hand, the PDF approximated by the SC method with 10 collocation points (plotted as the orange squared-shaped curve) is exactly the same as the reference PDF. Therefore, the SC method may be a better approach if the aim is to recover the output PDF in detail.

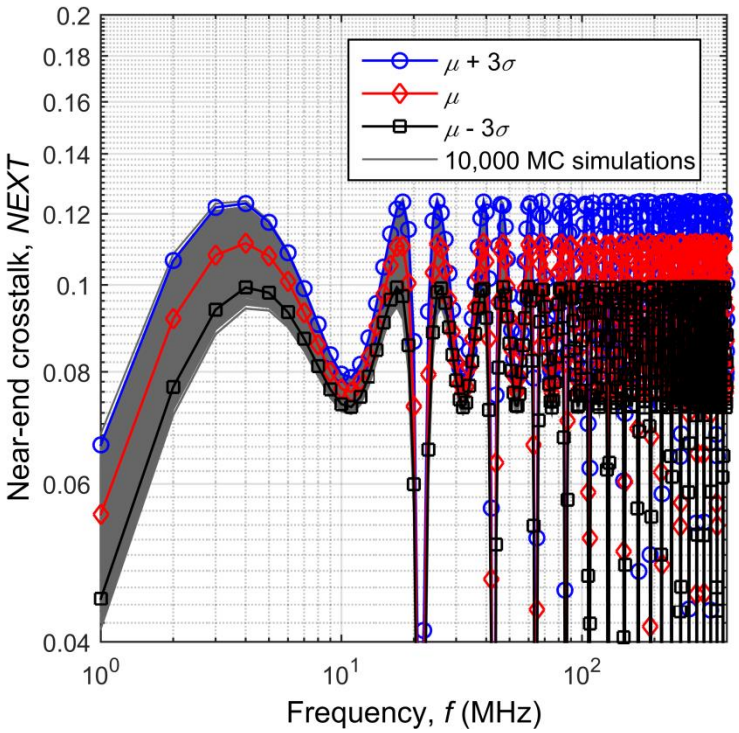

Fig. 4-7. Upper and lower boundaries obtained using the SROM method to bound the variation of *NEXT*. At each frequency, only 10 samples of the SROM-based $\widetilde{NEXT}$ are used. The uncertain variable is *H*.

As the SROM method can predict the accurate mean μ and standard deviation σ of *NEXT*, the variation range of *NEXT* can be bounded using the interval: $[\mu - 3\sigma, \mu + 3\sigma]$ as a mere heuristic choice to define approximate upper and lower bounds for practical purposes [67]. The boundaries of the *NEXT* variations are obtained by the SROM method and plotted from 1 MHz to 400 MHz in Fig. 4-7. It can be seen that only a small number of extreme cases are outside the variation range. It is worth noting that only 10 samples of $\widetilde{NEXT}$ are required at each frequency to obtain the variation range. Therefore, the SROM method is able to predict the accurate variation range of crosstalk with small computational cost. The frequencies for the peaks and troughs of the coupling level can be explained using the theory of predicting the frequency of the maximum coupling level and the period of the coupling variation.

4.3.2 Uncertain Frequency *f*

The effect of the uncertain frequency *f* is considered in this section to test the robustness of the SROM method, since the variation of *f* can have significant influence on the distribution of crosstalk, especially when the peaks and troughs of crosstalk occur within the uncertain range of *f*. The uncertain variable *f* is modelled using a Gaussian distribution with mean $E(f)$ = 400 MHz and standard deviation $\sigma(f)$ = 5 MHz. The variables *L*, *r*, *d*, *T* and *H* are assumed to take the deterministic values presented in Table 4-1.

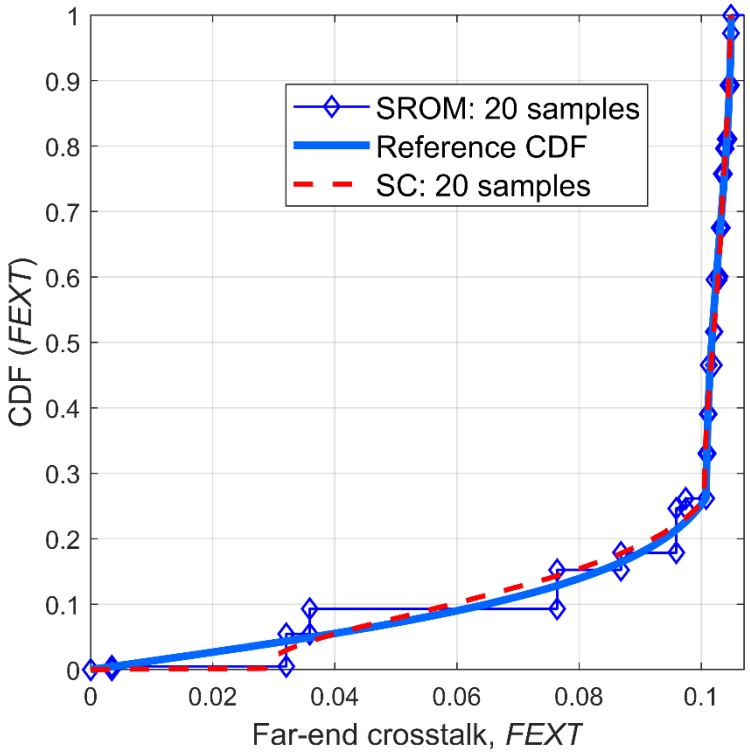

Fig. 4-8. The reference CDF of *FEXT*, the CDF approximated by the SROM-based $\widehat{FEXT}$ with a sample size of 20, and the CDF approximated by the SC method with 20 collocation points.

As the uncertain variable *f* has sizable effect on crosstalk variation, 20 samples are used to construct the SROM $\tilde{f}$ and propagate the uncertainty to *FEXT*. As shown in Fig. 4-8, the distribution of *FEXT* is highly concentrated in the range of *FEXT* being larger than 0.1, and is well approximated by the CDF of the SROM-based $\widehat{FEXT}$. It is worth noting that the stepped shape of the SROM-based CDF is due to the inherent nature of the SROM implementation (discrete sample probability). When implementing the SC method with the Lagrange

interpolating function for this example, it is found that the proposed SC method may generate non-physical output samples, i.e., samples taking values outside the reasonable range. This may contaminate the output statistics, such as the mean value and standard deviation. For this reason, the presented result of the proposed SC method in this study is obtained after data refinement, i.e., discarding non-physical samples of crosstalk. By contrast, the SROM method only produces output samples in the physical range. As shown in Fig. 4-8, the approximated CDF by the SC method with 20 collocation points is also in good agreement with the reference CDF.

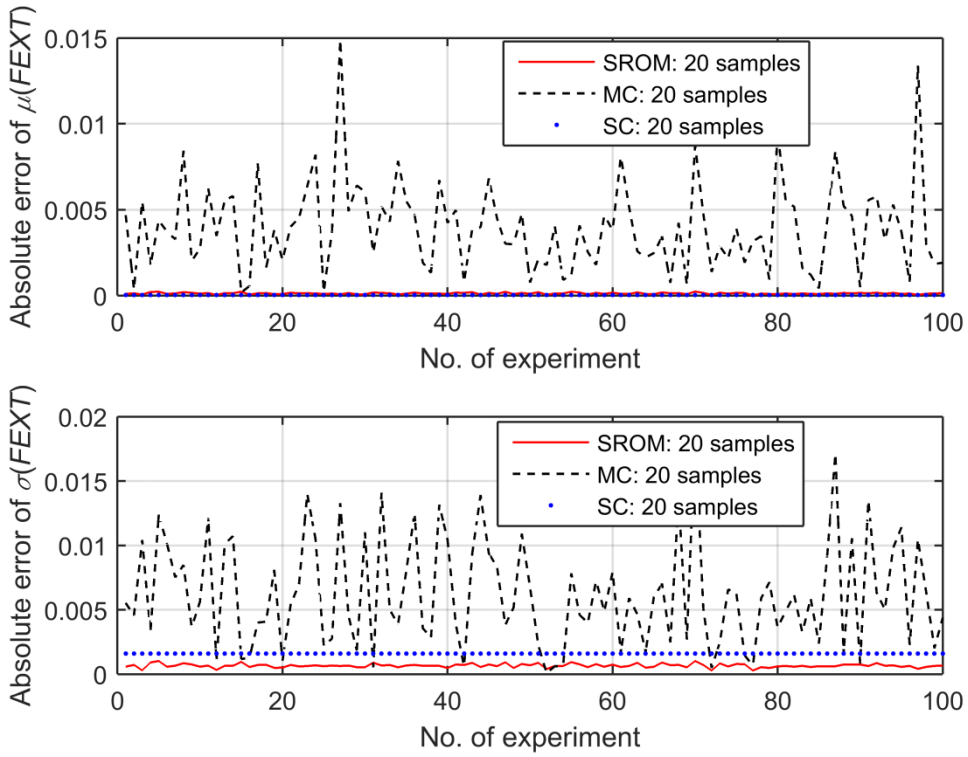

Fig. 4-9. Absolute errors of the mean value and standard deviation of *FEXT* obtained by performing the SROM, MC and SC methods with 20 samples for 100 times.

Then, the experiments of using 20 samples (or known as collocation points for SC) for the SROM, MC, and SC methods are repeatedly performed for 100 times. The absolute errors of the mean value and standard deviation are plotted against the *No. of experiment* in Fig. 4-9. For example, the result at the *No. of experiment* of 40 denotes the absolute error of the 40th (SROM, SC, or MC) stochastic analysis of using 20 samples. As shown in Fig. 4-9, it is clear that when repeating the stochastic analysis, both the SC and SROM methods constantly produce very accurate mean values, but the standard deviation of the SROM method is more

accurate than that of the SC method. On the other hand, the results given by the MC method vary significantly, and mostly are inaccurate.

4.3.3 Two Uncertainty Sources

In this section, the SROM method is applied in the presence of two random variables: the wire height H and distance d between two wires. To tackle multiple uncertainty sources with the SROM method, the idea is to regard each uncertainty source as a 1-dimensional variable, and integrate these uncertainty sources into a multidimensional variable. Then, a SROM can be constructed for this multidimensional variable to globally approximate the overall uncertain input space. For example, we can use the N-dimensional random variable $\boldsymbol{X}$ described in Section 2.3 to contain two 1-dimensional variables H and d, i.e., $\boldsymbol{X} = [H, d]$. In this case, $\boldsymbol{X}$ is a bivariate variable and $N = 2$. Each sample of $\boldsymbol{X}$ represents a point in a plane formed with H as the *x-axis* and d as the *y-axis*. The coordinates of the point contain a set of possible values of H and d to run the deterministic solver once. As a result, the uncertainties of H and d can be jointly approximated by building a SROM for $\boldsymbol{X} = [H, d]$.

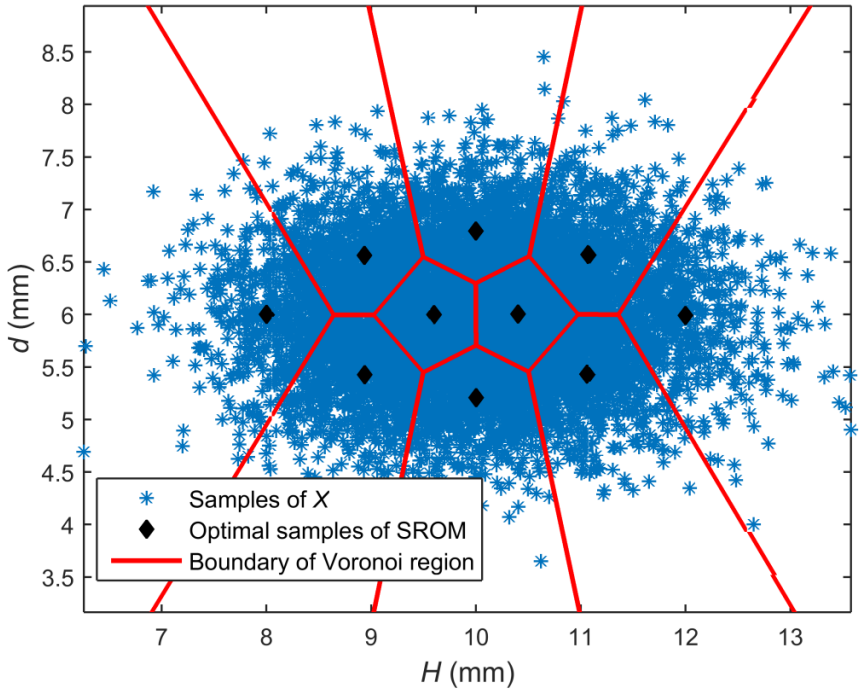

Fig. 4-10. The distribution of 10,000 samples of X, and 10 optimal samples of $\widetilde{X}$ in corresponding Voronoi regions.

The height H and distance d are assumed to follow the Gaussian distribution with the mean values $E(H)$ = 10 mm and $E(d)$ = 6 mm, and the standard deviations $\sigma(H)$ = 1 mm and $\sigma(d)$ = 0.6 mm. Other variables are considered as deterministic values in Table 4-1. A SROM $\widetilde{\boldsymbol{X}}$ with a sample size of 10 is used to visualise the concept of the SROM of the 2-dimensional variable $\boldsymbol{X}$= [H, d]. Fig. 4-10 shows the distribution of 10,000 samples of $\boldsymbol{X}$. In addition, 10 optimal samples of $\widetilde{\boldsymbol{X}}$ are selected from the 10,000 samples of $\boldsymbol{X}$ using the algorithm introduced in Section 2.3.2, and are plotted in the Voronoi tessellation in Fig. 4-10. As these 10 samples of $\widetilde{\boldsymbol{X}}$ are widely separated from each other, the entire uncertain region of $\boldsymbol{X}$ is explored, rather than only focusing on highly likely or marginal regions.

The probability of each optimal sample in $\widetilde{\boldsymbol{X}}$ can be calculated using the number of samples in the corresponding Voronoi region. Having obtained the sample and probability sets, the optimal SROM $\widetilde{\boldsymbol{X}}$ is constructed and visualised versus the PDF of $\boldsymbol{X}$ in Fig. 4-11. As shown in Fig. 4-11, the coordinates of a red dot on the H-d plane indicate the values of H and d contained in this optimal sample, and the height of the red dot represents the corresponding probability.

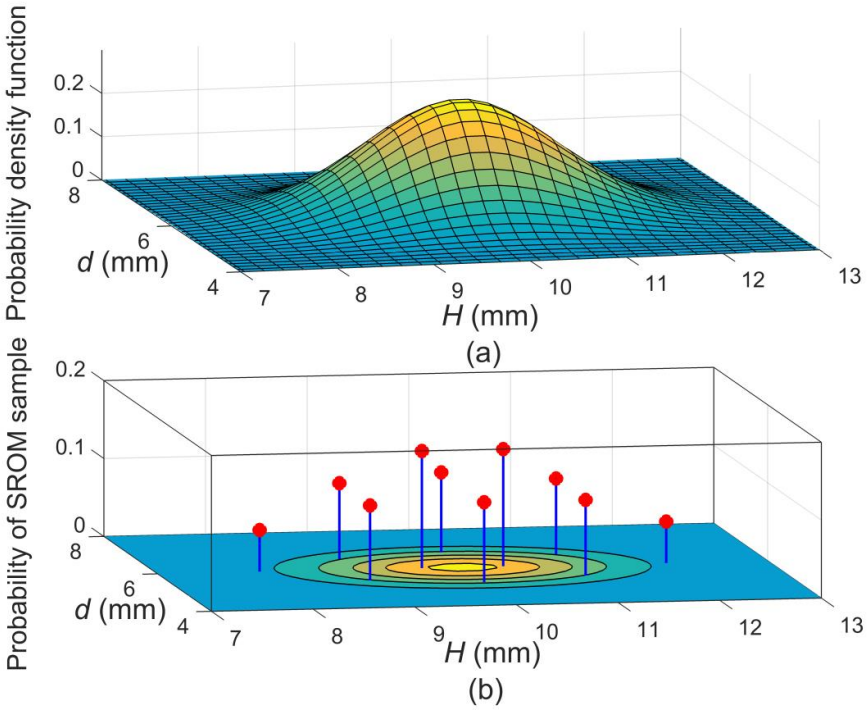

Fig. 4-11. (a) The PDF of a bivariate variable X = [H, d]. (b) The visualisation of an optimal SROM $\widetilde{X}$ with sample size of 10.

Both the SROM and SC methods are used to propagate the uncertainty from $\boldsymbol{X}$ = [H, d] to

NEXT. In this example, the SC method based on tensor-product sampling is implemented using the cubic Hermite interpolating function [91]. The number of collocation points on the *H-d* plane is set to 3 × 3, 4 × 4 and 5 × 5, respectively. Here, 3 × 3 means there are 3 collocation points in the uncertain ranges of H and d, respectively. To ensure the deterministic solver is evaluated by the SROM method with the same number of times, the sample size of the SROM $\widetilde{\boldsymbol{X}}$ is set to 9, 16 and 25 accordingly.

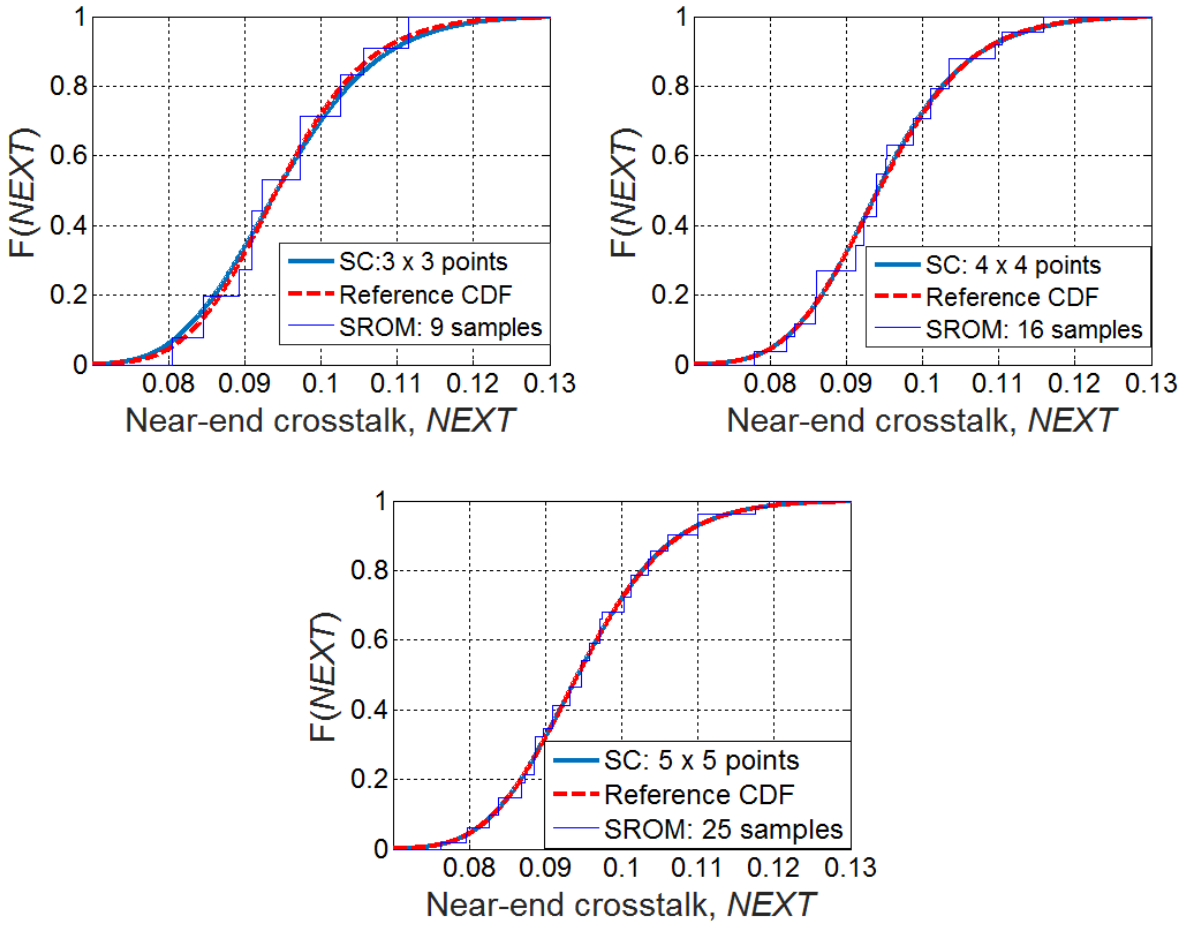

Fig. 4-12. The reference CDF of *NEXT*, the CDF approximated by the SC method (using Cubic Hermite interpolating function) with 9, 16 and 25 collocation points, and the CDF approximated by the SROMs $\widetilde{NEXT}$ with sizes of 9, 16 and 25.

At each sample size, the predicted CDFs of *NEXT* using the SROM and SC methods are plotted in Fig. 4-12. It is seen that the CDF obtained by the SROM method with size of 9 can recover the general shape of the reference CDF. At the size of 25, the difference between the SROM-based and reference CDFs becomes very small. On the other hand, the CDF approximated by the SC method is very close to the reference CDF by using 9 collocation points. When increasing the number of collocation points to 16, the difference between the

SC-based and reference CDFs becomes indistinguishable.

In Fig. 4-13, the convergence rates of the SROM, SC and MC methods are compared at the sample sizes (i.e., the number of collocation points for the SC method) of 9 (3 × 3 for SC), 16 (4 × 4), 25 (5 × 5), 36 (6 × 6), 49 (7 × 7), 64 (8 × 8), 81 (9 × 9) and 100 (10 × 10). It is clear that both the SROM and SC methods steadily converge to the reference result when increasing the sample size, but the convergence rates are different. Specifically, the SROM and SC methods have almost the same performance to predict accurate mean value using small sample sizes, but the convergence rate to the reference standard deviation by the SC method is faster than that by the SROM method. Despite this, the standard deviation evaluated by the SROM method is still accurate to a certain extent. For example, at the sample size of 16, the SROM-based standard deviation is within the error of 7%. Here, the SROM error of 7% is the ratio of the absolute error of $\sigma(NEXT)$ given by SROM to the theoretical value of $\sigma(NEXT)$, which is 0.0007 / 0.0098 × 100% = 7%.

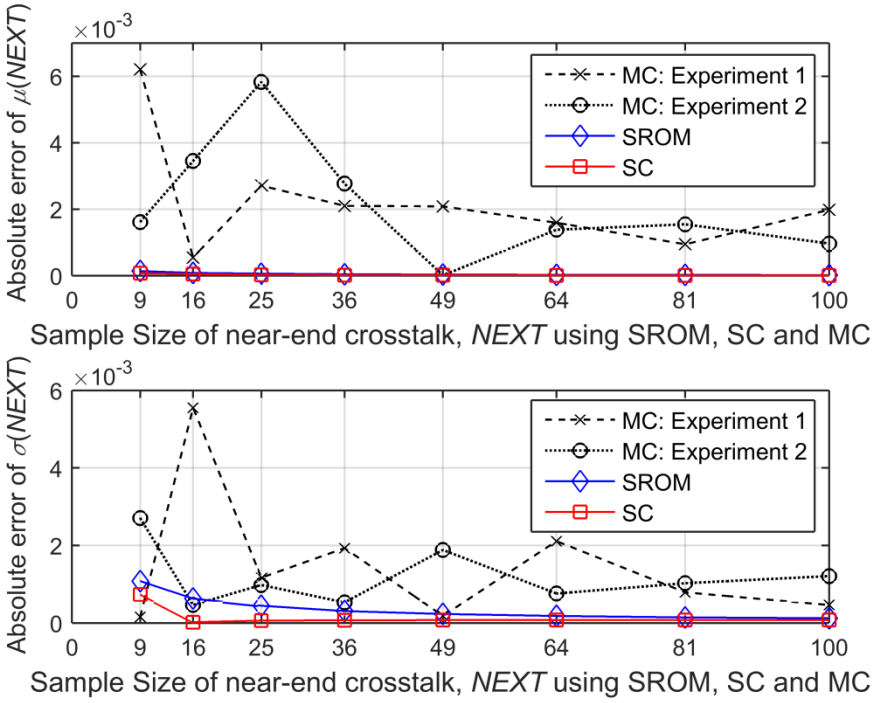

Fig. 4-13. Convergence rates of the SROM, SC and MC methods under 100 samples, when the random variables are *H* and *d*.

Unlike the SC and SROM methods, increasing the sample size for the MC method may not guarantee an increase in the accuracy of the result. As seen in Fig. 4-13, the MC method only produces accurate results because of the stochastic nature of the process using small sample

sizes, as the approximated statistical results in two MC experiments experience random variations and fail to converge under the sample size of 100. Therefore, it is clear that for small sample sizes, the MC method only produces different and inaccurate results, whereas the SC and SROM methods are accurate, stable and fast converging.

Fig. 4-14 shows the variation range of *NEXT* obtained using the SROM method with a sample size of 25. It can be seen that nearly all the 10,000 MC simulations, except for a small number of extreme cases, are well enclosed by the upper and lower boundaries.

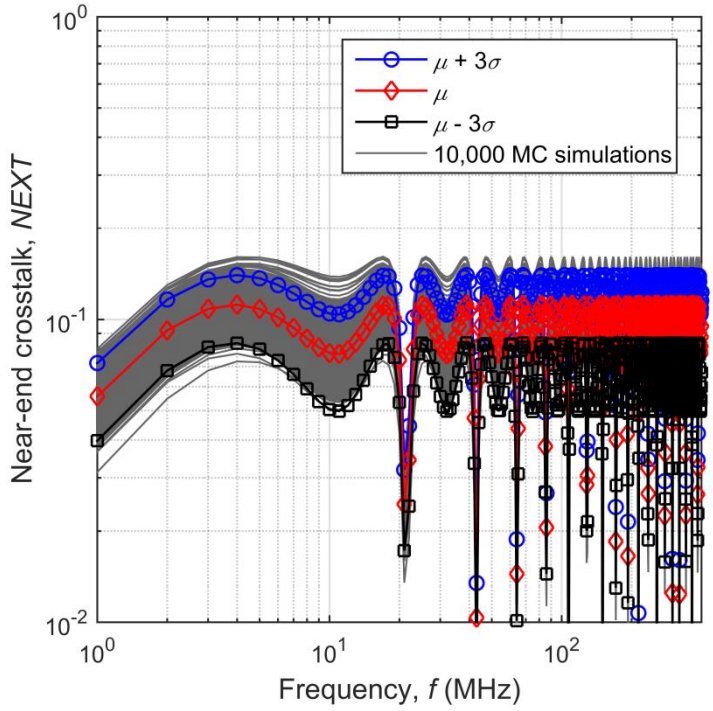

Fig. 4-14. Upper and lower boundaries obtained using the SROM method to bound the variation of *NEXT*. At each frequency, only 25 samples of the SROM-based $\widetilde{NEXT}$ are needed. The uncertain variables are *H* and *d*.

4.3.4 Four Uncertainty Sources

In this example, the efficacy of the SROM method to recover the statistics of *FEXT* in the presence of four random variables is demonstrated and compared with that of the SC method based on tensor-product sampling. The four uncertain variables are selected as the wire height H, distance d, termination load T and wire radius r, following the Gaussian distribution with mean values $E(H)$ = 10 mm, $E(d)$ = 6 mm, $E(T)$ = 50 Ω and $E(r)$ = 1.024 mm, and standard deviations $\sigma(H)$ = 1 mm, $\sigma(d)$ = 0.6 mm, $\sigma(T)$ = 5 Ω and $\sigma(r)$ = 0.1024 mm. The frequency f

and wire length L are assumed to take deterministic values in Table 4-1. In this example, the nominal values of random variables can be different by orders of magnitude. Therefore, this example can demonstrate the potential applicability of the SROM method for stochastic problems where input variables represent different physical quantities.

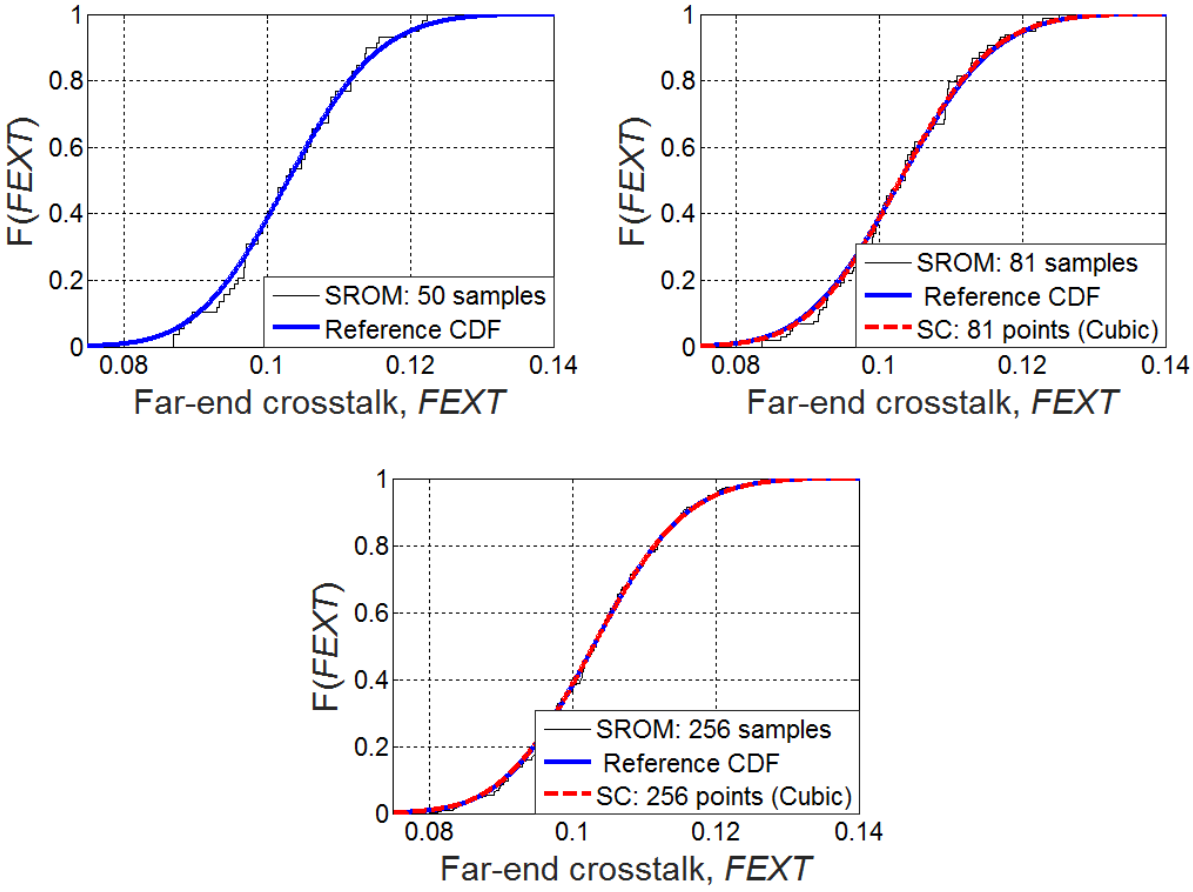

Fig. 4-15. Comparison of the reference CDF of *FEXT*, the CDF approximated by the SROMs $\widetilde{FEXT}$ with sizes of 50, 81 and 256, and the CDF approximated by the SC method (using Cubic Hermite interpolating function) with 81 and 256 collocation points.

Let $\boldsymbol{X}$ be a 4-dimensional variable containing all the uncertain variables, i.e., $\boldsymbol{X} = [H, d, T, r]$. In this case, the optimal SROM $\widetilde{\boldsymbol{X}}$ of $\boldsymbol{X}$ cannot be visualised as in the 2-dimensional example, but the concept and the construction of the optimal $\widetilde{\boldsymbol{X}}$ follow the same principle. Fig. 4-15 shows the predicted CDFs of *FEXT* using the SROM method with the sample size of 50, 81 and 256. It is clear that at the size of 50, the CDF given by the SROM method recovers the general shape of the reference CDF. Then, the difference between the SROM-based and reference CDFs is further reduced at size of 81, and becomes indistinguishable at size of 256.

In order to use the cubic Hermite interpolating function for the SC method, at least 3 collocation points are needed in each random dimension. Therefore, the illustrated SC method based on tensor-product sampling needs a minimum of $3^4 = 81$ collocation points in total. If 4 collocation points are selected in each random dimension, the total number of collocation points will be $4^4 = 256$. For the SROM method, the choice of sample size is flexible. As shown in Fig. 4-15, the CDF predicted by the SC method using 81 samples is almost the same as the reference CDF. Therefore, the SC method may be a better approach to recover the CDF of the system output in some cases.

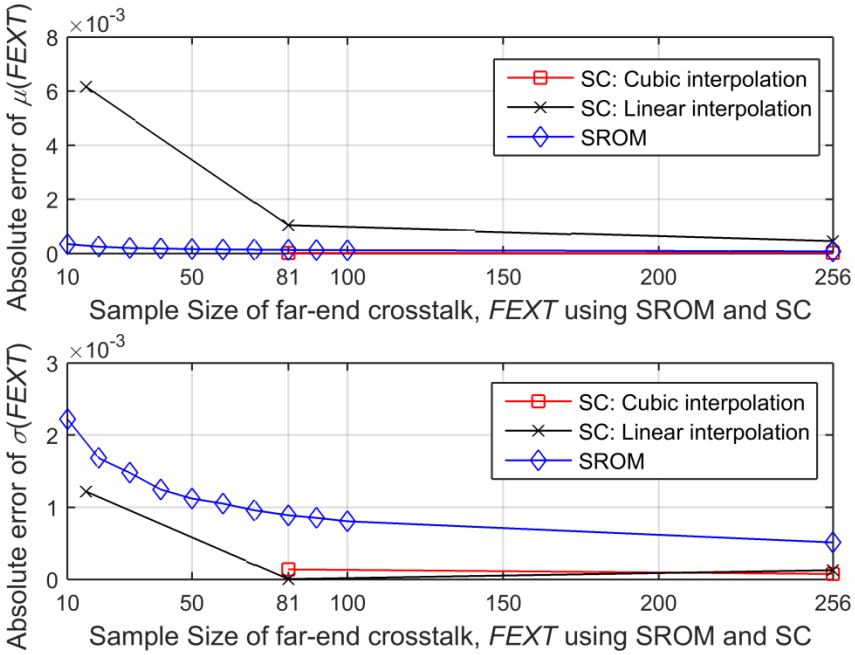

Fig. 4-16. Convergence rates of the SROM method and the SC method using cubic and linear interpolating functions, when the random variables are *H*, *d*, *r* and *T*.

Fig. 4-16 shows the convergence rates of the SROM method and the SC method using both the linear interpolating function [92] and the cubic Hermite interpolating function. For the SC implementation using linear interpolation and tensor-product sampling, the minimum required number of collocation points is $2^4 = 16$, as each random dimension needs at least 2 collocation points. As shown in Fig. 4-16, the result of the SC method is sensitive to the choice of the interpolating function, as the mean value given by the cubic interpolation is more accurate than that by the linear interpolation. It is also seen in Fig. 4-16 that both the SROM method and the SC method using the cubic interpolation and tensor-product sampling can produce very accurate mean values. In Fig. 4-16, a steady convergence is observed for

the standard deviation by the SROM method, which means a better accuracy is guaranteed by increasing the sample size. We note that the convergence rate of the SROM method to the reference standard deviation is slower than that of the SC method. However, the SROM-based result is still accurate to a certain degree. For example, the standard deviation by the SROM method at sample size of 50 is within the error of 10%.

In Fig. 4-17, the variation range of *FEXT* is obtained using the SROM method with a sample size of 50. It can be seen that the SROM method can provide accurate upper and lower boundaries to enclose most of the 10,000 MC simulations, except for a small number of extreme occurrences. It is clear that in the case of four uncertainty sources, only a small computational cost is needed to predict the variation range of crosstalk using the SROM method.

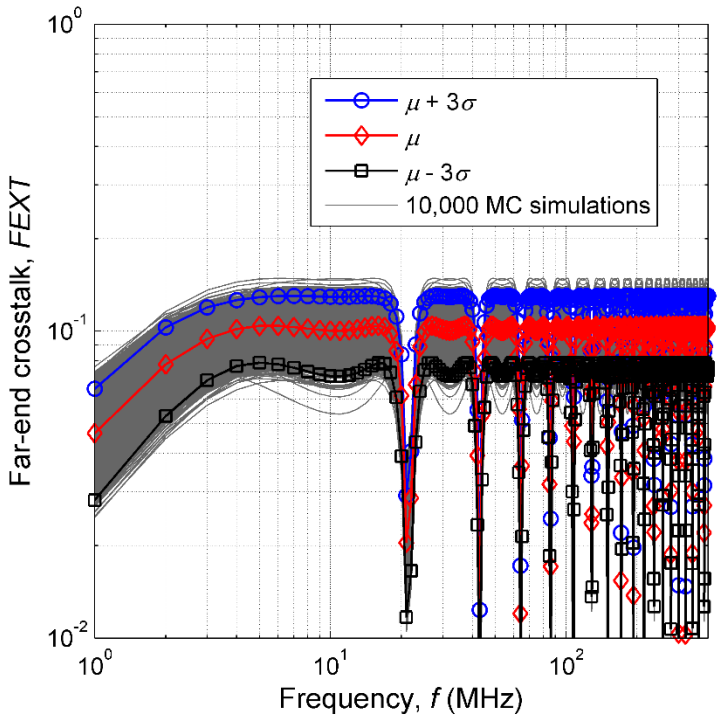

Fig. 4-17. Upper and lower boundaries obtained with the SROM method to bound the variation of *FEXT*. At each frequency, only 50 samples of the SROM-based $\widehat{FEXT}$ are used. The uncertain variables are *H*, *d*, *r* and *T*.

From the examples of this study, it is clear that the SC method can produce very accurate statistics of crosstalk using the appropriate interpolating function. On the other hand, the SROM method can provide the mean value of crosstalk as accurate as that of the SC method, but is less accurate than the SC method to predict standard deviation in some cases. Also,

choosing the sample size for the SROM method is flexible. The overhead of implementing the SROM and SC methods is also different. Specifically, after the samples of the SROM-based output are obtained, it is straightforward for the SROM method to calculate statistics. For the SC method, having known the output samples at collocation points, the analytical approximation of the output needs to be derived before estimating output statistics. With a CPU of 3.4 GHz and RAM of 8 GB, the computation time of the SROM, SC and MC methods for each example is given in Table 4-2 to demonstrate the efficiency of the SROM and SC methods. Please note that the time listed in Table 4-2 is for the complete process of each method. More specifically, the time spent by the SROM method includes building the SROM-based input, running the deterministic solver, and deriving the crosstalk statistics. For the SC method, the overall time includes the procedures of running the deterministic solver, deriving the analytical formula of the crosstalk, and finally estimating the statistics of the crosstalk. On the other hand, the time consumed by the MC method is mainly due to the cost of running the deterministic solver for a large number of times.

Table 4-2. Efficiency of the SROM and SC Methods

EXAMPLE		$\boldsymbol{X}=[H]$	$\boldsymbol{X}=[f]$	$\boldsymbol{X}=[H, d]$	$\boldsymbol{X}=[H, d, r, T]$
SROM	Time (s)	0.25	1.02	0.56	4.72
	Samples	10	20	25	81
SC	Time (s)	11.03	16.79	16.57	18.48
	Samples	10	20	25	81
MC	Time (s)	125.51	126.82	124.95	126.37
	Samples	10,000	10,000	10,000	10,000

We note that it is possible to obtain more accurate results by using other interpolating functions for the SC method. Also, the illustrated SC implementation could be more efficient using sparse-grid sampling computed via the Smolyak algorithm [71]. However, such an exhaustive comparison is beyond the scope of this study. The advantage of one method over another only holds true in the examples of this study.

There are also some remaining questions about the SROM method itself. Specifically,

although a randomness dimensionality of four is tackled using the SROM method in this chapter, the maximum randomness dimensionality that the SROM method can handle is still unclear and needs further investigation. Also, it would be beneficial to develop an *a-priori* evaluation method which provides bounds on the errors of the SROM solution. Such an evaluation can be used to select the minimum SROM sample number to keep the computational cost as small as possible whilst guaranteeing sufficient accuracy.

4.4 Summary

In this chapter, a new non-intrusive stochastic approach known as the SROM method has been applied to quantify the uncertainties of cable crosstalk. A simple three-conductor transmission line has been taken as the demonstration scenario. The SROM, SC (based on the tensor-product sampling strategy) and MC methods have been applied to obtain the statistics of crosstalk subject to multiple uncertainty sources. With the SROM method, the statistics of the actual crosstalk have been accurately approximated, and the variation range of crosstalk has been successfully obtained.

The results from the three methods have been carefully compared and it has been found that the SROM method is more efficient than the MC method, and offers a good accuracy in estimating statistical information. In addition, the sample size for the SROM method has been shown to be flexible depending on the requirement of the result accuracy. It has also been noted that the SC method has a better performance to predict the standard deviation of crosstalk compared with the SROM method. The overhead of the SROM and SC methods has been shown to be different, as the SROM method only needs numerical calculation to obtain the optimal SROM for random variables, whereas the SC method involves algebraic calculation to derive the approximated expression of the output.

With the non-intrusive, accurate, and efficient features of the SROM method demonstrated, it is hoped that the SROM method can be applied to the uncertainty prediction for other EMC problems which may not be easily solved by the MC and SC methods due to impractical computational cost.

At this stage, the sensitivity of crosstalk to different cable variables awaits to be revealed. Also, the feasibility of simplifying stochastic EMC problems by reducing randomness dimension needs to be investigated. These questions will be addressed in the next chapter.

Chapter 5 Sensitivity Analysis of Cable Crosstalk to Uncertain Parameters Using Stochastic Reduced Order Models

As demonstrated in Chapter 4, the statistics of cable crosstalk can be efficiently obtained using the SROM method in the presence of multiple uncertainty sources. Despite the superior efficacy of the SROM method to deal with multivariate stochastic processes, it is yet desirable to reduce the number of random variables considered in the problem, in order to further reduce the computational cost. To this end, the sensitivity analysis needs to be performed to identify the weak variables affecting the cable crosstalk. This motivation also coincides with the unsolved task raised in Chapter 3: to rank cable variables based on their isolated effects on the uncertainty degree of crosstalk.

Therefore, this chapter presents the sensitivity analysis of cable crosstalk against different uncertain variables using the *stochastic reduced order model* (SROM) method. Taking the three-conductor transmission line as the cable model, a ranking of these uncertain variables is produced based on their impact on the crosstalk. The result shows that the accuracy of the crosstalk statistics is preserved after ignoring the uncertainty of the weak variable. Therefore, it is confirmed that the complexity of the statistical problem can be reduced by ignoring the weak variables without affecting the accuracy. The SROM and Monte-Carlo (MC) methods are applied to study the sensitivity of the crosstalk variation to different uncertainty variables separately. Comparing the SROM performance with that of the conventional MC performance, it is found that the SROM method can reduce the computational cost required by the converged MC result by at least two orders of magnitude.

5.1 Introduction

From the previous chapters, it is clear that the cable crosstalk is an important aspect of the cable EMC performance, as it determines if the cable may suffer from malfunctions. Also, the cable crosstalk is always an uncertain quantity in reality due to the inevitable uncertainty in cable variables. Therefore, as emphasised in [21], the statistics of crosstalk rather than a seemingly accurate value is more desired.

To obtain the statistics of crosstalk, statistical approaches need to be applied [28], [29], [30]. However, a common bottleneck confronting the statistical method is the dimension of randomness, i.e., the number of uncertain input variables. If the dimension of randomness is high, the implementation of the statistical analysis becomes prohibitive due to the curse of dimensionality. For this reason, reducing the dimension of randomness is able to ease statistical analysis. To do this, sensitivity analysis should be performed to identify the uncertain input variables with weak influences on the uncertainty of the output [93]. Once being found, the statistical analysis can be simplified by ignoring the uncertainties of the weak input variables and regarding them as nominal values. As a result, the number of uncertain variables to be considered is reduced, whilst the accuracy of the output statistics is negligibly affected.

Statistical approaches are required to perform sensitivity analysis. In this chapter, the *stochastic reduced order model* (SROM) method is used to obtain the statistics of the cable crosstalk. The detailed introduction of the SROM method is presented in Section 2.3, and therefore, not repeated herein.

In this study, the SROM and MC methods are applied to study the sensitivity of the crosstalk variation to different uncertain variables separately. Then, a ranking is produced to show the variable effects on the uncertainty degree of the crosstalk. This chapter also shows that the accuracy of the crosstalk statistics is preserved after ignoring the uncertainty of the weak variable. The remaining part of this chapter is organised as follows: Section 5.2 introduces the investigated cable variables of the sensitivity analysis in the cable modelled using a three-conductor transmission line. In Section 5.3, the result of the sensitivity analysis obtained using the SROM method is compared with that of the MC method and discussed. Finally, the summary of the chapter is given in Section 5.4.

5.2 Investigated Cable Variables of Sensitivity Analysis

A three-conductor transmission line is selected as the model of the cable in this chapter. This is because each cable variable to be investigated can be clearly defined due to the integrity of this cable model.

The crosstalk is jointly determined by electrical and geometrical variables of the cable model shown in Fig. 5-1. The electrical variables include the source impedance R_S and the load impedance R_L of the generator circuit, and the *near-end* load R_{NE} and the *far-end* load R_{FE} of the receptor circuit. The geometrical variables comprise the radius r_G and height H_G of the generator wire, the radius r_R and height H_R of the receptor wire, the distance d between the generator and receptor wires, and the length L over which the two conductors are parallel.

It is assumed that $r_G = r_R = r$, $H_G = H_R = H$, and $R_S = R_L = R_{NE} = R_{FE} = T$. As a result, the four uncertain cable variables to be investigated are H, d, r, and T.

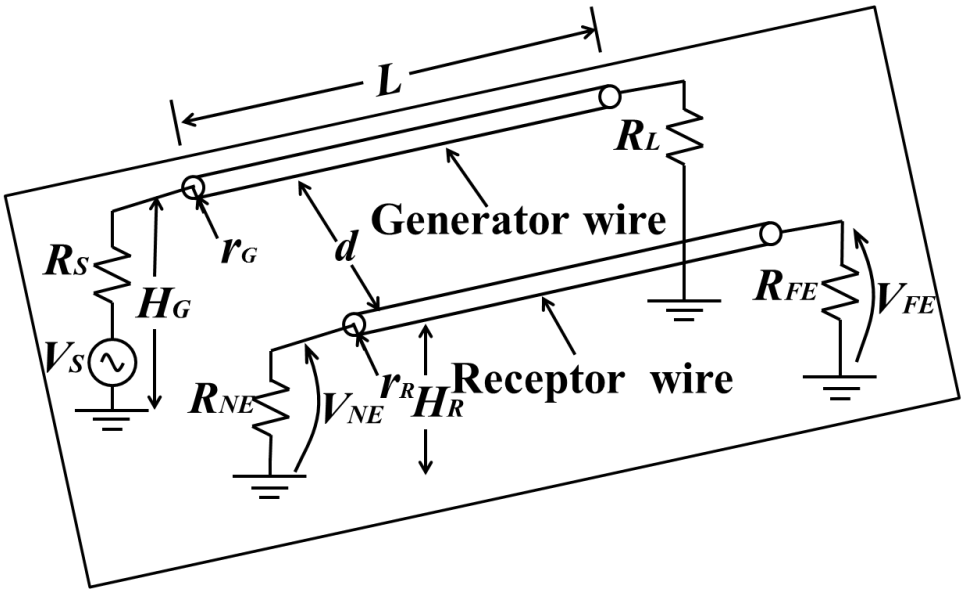

Fig. 5-1. The model of the three-conductor transmission line.

The interference induced to the receptor circuit is represented using the *near-end* crosstalk (*NEXT*) with the same definition as in Section 4.2.2. The analytical solution of cable crosstalk derived in [15] is used as the deterministic solver to calculate the crosstalk level from the values of cable variables.

5.3 Sensitivity Analysis with SROM and MC Methods

In this section, we investigate the sensitivity of the crosstalk uncertainty to each uncertain source. Before conducting the sensitivity analysis, let us introduce a relative measure referred to as the coefficient of variance (*COV*) to describe the uncertainty degree of a random variable [93]. The *COV* of a random variable $\boldsymbol{A}$ is defined as:

$$COV(\boldsymbol{A}) = \frac{\sigma(\boldsymbol{A})}{E(\boldsymbol{A})} \tag{5.1}$$

where $E(\boldsymbol{A})$ is the mean value of $\boldsymbol{A}$, and $\sigma(\boldsymbol{A})$ is the standard deviation of $\boldsymbol{A}$.

In the sensitivity analysis of a certain input variable, the SROM and MC methods are used to obtain the uncertainty degree (*COV*) of the crosstalk, while only considering this input variable to be uncertain and regarding other input variables as their mean values. By comparing the uncertainty degrees of this variable and the crosstalk, the isolated effect of the variable on the crosstalk uncertainty can be evaluated.

Sensitivity analyses are performed for *H*, *d*, *r*, and *T* under the conditions *f* = 400 MHz and *L* = 8 m. In each analysis, the uncertain input variable is assumed to have Gaussian distribution with the same uncertainty degree of *COV* = 0.1 for fair comparison. The assumption of *COV* = 0.1 is realistic as it implies a probability of 68%, 95% and 99.7% for the random variable taking a value within the range of $\pm$10%, $\pm$20%, and $\pm$30% with respect to the mean value, respectively. The statistics of uncertain input variables are shown in Table 5-1. The MC results obtained using 1,000,000 samples are referred to as reference values to set benchmarks.

Table 5-1. Statistical Properties of the Input Variables

Input Variable	Mean	σ	*COV*
H (mm)	10	1	0.1
d (mm)	8	0.8	0.1
r (mm)	0.4064	0.0406	0.1
T (Ω)	50	5	0.1

5.3.1 Sensitivity Analysis of Height *H*

As shown in Table 5-2, the cable crosstalk *NEXT* receives an uncertainty degree of *COV* (*NEXT*) = 0.0399 as a response to the uncertainty source *H* with the uncertainty degree of *COV* (*H*) = 0.1. Here, the influence of the cable variable on the crosstalk variation is judged by comparing the uncertainty degrees of the cable variable and crosstalk. As shown herein, the uncertainty degree of *NEXT* (i.e., *COV* (*NEXT*) = 0.0399) is much smaller than that of the height *H* (i.e., *COV* (*H*) = 0.1). This means that in the presence of the uncertain cable height *H*, the crosstalk receives a very small fraction (around 40%) of the input uncertainty. As a result, one may deem the variable *H* to be a weak variable in the stochastic analysis of the crosstalk. The effect of the cable height *H* on the variation of the crosstalk *NEXT* will be further justified in Section 5.3.5.

Table 5-2. Theoretical Statistics of *NEXT* When Only the Cable Height *H* is Uncertain with *COV* = 0.1

Output Response	Mean	σ	*COV*
NEXT	0.0351	0.0014	0.0399

The error of the SROM and MC results is used to evaluate the performance of the both methods. The error is defined as:

$$Error = \frac{|simulation\ result - reference\ result|}{reference\ result} \tag{5.2}$$

As can be seen in Fig. 5-2, to converge to the theoretical *COV* (*NEXT*) within the error of 2%, the SROM method only needs 14 selected samples for *H*, resulting in 14 samples of the SROM-based output $\widetilde{NEXT}$, whereas the MC method needs at least 10,000 random samples. Therefore, the computational cost is reduced by a factor of 10,000/14 ≈ 714, which is a remarkable acceleration for statistical analysis. Apart from the superior efficiency, the SROM method is also very stable. Unlike the SROM method, the accuracy of the MC method fluctuates significantly even at large sample sizes (1,000 ~ 10,000).

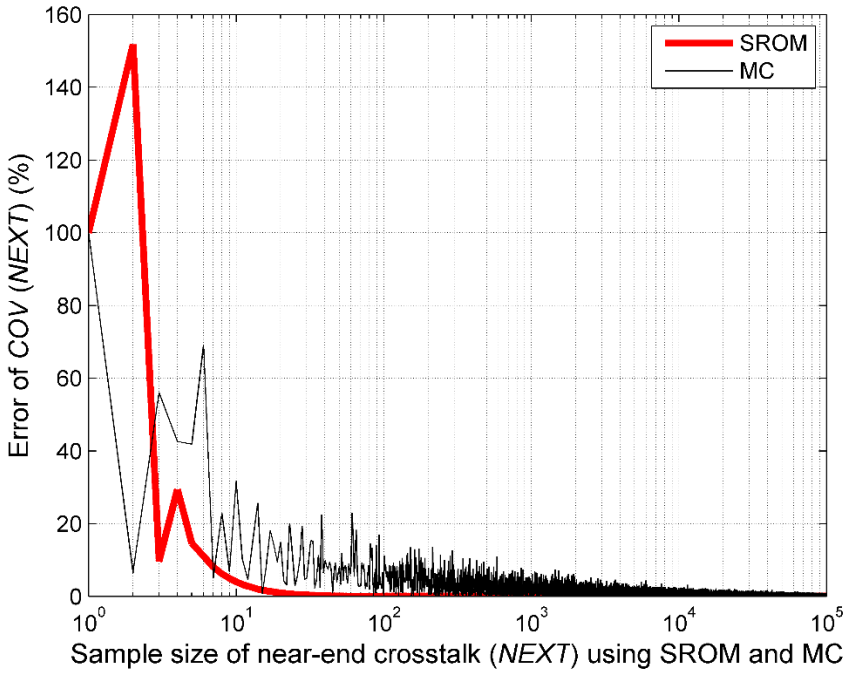

Fig. 5-2. Convergence rates of the SROM and MC methods to the theoretical *COV* of *NEXT*, when *H* is the uncertain input variable.

5.3.2 Sensitivity Analysis of Distance *d*

It can be seen from Table 5-3 that the distance *d* is stronger than *H* to affect the crosstalk uncertainty, causing *COV* (*NEXT*) = 0.1014. This means when *d* is the only uncertain variable, the propagated uncertainty to crosstalk is nearly the same as that of the random input. In terms of the convergence rates shown in Fig. 5-3, the SROM method needs 15 samples to yield accurate statistics within the error of 2%. In contrast, around 10,000 samples are in demand by the MC method to have the same performance. In this case, the statistical analysis accelerates by a factor of 10,000/15 ≈ 667 with the SROM method.

Table 5-3. Theoretical Statistics of *NEXT* When Only the Distance *d* is Uncertain with *COV* = 0.1

Output Response	Mean	σ	*COV*
NEXT	0.0355	0.0036	0.1014

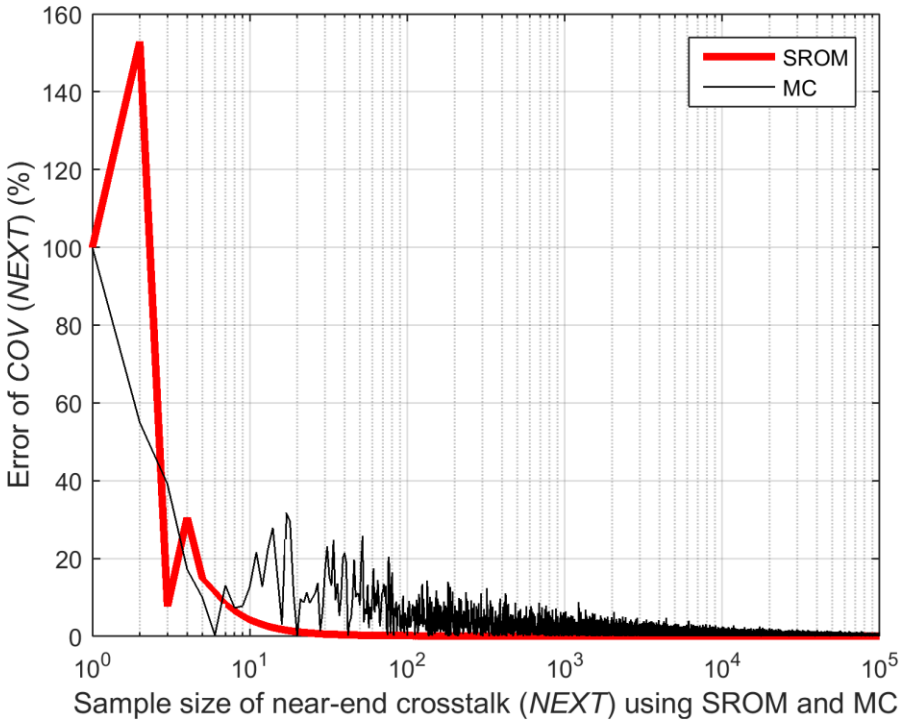

Fig. 5-3. Convergence rates of the SROM and MC methods to the theoretical *COV* of *NEXT*, when *d* is the uncertain input variable.

5.3.3 Sensitivity Analysis of Wire Radius *r*

Table 5-4 shows that with *COV* (*NEXT*) = 0.0597, the influence of the wire radius *r* on the uncertainty of *NEXT* is between those of *d* and *H*. Again, an overwhelming efficiency of the SROM method over the MC method is shown in Fig. 5-4, since 14 and 10,000 samples are needed by the SROM and MC methods to produce the accuracy within the error of 2%, respectively. As a result, an acceleration factor of 714 is seen in this case with the SROM method.

Table 5-4. Theoretical Statistics of *NEXT* When Only the Wire Radius *r* is Uncertain with *COV* = 0.1

Output Response	Mean	σ	*COV*
NEXT	0.0352	0.0021	0.0597

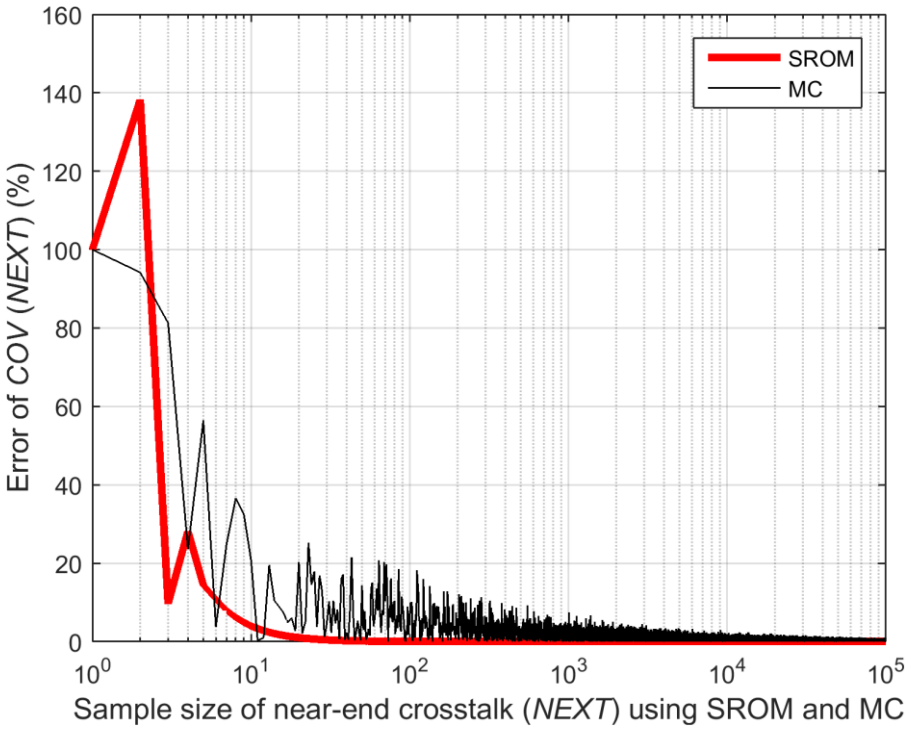

Fig. 5-4. Convergence rates of the SROM and MC methods to the theoretical *COV* of *NEXT*, when *r* is the uncertain input variable.

5.3.4 Sensitivity Analysis of Termination Load *T*

As shown in Table 5-5, the uncertain termination impedance T is the strongest variable to deviate the crosstalk from the nominal value. As the *COV* (*NEXT*) of 0.1161 is larger than the *COV* (*T*) of 0.1, the uncertainty is increased when propagated from the input T to the output *NEXT*. Similar to H, d, and r, Fig. 5-5 shows that a speed-up of the statistical analysis could be 10,000/14 = 714 times if the SROM method is used.

Table 5-5. Theoretical Statistics of *NEXT* When Only the Termination Load *T* is Uncertain with *COV* = 0.1

Output Response	Mean	σ	*COV*
NEXT	0.0353	0.0041	0.1161

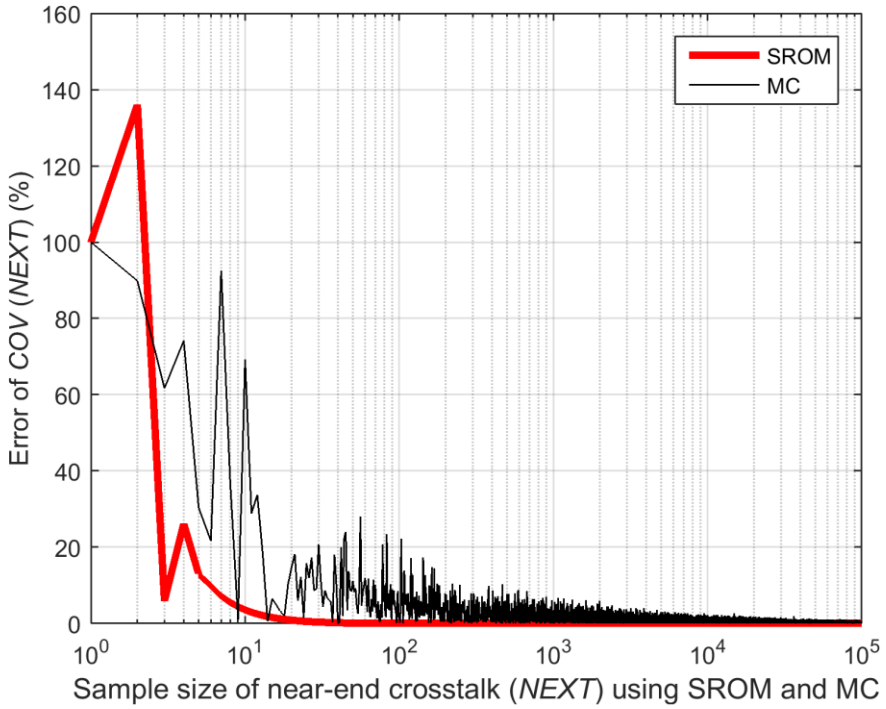

Fig. 5-5. Convergence rates of the SROM and MC methods to the theoretical *COV* of *NEXT*, when *T* is the uncertain input variable.

It is worth noting that the SROM convergence curves in Fig. 5-2 and Fig. 5-3 for H and d appear to be identical, but are not exactly the same. The same phenomenon is observed for the SROM convergence curves in Fig. 5-4 for r and Fig. 5-5 for T as well. This can be explained by the facts that: 1) *NEXT* is almost linearly related to each uncertain variable in the uncertain range; and 2) all the uncertain variables are assumed to have Gaussian distributions. Therefore, the performance of the SROM method follows very similar pattern as shown in Fig. 5-2, Fig. 5-3, Fig. 5-4, and Fig. 5-5.

5.3.5 Reduction of Randomness Dimension

With the sensitivity analyses finished, a ranking of the influences of each variable on the variation of the crosstalk is plotted in Fig. 5-6. The amplitude of each variable shows the impact of this variable on crosstalk variability. It is clear that the cable height H is the most insignificant variable compared to the other variables, but is still relatively significant. As the curse of dimensionality is an issue for statistical analysis, it is desirable to reduce the randomness dimension.

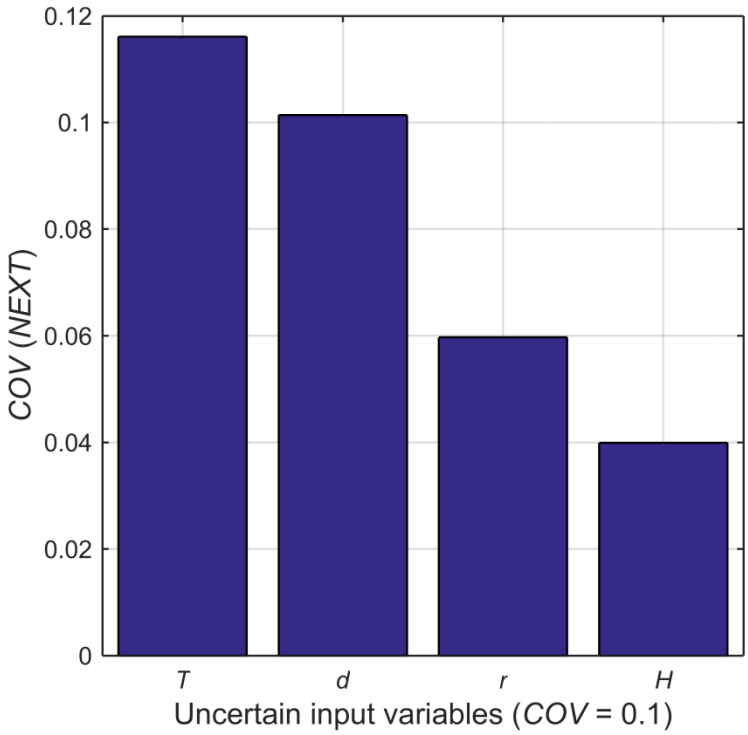

Fig. 5-6. Influences of each uncertain variable on the uncertainty of *NEXT*.

Let us first justify if the effect of the cable height H on the crosstalk *NEXT* is negligible. This can be done by treating the variable H as the mean value to ignore its uncertainty, while keeping other variables stochastic. For this case, the results are shown in Table 5-6 and Fig. 5-7.

Table 5-6. Theoretical Statistics of *NEXT* Before and After the Uncertainty of *H* is Ignored, While Other Variables are Uncertain with *COV* = 0.1

Output response	Mean	σ	*COV*
NEXT (Before)	0.0354	0.0061	0.1723
NEXT (After)	0.0355	0.0059	0.1662

As can be seen from Table 5-6, after the uncertainty of H is discarded, the statistics of *NEXT* remain very close to the case where all the variables (including H) are considered uncertain. In addition, Fig. 5-7 shows a good agreement when comparing the distributions of *NEXT* before and after ignoring the uncertainty of H. Specifically, the peaks of PDF (*NEXT*) are 67 and 69 for the two cases: (1) before ignoring the uncertainty of H, and (2) after ignoring the

uncertainty of H, respectively. This gives a small distortion of the PDF of *NEXT*. The distortion is justified by the relative error of the peak of the PDF (*NEXT*) after ignoring parametric uncertainty, which is (69-67) / 67 ≈ 3% in this case. Therefore, from this perspective, one may regard the cable height H as a negligible variable in the statistical analysis of crosstalk.

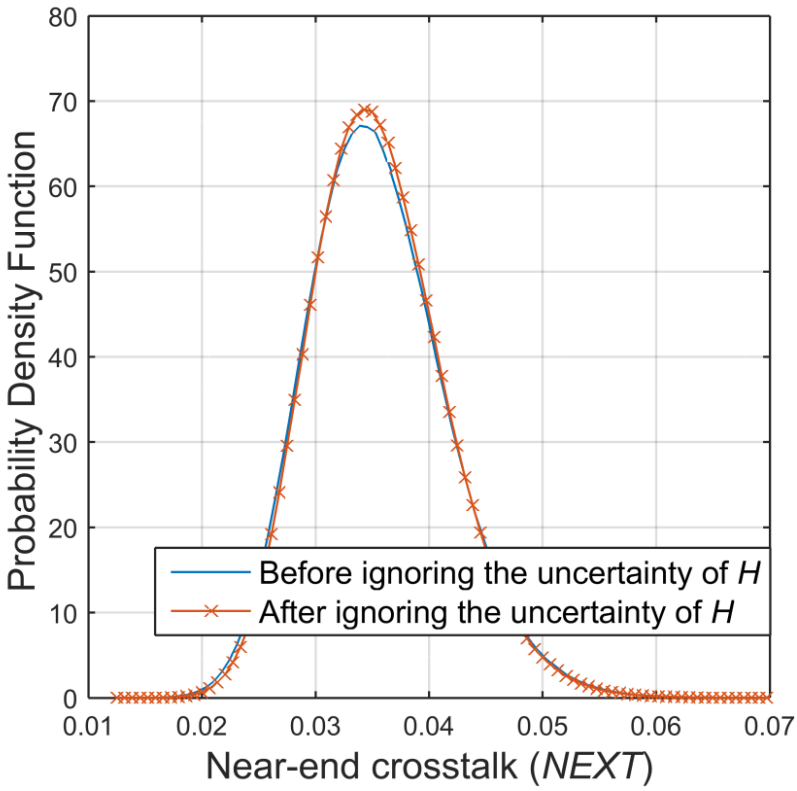

Fig. 5-7. Distributions of *NEXT* before and after the uncertainty of *H* is ignored, while other variables are considered uncertain.

Now let us investigate if the randomness dimension of the cable crosstalk problem can be further reduced. To this end, one can ignore the uncertainty of the second weakest variable r together with that of H, and the result is shown in Fig. 5-8. As can be seen in this case, severe distortion is introduced to the distribution of *NEXT*. Specifically, the peaks of the PDF of the crosstalk *NEXT* are 67 and 74 for the two cases: (1) every variable (including H and r) are random, and (2) after ignoring the uncertainty of H and r (whilst other variables are still stochastic), respectively. Now the distortion of the PDF (*NEXT*) obtained after reducing randomness dimension is quantified to be (74-67) / 67 ≈ 10%, resulting in a significant deviation from the theoretical PDF of *NEXT*. As a result, the ignorance of the uncertainty of both the variables H and r is shown to have non-negligible effect on the statistics of the

crosstalk *NEXT*. Therefore, it is feasible to simplify the stochastic analysis by reducing the dimension of randomness, and still retaining accurate statistical results, but the number of ignored weak variables should be carefully selected.

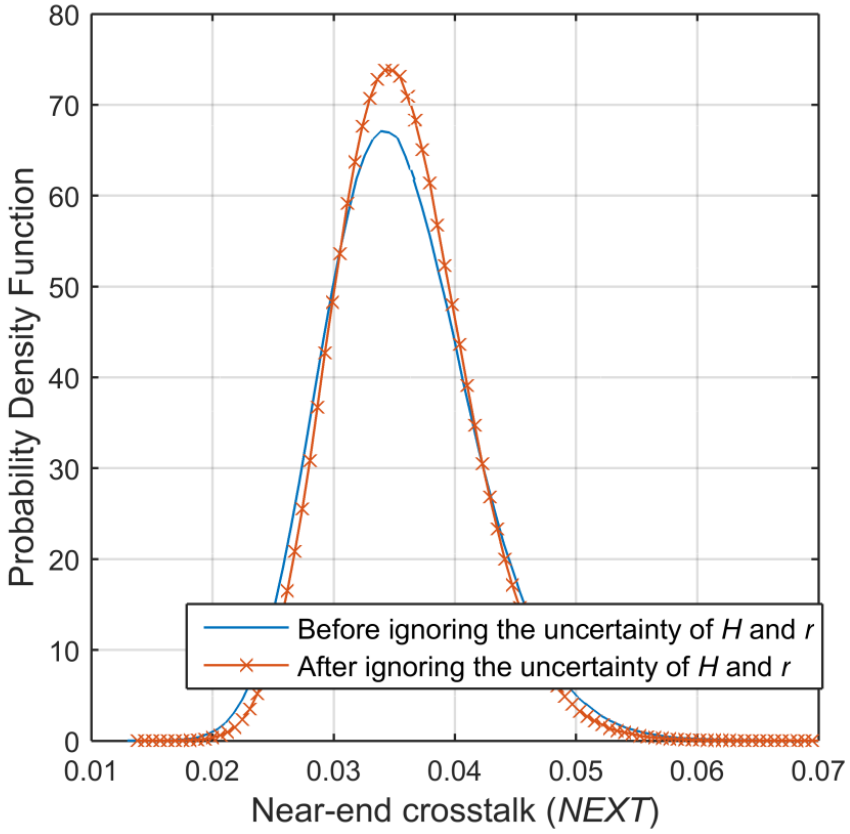

Fig. 5-8. Distributions of *NEXT* before and after the uncertainties of *H* and *r* are ignored, while other variables are considered uncertain.

5.4 Summary

In this chapter, sensitivity analyses have been performed using the SROM method to rank the isolated influences of each cable variable on the crosstalk uncertainty. The contributions of this work are threefold. First, the weakest cable variable has been identified to reduce the dimension of randomness, thus to reduce the complexity of the problem and make the computation more manageable. Second, the efficiency of the SROM method has been shown to be superior. With the SROM method, the computational cost has been reduced by at least two orders of magnitude compared with that of the conventional MC method, without compromising the accuracy of the results. Finally, it has been shown that ranking the

importance of the random variables and ignoring the weak variables is an efficient and effective approach to obtain the accurate statistics of crosstalk. This way of reducing the dimension of randomness could be applicable to other uncertainty-embedded EMC problems as well.

Chapter 6 Numerical Analysis of a Transmission Line Illuminated by a Random Plane-Wave Field Using Stochastic Reduced Order Models

As described in Chapter 1, the interference induced to the wire in the cable can be caused by other wires in close proximity, or due to the illumination of impinging electromagnetic field. These two scenarios can be investigated using the wire-to-wire coupling model and the field-to-wire coupling model, respectively. From Chapter 3 to Chapter 5, the cable interference due to the wire-to-wire coupling mechanism was analysed. In this chapter, the induced effect in the cable in the field-to-wire coupling scenario is investigated.

Specifically, in this chapter, the novel *stochastic reduced order model* (SROM) method is applied to efficiently estimate the statistical information of the terminal response (i.e., the induced current) in transmission lines excited by a random incident plane-wave field. The motivation is that the induced effect in the cable may be a potential threat to degrade the performance of electronic systems, especially for aerospace applications. Therefore, predicting the radiated susceptibility of cables to the impinging electromagnetic field is of great importance at the early stage to account for possible malfunctions. The efficiency and accuracy of the SROM method to obtain the statistics of the induced current are analysed using two examples where the complexity of the uncertain input space gradually increases. The performance of the SROM method is compared with that of the traditional Monte-Carlo (MC) method. The stochastic collocation (SC) method based on sparse-grid sampling strategy computed via the Smolyak algorithm is also implemented to fairly evaluate the SROM performance. The result shows that the SROM method is much more efficient than the MC method to obtain accurate statistics of the induced current, and even shows a faster convergence compared with that of the SC method in the examples considered. Therefore, the

SROM method is shown to be a suitable approach to investigate the variability of radiated susceptibility in electromagnetic compatibility problems with a random incident wave.

6.1 Introduction

The induced effect in cables caused by an incident electromagnetic field may be a potential threat to degrade the performance of the system. This phenomenon is especially of interest in aerospace systems. Therefore, it is important to estimate the terminal response (such as the induced current or voltage) of the cable to the impinging electromagnetic field at the early stage to prevent possible malfunctions.

For deterministic estimation, the pioneering work in [94] gave a closed-form solution for the terminal response of a two-conductor transmission line illuminated by an incident field. This work was later generalised for multiconductor transmission lines (MTLs) in [18] and [95]. Then, the field-to-wire coupling model was extended for some common configurations, such as a twisted-wire pair (TWP) in free space [96], a TWP or a bundle of TWPs above a ground plane in [97] and [98]. The estimation approach for non-uniform cable types was addressed in [99] and [100]. The induced effect resulting from the strong electromagnetic field such as lightning strikes was investigated in [17], [101].

The aforementioned work is very useful for deterministic analysis with a unique output, but may not be sufficient for practical cases. This is because the characteristics of the incident wave (such as the field strength and incident direction) could be unknown in practice. Therefore, the resultant induced effect in the cable also becomes an uncertain quantity. As a result, statistical analysis needs to be performed to account for the potential variability of the induced effect.

If the deterministic solver relating the input to output takes the form of an analytic formula, the theory of random variable transformation in [26] can be used to obtain the statistical information of the output. On this basis, pioneering contributions were presented in [102] and [103] to derive closed-form expressions for the statistical properties of the induced current. However, the probabilistic transformation involved may become prohibitively difficult if the deterministic solver takes complex algebraic forms or is an electromagnetic simulator. Other work was dedicated to the estimation of extreme induced current values using the controlled stratification method [104].

As reviewed in Chapter 2, to perform a general statistical analysis, one needs to consider using the conventional Monte-Carlo (MC) method [28], the well-established polynomial chaos expansion (PCE) [29] and stochastic collocation (SC) [30] methods, and the newly proposed *stochastic reduced order model* (SROM) method [27]. The MC method is non-intrusive, as the deterministic solver is used without any modifications. However, for the MC method, despite the ease of implementation, converged results are only produced after examining a sufficient number of possible occurrences, making the implementation inefficient. Applications of the MC method for field-to-wire coupling problems can be found in [105] and [106].

The PCE method [29] has been used as an efficient statistical tool in the last decade. The principle of the PCE method was well addressed in Section 2.2.2, and therefore is not repeated herein. Efforts were made via the PCE method to express the induced current at the termination load of the transmission line using an analytical formula with regard to variables characterising the incident wave [24]. On this basis, the statistics of the induced current can be efficiently estimated via the probability transformation technique in [26] or MC simulations. However, it is worth noting that in [24], the impinging field was not assumed to be fully random.

Similar to the PCE method, the SC method [30] is also aimed at expressing the deterministic solver using an analytical formula. How to perform the SC method was given in Section 2.2.3. With the analytical expression being obtained, the statistics of the output can be obtained using the same procedure as that for the PCE method. Like the MC method, the SC method is also non-intrusive. However, the SC method was yet to be applied for the stochastic field-to-wire coupling problem until the presentation in this chapter.

The SROM method [27] was recently proposed as a computationally efficient alternative to MC simulations for statistical analysis. This method is general, non-intrusive, and able to produce accurate output statistics by only using a small fraction of the MC computational cost. The applications of the SROM method in the uncertainty quantification and sensitivity analysis of cable crosstalk were given in Chapter 4 and Chapter 5, respectively.

Since the SROM method is a novel methodology, it is worth another specific investigation on its performances and advantages versus the brute-force MC approach and other efficient statistical methods. In this chapter, the SROM method is applied to efficiently estimate the statistics of the induced current in the multiconductor transmission line induced by a random

incident wave. It provides an incremental contribution to efficient statistical analysis of field-to-wire coupling problems. Also, although the SROM performance is compared to the SC method based on the tensor-product sampling technique in Chapter 4, the relative goodness of SROM over SC or vice versa in terms of efficiency is still obscure. Therefore, in this chapter, the SROM performance is also compared with the SC method based on a more efficient sparse-grid sampling technique. The introductions of the SROM and SC methods were given in Chapter 2 and not repeated herein. The remainder of the chapter is organised as follows: In Section 6.2, the deterministic solver of the field-to-wire coupling model is described. In Section 6.3, the implementation of SROM for uncertainty propagation in the case considered is presented. Also, the application of the SC method is briefly presented for comparison purposes. The discussion about the SROM and SC performances is given in Section 6.4. The summary of the chapter is presented in Section 6.5.

6.2 Deterministic System

In this section, the field-to-wire coupling model sketched in Fig. 6-1 is introduced. As shown in Fig. 6-1(a), the external excitation source is a plane-wave field characterised by the incidence angles θ (the elevation angle) and ψ (the azimuth angle), the polarisation angle η, and the electric field amplitude E_0.

The victim of the incident field is a uniform and lossless MTL with length l. This MTL consists of N perfect conductors placed in the *y-axis* direction above a ground plane. For the sake of the neatness of the MTL plot, only a representative (the ith, $1 \leq i \leq N$) conductor is shown in Fig. 6-1(b).

The position of the ith conductor in the x-z plane (the cross-section plane) is denoted by the coordinate (x_i, z_i). The ith conductor is connected to the ground plane via the termination loads R_{iL} at the left end and R_{iR} at the right end. The medium immersing the MTL is characterised by the electric permittivity ε_0 and magnetic permeability μ_0 in free space. The system response refers to the induced current in the right-end termination of the MTL. Given the characteristics of the field-to-wire coupling model, the induced current can be calculated using the deterministic solver (i.e., the calculation process).

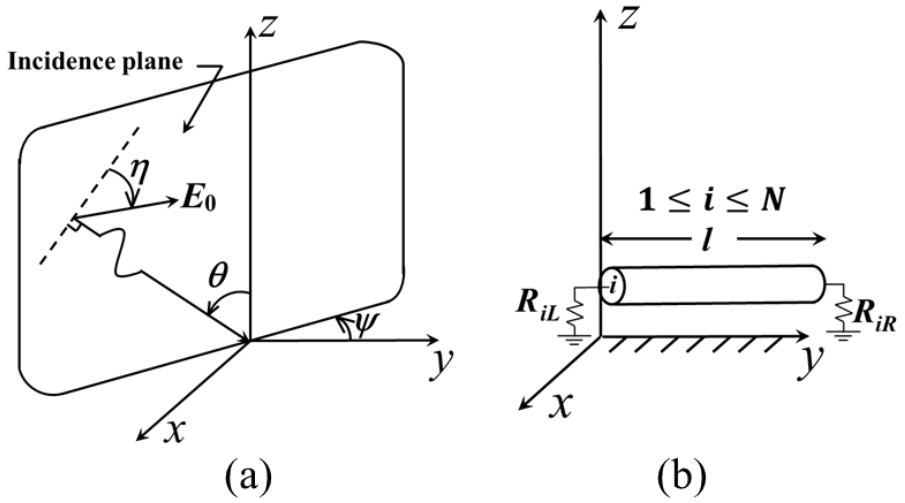

Fig. 6-1. (a) Variables characterising the incident plane-wave field. (b) Configuration of an arbitrary wire in the illuminated MTL [16]**.**

The induced current (i.e., the output of the deterministic solver) is observed at the right end of the MTL. To obtain the induced current, one needs to know the vectors $\boldsymbol{V}_{SL}$ and $\boldsymbol{V}_{SR}$ containing the induced equivalent open-end voltage sources at the left and right ends of each line, respectively. According to [16], the voltage sources $\boldsymbol{V}_{SL}$ (or $\boldsymbol{V}_{SR}$) comprise two contributions caused by the external field. The first contribution is distributed voltage sources contained in the vector $\boldsymbol{V}_{SL}^{H}$ (or $\boldsymbol{V}_{SR}^{H}$) due to the electric field component parallel to the MTL. The second contribution is lumped terminal sources caused by the vertical component of the field, and is denoted by the vector $\boldsymbol{V}_{SL}^{V}$ (or $\boldsymbol{V}_{SR}^{V}$). On this basis, the terms $\boldsymbol{V}_{SL}$ and $\boldsymbol{V}_{SR}$ can be expressed as:

$$\boldsymbol{V}_{SL} = \boldsymbol{V}_{SL}^{H} + \boldsymbol{V}_{SL}^{V} \tag{6.1}$$

$$\boldsymbol{V}_{SR} = \boldsymbol{V}_{SR}^{H} + \boldsymbol{V}_{SR}^{V} \tag{6.2}$$

The vectors $\boldsymbol{V}_{SL}^{H}$ and $\boldsymbol{V}_{SR}^{H}$ can be obtained using [16]:

$$\boldsymbol{V}_{SL}^{H} = \frac{\gamma_0 e^{-\hat{\gamma}_0 l} - \gamma_0 \cosh(\gamma_0 l) + \hat{\gamma}_0 \sinh(\gamma_0 l)}{(\gamma_0^2 - \hat{\gamma}_0^2)\sinh(\gamma_0 l)} \boldsymbol{V}_0 \tag{6.3}$$

$$\boldsymbol{V}_{SR}^{H} = \frac{-\gamma_0 e^{\hat{\gamma}_0 l} + \gamma_0 \cosh(\gamma_0 l) + \hat{\gamma}_0 \sinh(\gamma_0 l)}{(\gamma_0^2 - \hat{\gamma}_0^2)\sinh(\gamma_0 l)} e^{-\hat{\gamma}_0 l} \boldsymbol{V}_0 \tag{6.4}$$

where

$$\gamma_0 = j\omega\sqrt{\varepsilon_0\mu_0} \tag{6.5}$$

$$\hat{\gamma}_0 = \gamma_0 \sin\theta \cos\psi \tag{6.6}$$

$$\boldsymbol{V}_0 = E_0(\cos\theta\cos\psi\cos\eta + \sin\psi\sin\eta)\boldsymbol{P} \tag{6.7}$$

The column vector $\boldsymbol{P}$ in (6.7) contains phase factors and is calculated as follows:

$$\boldsymbol{P} = \begin{pmatrix} 2\sinh(\gamma_0 z_1\cos\theta)\, e^{\gamma_0 x_1 \sin\theta\sin\psi} \\ \vdots \\ 2\sinh(\gamma_0 z_N\cos\theta)\, e^{\gamma_0 x_N \sin\theta\sin\psi} \end{pmatrix} \tag{6.8}$$

The vectors $\boldsymbol{V}_{SL}^{V}$ and $\boldsymbol{V}_{SR}^{V}$ can be obtained using:

$$\boldsymbol{V}_{SL}^{V} = -\frac{E_0 \tan\theta\cos\eta}{\gamma_0}\boldsymbol{P} \tag{6.9}$$

$$\boldsymbol{V}_{SR}^{V} = e^{-\hat{\gamma}_0 l}\boldsymbol{V}_{SL}^{V} \tag{6.10}$$

The calculation process of the vectors $\boldsymbol{V}_{SL}$ and $\boldsymbol{V}_{SR}$ in (6.1) and (6.2) is clearly outlined in (6.3)-(6.10).

Having obtained $\boldsymbol{V}_{SL}$ and $\boldsymbol{V}_{SR}$, the induced currents $\boldsymbol{I}_R$ = [I_{R1}, …, I_{RN}] in the right-end termination of each line can be calculated using (6.11)-(6.22) shown below. Specifically, the vector $\boldsymbol{I}_R$ can be related to $\boldsymbol{V}_{SL}$ and $\boldsymbol{V}_{SR}$ using:

$$\boldsymbol{I}_R = \boldsymbol{A}\cdot\boldsymbol{V}_{SL} + \boldsymbol{B}\cdot\boldsymbol{V}_{SR} \tag{6.11}$$

The terms $\boldsymbol{A}$ and $\boldsymbol{B}$ in (6.11) are matrices defined by:

$$\boldsymbol{A} = (\mathbf{1}_{\square} - \boldsymbol{M}\cdot\boldsymbol{Z_R})^{-1}\cdot(\boldsymbol{M}\cdot\boldsymbol{\Phi_{11}} - \boldsymbol{\Phi_{21}}) \tag{6.12}$$

$$\boldsymbol{B} = -(\mathbf{1}_{\square} - \boldsymbol{M}\cdot\boldsymbol{Z_R})^{-1}\cdot\boldsymbol{M} \tag{6.13}$$

where

$$\boldsymbol{M} = (\boldsymbol{\Phi_{22}} - \boldsymbol{\Phi_{21}}\cdot\boldsymbol{Z_L})\cdot(\boldsymbol{\Phi_{12}} - \boldsymbol{\Phi_{11}}\cdot\boldsymbol{Z_L})^{-1} \tag{6.14}$$

The symbol $\mathbf{1}_{\square}$ in (6.12) means the $N \times N$ identity matrix. The terms $\boldsymbol{Z_L}$ and $\boldsymbol{Z_R}$ are the impedance matrices at the left and right ends, respectively, and are defined by:

$$\boldsymbol{Z_L} = \begin{bmatrix} R_{1L} & \cdots & 0 \\ \vdots & \ddots & \vdots \\ 0 & \cdots & R_{NL} \end{bmatrix} \tag{6.15}$$

$$\boldsymbol{Z_R} = \begin{bmatrix} R_{1R} & \cdots & 0 \\ \vdots & \ddots & \vdots \\ 0 & \cdots & R_{NR} \end{bmatrix} \tag{6.16}$$

The matrices $\boldsymbol{\Phi_{11}}$, $\boldsymbol{\Phi_{12}}$, $\boldsymbol{\Phi_{21}}$ and $\boldsymbol{\Phi_{22}}$ in (6.12) and (6.14) are cast as follows:

$$\boldsymbol{\Phi_{11}} = \cosh(\gamma_0 l)\mathbf{1}_{\square} \tag{6.17}$$

$$\boldsymbol{\Phi_{12}} = -\sinh(\gamma_0 l)\,\boldsymbol{Z_C} \tag{6.18}$$

$$\boldsymbol{\Phi_{21}} = -\sinh(\gamma_0 l)\,\boldsymbol{Z_C^{-1}} \tag{6.19}$$

$$\boldsymbol{\Phi_{22}} = \cosh(\gamma_0 l)\mathbf{1}_{\square} \tag{6.20}$$

The term $\boldsymbol{Z_C}$ in (6.18) is the characteristic impedance matrix whose entries are given by [18]:

$$[\boldsymbol{Z_C}]_{ii} = \frac{377}{2\pi}\log\left(\frac{2z_i}{r}\right) \tag{6.21}$$

$$[\boldsymbol{Z_C}]_{\substack{ij \\ i\neq j}} = \frac{377}{4\pi}\log\left(1 + \frac{4z_i z_j}{\left(z_i - z_j\right)^2 + \left(x_i - x_j\right)^2}\right) \tag{6.22}$$

where $1 \leq i, j \leq N$, and r is the radius of the conductor in the MTL.

The uncertainty is assumed to be embedded in the incident field, whereas the features of the MTL are deterministically characterised. Specifically, the length of the MTL is l = 2 m, and the radius of each conductor is r = 1 mm. The cross-section detail of the MTL is shown in Fig. 6-2. Each line is terminated using 50 Ω loads at the left and right ends. By default, the analysis is performed at the frequency of 50 MHz unless specifically stated. A clarification of the stochastic and deterministic variables assumed in this chapter is given in Table 6-1.

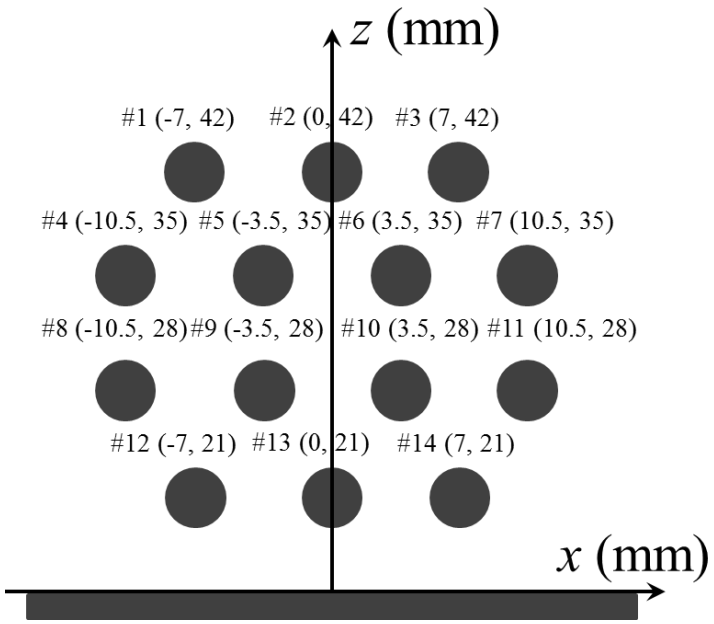

Fig. 6-2. Positions of each line denoted by the coordinates (x_i, z_i) in the cross-section of the MTL.

Table 6-1. Clarification of Stochastic and Deterministic Variables

θ (elevation angle)	Stochastic
ψ (azimuth angle)	Stochastic
E_0 (electric field strength)	Deterministic in Section 6.3.1, stochastic in Section 6.3.2.
η (polarisation angle)	Deterministic in Section 6.3.1, stochastic in Section 6.3.2.
x_i (position of ith conductor in x-axis)	Deterministic
z_i (position of ith conductor in z-axis)	Deterministic
R_{iL} (left-end termination load of ith conductor)	Deterministic
R_{iR} (right-end termination load of ith conductor)	Deterministic

6.3 Numerical Examples

In this section, taking the MTL with 14 conductors as the victim, the SROM method is applied to derive the statistics of the induced current excited by a random incident plane-wave. Specifically, the induced current (I_{R3}) in the right-end termination of wire #3 is observed for the demonstration purpose.

To test the efficacy and robustness of the proposed SROM method, two examples are considered, and the complexity of the uncertain input space in the second example is increased with respect to the first one. In addition, the SC method using Lagrange interpolation is also applied to random field coupling problems for the first time. But the aim of introducing the SC method is to provide a competing technique for comparison with the SROM method. MC results from 200000 simulations are used as the reference to benchmark the accuracy of the SROM and SC results.

6.3.1 Random θ and ψ

In this section, the SROM method is applied to quantify the variability of the induced current I_{R3} due to two uncertain variables, and its performance is discussed with respect to the SC method. The two random variables are chosen as the incidence angles θ and ψ following uniform distributions in [0, π/2] and [0, π], respectively. This assumption means that the incident plane-wave field could illuminate the MTL from any direction above the ground plane. Please note that the variation range of the azimuth ψ is chosen as [0, π] instead of [0, 2π]. This is because the cross-section of the MTL is symmetrical. Such a choice can avoid analysing a redundant space of the variable ψ. It is to be noted that the random variables in this chapter are uncorrelated by nature, but the SROM method is also applicable to correlated input variables, please see [27] for example. The field strength E_0 and polarisation angle η are assumed to take deterministic values of 1 V/m and 0°, respectively.

The first step of the SROM implementation process is to construct a SROM-based input model as the approximation of the uncertain input space. Let $\boldsymbol{X}$ be a bivariate random variable containing the two uncertain variables θ and ψ, i.e., $\boldsymbol{X} = [\theta, \psi]$ and the dimension $N = 2$. Each sample of $\boldsymbol{X}$ represents a point on the 2-D plane dimensioned using θ and ψ as orthogonal axes. The coordinates of the point indicate the input information, i.e., the values of θ and ψ.

This information can be used to run the deterministic solver once and obtain the corresponding output value (i.e., the induced current in this case). The construction process of the SROM-based input $\tilde{\boldsymbol{X}}$ for $\boldsymbol{X}$ is visualised in Fig. 6-3.

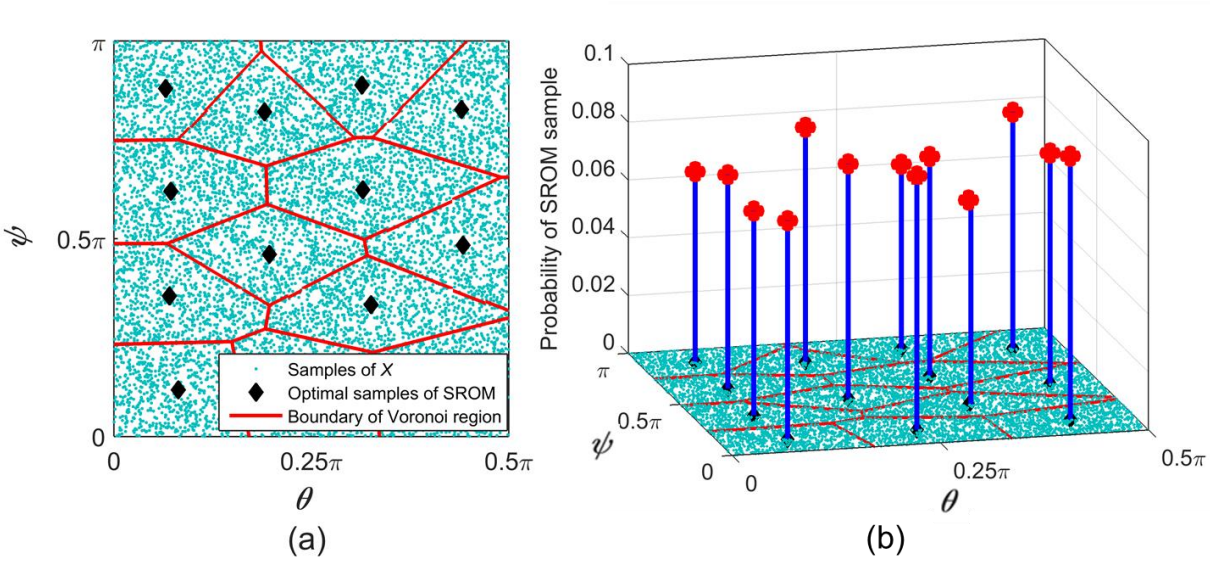

Fig. 6-3. (a) Distribution of 10000 samples of X = [θ, ψ] and 13 samples of $\tilde{X}$ in corresponding Voronoi regions. (b) Visualisation of SROM $\tilde{X}$ with sample size of 13.

As shown in Fig. 6-3(a), 10000 independent samples of $\boldsymbol{X}$ = [θ, ψ] are randomly generated according to the probability distributions of θ and ψ. The samples of $\tilde{\boldsymbol{X}}$ can be selected using the pattern classification algorithm, and are shown in Fig. 6-3(a) for sample size m = 13. Having determined the samples of $\tilde{\boldsymbol{X}}$, the probability of the sample in $\tilde{\boldsymbol{X}}$ can be obtained using the sample number of $\boldsymbol{X}$ in that specific Voronoi region. Now the SROM-based input $\tilde{\boldsymbol{X}}$ is completely constructed and visualised using red dots in Fig. 6-3(b). Specifically, the projection of the red dot on the θ-ψ plane tells the coordinates of the SROM sample, and the height of the red dot represents the probability assigned to this SROM sample. It is clear that the SROM samples in $\tilde{\boldsymbol{X}}$ are assigned very similar probabilities, and are evenly located in the uncertain region: [0, 0.5π] × [0, π]. This is due to the probabilistic nature of the input $\boldsymbol{X}$ (i.e., following uniform distributions in the dimensions of θ and ψ). Please note that a different set of 10000 MC samples in Fig. 6-3(a) (but still accurately characterising the statistics of the input) would yield variations in the choice of SROM samples and probabilities. But such variations are very small and the influence on the accuracy of the result is negligible. Due to the importance of assumed input statistical distributions on the result, one could also consider the influence of assuming Gaussian distributed incidence angles of the plane wave. Such an

investigation would be similar to the example of bivariate Gaussian distributions in [13].

Having constructed the SROM-based input $\widetilde{\boldsymbol{X}}$ for $\boldsymbol{X} = [\theta, \psi]$, the SROM-based output $\widetilde{I_{R3}}$ can be obtained according to Section 2.3.3. Specifically, the samples of $\widetilde{I_{R3}}$ are produced using the deterministic solver, and the probabilities of the samples in $\widetilde{I_{R3}}$ are the same as those in $\widetilde{\boldsymbol{X}}$. On this basis, the statistics (i.e., CDF, mean value, and standard deviation) of the actual induced current I_{R3} can be derived using (2.56)-(2.58) in Chapter 2.

On the other hand, the SC method is also implemented based on sparse-grid sampling computed via the Smolyak algorithm. This sampling technique can significantly reduce the number of times of running the deterministic solver for high random dimensions, compared with the tensor-product sampling. The SC implementation process is decomposed as follows. First, collocation points are selected in the uncertain input region using sparse-grid sampling. Here, SC collocation points are essentially the same as SROM samples, in the sense that the coordinates of each collocation point also contain the value of each random variable to run the deterministic solver once. In other words, the number of collocation points is equal to the number of simulations for SC to derive the analytical relationship between random inputs and the output. The number of collocation points is determined by the random dimension N and the Smolyak construction level k. If N is fixed, the number of collocation points is increased by increasing k, so are the accuracy and computational cost. The coordinates of the collocation point in each dimension can be calculated based on the extrema of Chebyshev polynomials [30]. Having obtained collocation points, the output values at collocation points are calculated using the deterministic solver. On this basis, the Lagrange interpolating function (a common choice of polynomials in the SC implementation) can be used to derive the analytical formula representing the deterministic solver. Now the statistics (mean, standard deviation, and CDF) of the output can be extracted from the output samples obtained by evaluating a sufficient number of input samples using this analytical formula (i.e., the derived efficient form of the deterministic solver).

It is clear that the accuracy of the SC result is dependent on the resolution of the derived analytical formula with respect to the deterministic solver. Since the SC method is not the core of this study, only a concise description of the SC method is given above, and further details can be found in [30] and [74]. The SC application in this chapter is realised using the sparse-grid interpolation toolbox in [76].

In each comparison, the number of SROM samples is chosen the same as that of the SC collocation points. As a result, the two methods consume the same computational cost of running the deterministic solver. Fig. 6-4(a) shows 13 collocation points in the uncertain input region: $[0, 0.5\pi] \times [0, \pi]$, with $k = 2$. In Fig. 6-4(b), the absolute error of the derived SC response for the induced current I_{R3} is plotted together with the theoretical response of I_{R3} (obtained from 200000 MC simulations). As shown in Fig. 6-4(b), the approximated response by the SC method gives exact induced currents at collocation points (i.e., absolute error = 0), but is generally very different from the theoretical response. With the approximated response of I_{R3} being obtained, the statistics of I_{R3} can be efficiently obtained. Please note that the theoretical response of this bivariate example in Fig. 6-4(b) does not present symmetry in the space of random variables. This implies that the proposed example is suitable for evaluation purposes, as symmetry could make SROM, SC, and MC uselessly inefficient.

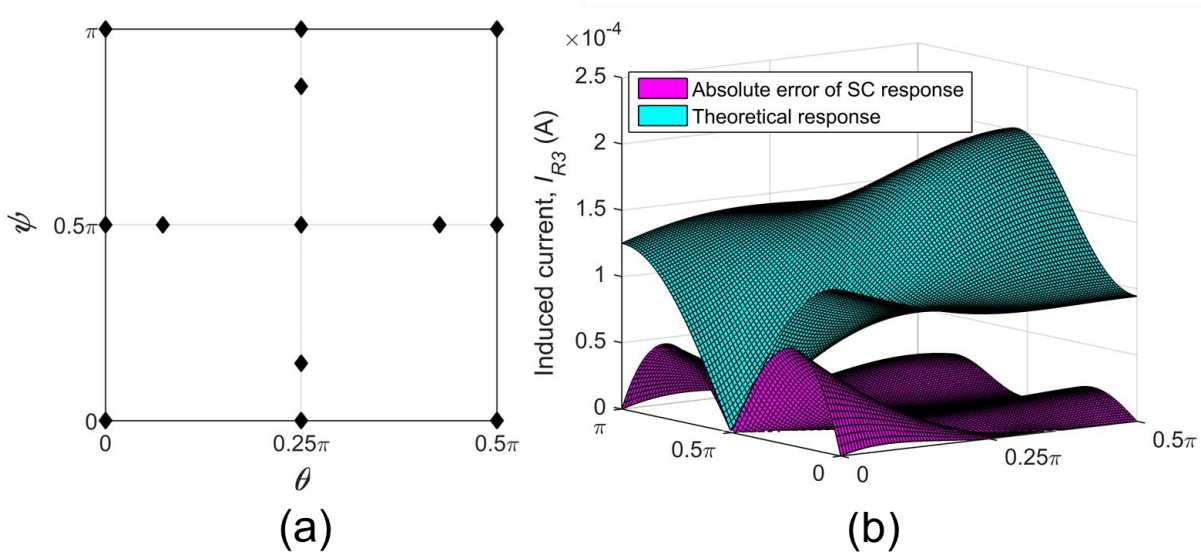

Fig. 6-4. (a) 13 collocation points obtained using sparse-grids based on the extrema of Chebyshev polynomials, with $N = 2$ and $k = 2$. (b) Theoretical response and the error of the SC approximated response using 13 collocation points.

In Fig. 6-5, the derived CDFs of I_{R3} obtained by the SROM and SC methods are compared. Here, the SROM sample number is set to 13, 29, 65, and 145, to equalise the number of SC collocation points at $k = 2$, 3, 4, and 5, respectively. Hereinafter, the sample size can refer to the SROM sample number as well as the SC collocation point number, depending on which method is being discussed. It is clear in Fig. 6-5 that for each method, the derived CDF becomes closer to the reference CDF (given by 200,000 MC simulations) by increasing the

sample size. But the performances of SROM and SC could be different. Specifically, at the sample size of 13, the SROM method gives a more accurate CDF compared to that of SC. However, at the sample size of 29, the CDF given by SC becomes very close to the reference CDF, whereas the SROM-based CDF is still noticeably different (although significantly improved compared to the CDF at 13 samples). This noticeable discrepancy from the staircase-shaped CDF is due to the discontinuity nature of the CDF approximation mechanism in (2.56). To improve the resolution of the SROM-based CDF, one needs to increase the sample size. Seeing the 65-sample case in Fig. 6-5 for example, the difference between the SROM-based and reference CDFs becomes almost indistinguishable. Finally, at the sample size of 145, both methods give the error-free CDF of I_{R3}. In Fig. 6-5, no method shows overwhelming accuracy over the counterpart to predict the CDF of the induced current I_{R3} in the case of random incidence angles θ and ψ.

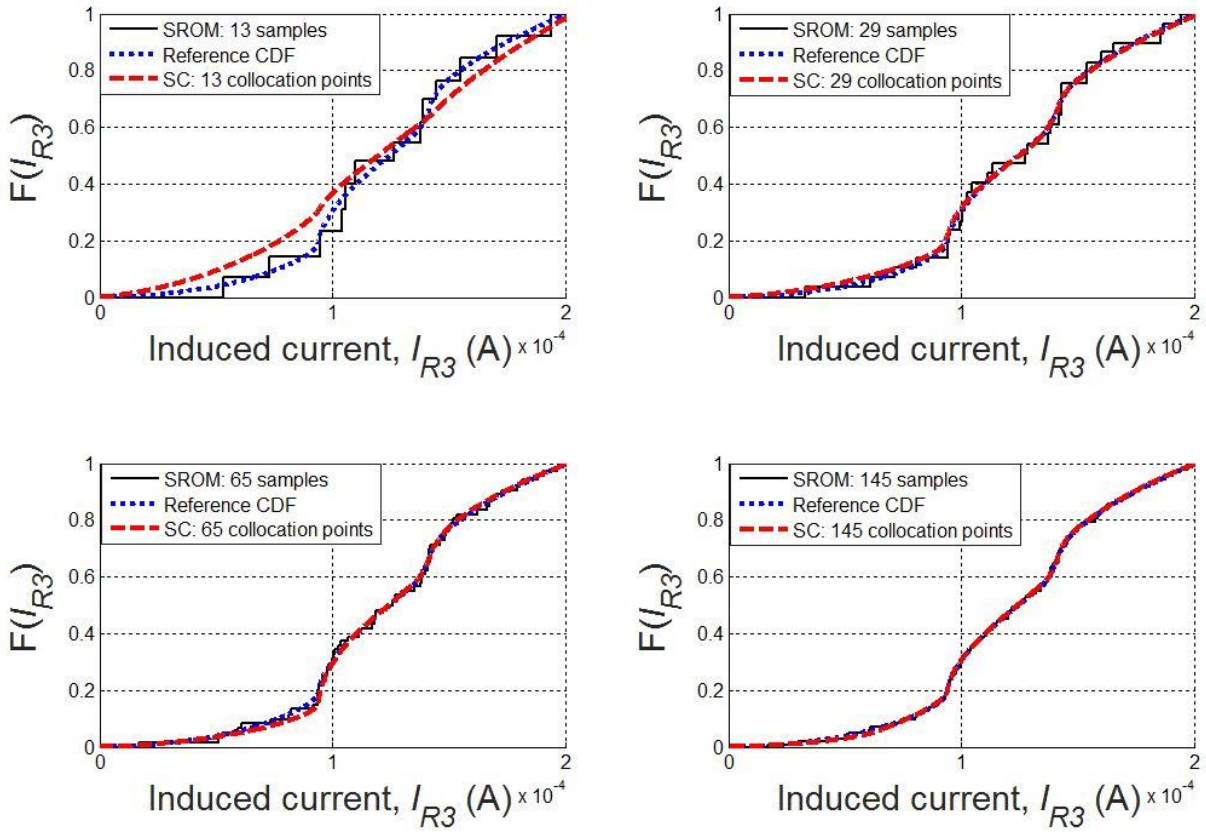

Fig. 6-5. Comparison of the reference CDF of I_{R3}, the CDFs approximated by the SROM-based output $\widetilde{I_{R3}}$ with the sample sizes of 13, 29, 65, and 145, and the CDFs approximated by the SC method with 13, 29, 65, and 145 collocation points (corresponding to k = 2, 3, 4, and 5, respectively).

As shown in Fig. 6-6, the performances of the SROM and SC methods to estimate the mean value μ and standard deviation σ of the induced current I_{R3} are compared at the sample sizes of 5, 13, 29, 65, 145, 321, 705, 1537, and 3329, corresponding to k = 1, 2, …, and 9, respectively. It is clear that in this case the SROM method is more efficient than the SC method to converge with sufficient accuracy.

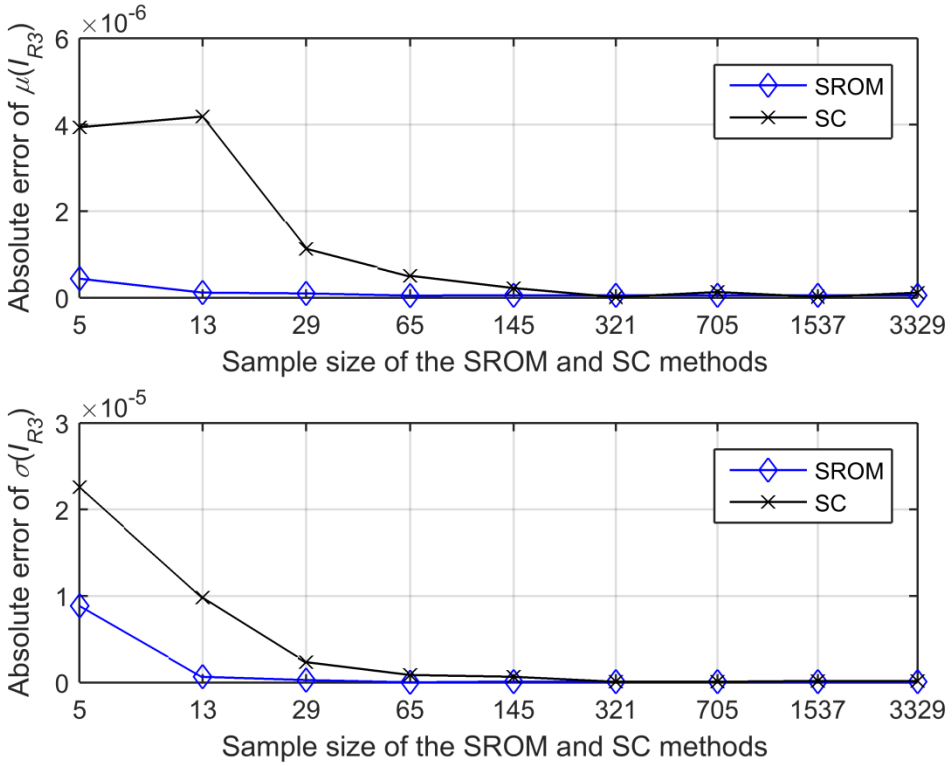

Fig. 6-6. Convergence rates of the SROM and SC methods at the frequency of 50 MHz, when the two random variables are θ and ψ.

Specifically, the SROM method only needs 13 samples to produce accurate μ (I_{R3}) and σ (I_{R3}) (both within the error of 2% with respect to the MC result using 200000 simulations). In contrast, at least 145 collocation points are required for the SC-based μ (I_{R3}) and σ (I_{R3}) to simultaneously converge to the good accuracy level given by SROM at the sample size of 13. The reason is that the approximated response of I_{R3} by the SC method only becomes sufficiently detailed when using 145 collocation points or more.

This can be clearly demonstrated using Fig. 6-7. Specifically, Fig. 6-7(a) shows 145 collocation points in the uncertain input region, and Fig. 6-7(b) shows the absolute error of the derived SC response of I_{R3} together with the theoretical response of I_{R3}. Specifically, in

this case, the derived SC response of I_{R3} is very close to the theoretical response, as the error of the SC response is very small (i.e., almost zero over the uncertain region: [0, 0.5π] × [0, π]). Clearly, increasing the number of SC collocation points is able to improve the accuracy of the derived SC response of the induced current. Please see the obvious error using 13 collocation points in Fig. 6-4(b) for example. Therefore, to obtain accurate μ (I_{R3}) and σ (I_{R3}) in the presence of uncertain θ and ψ, the number of repeated deterministic runs can be reduced by a factor of 145/13 ≈ 11 by replacing the SC method with the SROM method. Finally, the MC method needs around 9000 simulations to converge to the same accuracy level. Hence, the MC process can be expedited by 9000/13 ≈ 692 times using the SROM method.

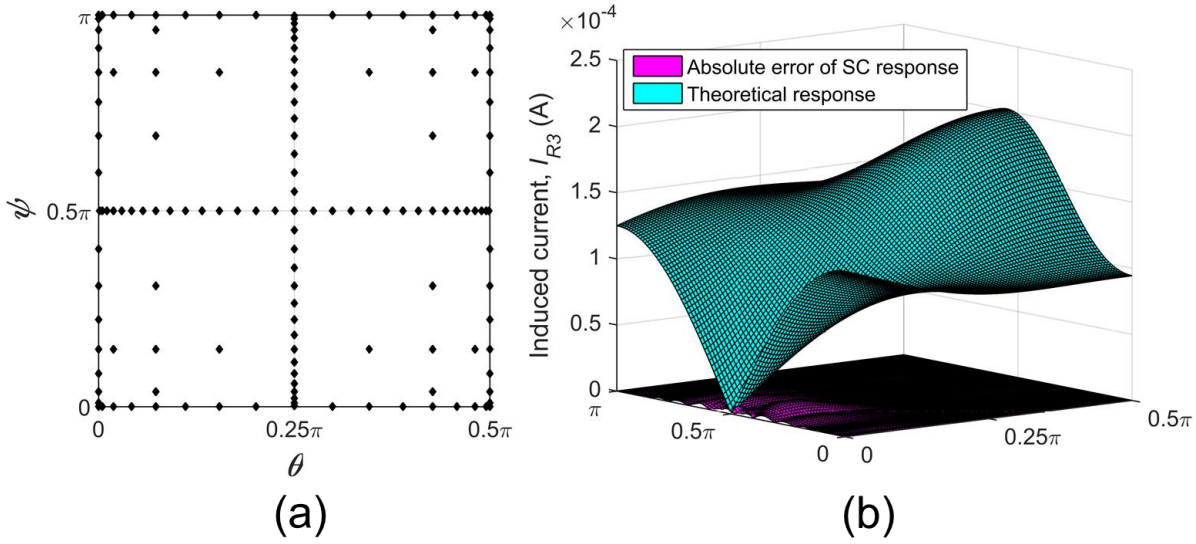

Fig. 6-7. (a) 145 collocation points obtained using sparse-grids based on the extrema of Chebyshev polynomials, with N = 2 and k = 5. (b) Theoretical response and the error of the accurate SC approximated response using 145 collocation points.

Instead of aforementioned discussion at the single frequency of 50 MHz, the comparison between the SROM and SC performances is widened to the frequency range: [10 MHz, 100 MHz] in Fig. 6-8. It is clear that at the sample size of 13, the SROM-based μ (I_{R3}) and σ (I_{R3}) are more accurate than the SC results, especially at the resonance frequency around 80 MHz. It is interesting to see that the errors are increasing when dealing with resonance frequency. This shows that the quality of the approaches could be subject to the complexity of the deterministic mapping. More specifically, the resonating nature of the problem makes the induced current more sensitive to random incidence angles, and consequently degrades the

result accuracy.

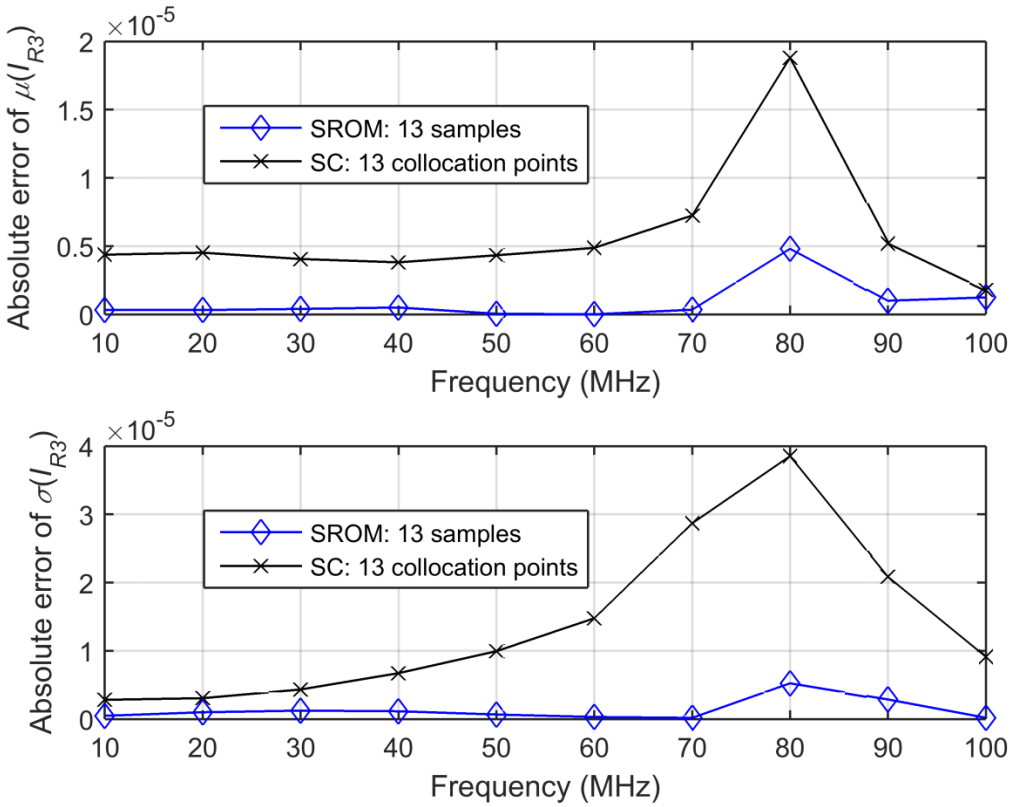

Fig. 6-8. Comparison of the SROM and SC performances to estimate the mean value μ (I_{R3}) and standard deviation σ (I_{R3}) in the frequency range: [10 MHz, 100 MHz].

As shown above, accurate mean value μ and standard deviation σ of the induced current I_{R3} can be obtained at each frequency using the SROM method with 13 samples. For practical purposes, the interval $[\mu - 3\sigma, \mu + 3\sigma]$ can be used as a heuristic and general choice to define approximate upper and lower bounds. On this basis, the variability of I_{R3} can be bounded. To ensure it is worth assuming $\mu + 3\sigma$ as the maximum, one may need to validate with high quantile assessment (such as 0.95, 0.99, 0.995 quantile), which is beyond the scope of this chapter. Please note that Fig. 6-9 only presents the upper boundary in the frequency range: [1 MHz, 100 MHz]. This is because: 1) the upper bound is of more interest for field-to-wire coupling problems, and 2) the lower bound based on $\mu - 3\sigma$ could give minus (i.e., not physically sound) induced currents at some frequencies, and, therefore, is omitted in Fig. 6-9. As shown in Fig. 6-9, it is remarkable that the accurate upper boundary obtained using only 13 SROM samples (i.e., 13 simulations) can hold underneath almost 10000 random simulation results. Comparing 13 simulations by SROM to 10000 simulations by MC, it is

obvious to see the sizable acceleration given by the SROM method.

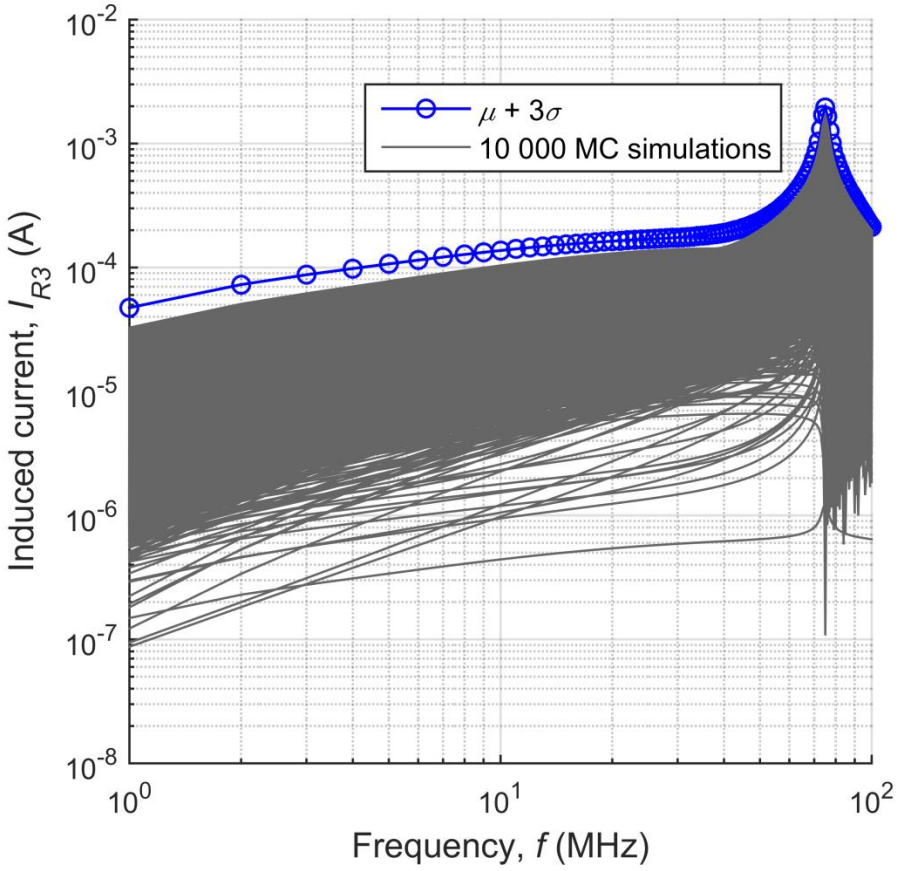

Fig. 6-9. Upper bound of the induced current I_{R3} obtained using the SROM method with only 13 samples, in the presence of the two random variables: θ and ψ.

6.3.2 Random θ, ψ, η, and E_0

In this section, the incident plane-wave field is assumed to be fully stochastically characterised by all four random variables: the incidence angles θ and ψ, field strength E_0, and polarisation angle η. To further complicate the investigated problem, random variables are assumed to follow different probability distribution types. Specifically, the random variables θ, ψ, and η are uniformly distributed in the ranges [0, π/2], [0, π], and [0, 2π], respectively. These variation ranges of the angles cover all possible physical values of the plane wave in the upper half-space without redundancy. Also, E_0 is regarded as a Gaussian random variable with the mean value E (E_0) = 1 V/m and standard deviation σ (E_0) = 0.2 V/m.

In this case, the SROM-based input $\widetilde{\boldsymbol{X}}$ needs to be constructed for the 4-D random variable $\boldsymbol{X} = [\theta, \psi, E_0, \eta]$. For the SC method, at the random dimension $N = 4$, the number of collocation points based on sparse-grid sampling is 9, 41, 137, 401, 1105, 2929, and 7537, corresponding to $k = 1, 2, 3, 4, 5, 6,$ and 7, respectively. It is worth noting the efficiency of sparse-grid sampling over tensor-product sampling in this case. Specifically, the top three minimum numbers of collocation points based on tensor-product sampling are $2^4 = 16$, $3^4 = 81$, and $4^4 = 256$, and can be reduced to 9, 41, and 137 using sparse-grid sampling. Again, the sample sizes for the SROM and SC methods are the same in each comparison. The implementation of the SROM and SC methods follows the same process demonstrated in Section 6.3.1, and, therefore, is not detailed herein.

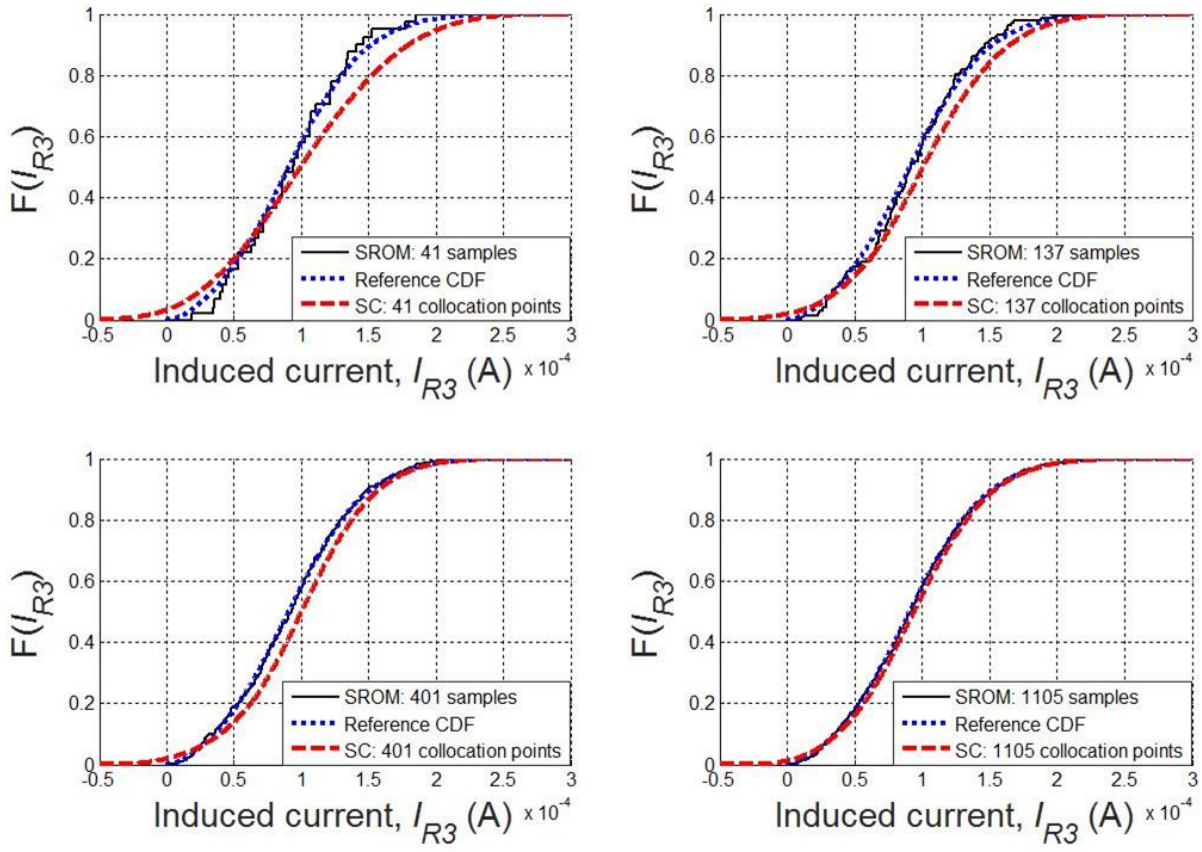

Fig. 6-10. Comparison of the reference CDF of I_{R3}, the CDFs approximated by the SROM-based output $\widetilde{I_{R3}}$ with the sample sizes of 41, 137, 401, and 1105, and the CDFs approximated by the SC method with 41, 137, 401, and 1105 collocation points (corresponding to k = 2, 3, 4, and 5, respectively).

Fig. 6-10 shows the CDFs of the induced current I_{R3} given by the SROM and SC methods using the sample sizes of 41, 137, 401, and 1105. Clearly, the CDF given by each method

becomes more accurate by increasing the sample size. But the SROM-based CDF is generally more accurate than the SC-based CDF. At the sample sizes of 137 and 401, the CDFs given by SROM are already in good agreement with the reference CDF, whereas the CDFs given by SC exhibit obvious discrepancy. The SC method can only produce accurate CDFs by using 1105 collocation points. This is because at least 1105 collocation points are needed to give sufficient resolution to the SC approximated response of I_{R3}. Please note that in this example, the SC method could generate minus (i.e., non-physical) induced currents at the sample size of 41, due to the insufficient resolution of the approximated response. This behaviour could contaminate the statistical information of the induced current. To resolve this problem, one should increase the number of SC collocation points, thus to increase the resolution of the approximated response. Please see the reduced probability of the non-physical current in the 137-sample case in Fig. 6-10 for example.

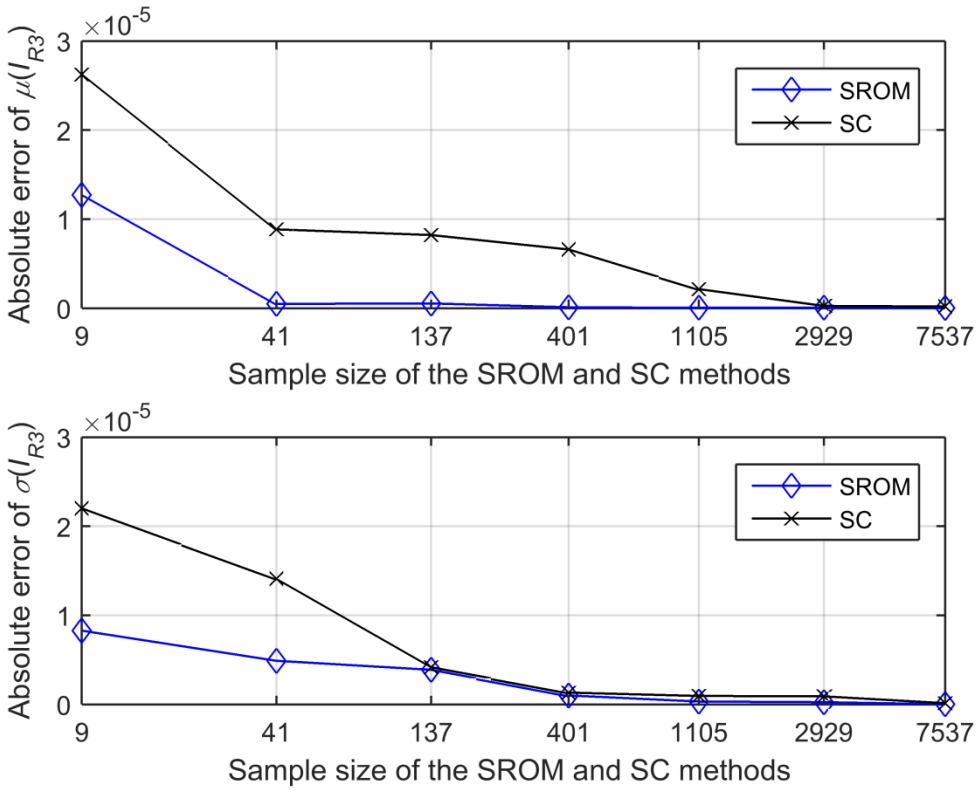

Fig. 6-11. Convergence rates of the SROM and SC methods at the frequency of 50 MHz, when the four random variables are θ, ψ, E_0, and η.

In Fig. 6-11, the convergence rates of the SROM and SC methods are compared at the sample sizes of 9, 41, 137, 401, 1105, 2929, and 7537. It is clear that in this case, the SROM method is more efficient than the SC method to obtain the converged mean value μ (I_{R3}) and standard

deviation σ (I_{R3}). Specifically, the sample size of 401 is sufficient for the SROM method to converge to accurate μ (I_{R3}) and σ (I_{R3}), both within the error of 2%. In contrast, the SC method needs at least a sample size of 1105 to converge to around the same accuracy level. This is in line with the accurate SC-based CDF given by 1105 collocation points in Fig. 6-10. By switching from the SC method to the SROM method, the number of deterministic runs needed for accurate results can be reduced by a factor of 1105/401 ≈ 2.8. Meanwhile, the MC method needs around 23000 simulations to converge to the SROM accuracy level at the sample size of 401. Therefore, the MC analysis can be expedited by 23000/401 ≈ 57 times using the SROM method.

Please note that each method (SROM, SC, and MC) needs a larger sample size to converge in this case than in Section 6.3.1, due to the increment of the random dimension. Please also note that the convergence rate of SC in Fig. 6-11 does not exhibit the exponential feature claimed in [64]. This is because the efficacy of SC can be influenced by the complexity of the deterministic mapping between the input and the output. It is worth noting that the SROM-based μ (I_{R3}) and σ (I_{R3}) at the sample size of 41 are already accurate to some extent, specifically with the errors of 1% and 7%, respectively. Please note that the absolute error in Fig. 6-11 is a small number. This is because the induced current in this case is physically small.

On this basis, Fig. 6-12 shows the heuristic upper bound of the induced current I_{R3} obtained by the SROM method with the sample size of 41. It is clear that almost 10000 MC simulations (except for very few extreme occurrences) are held underneath this upper bound. Therefore, the efficiency of obtaining the upper bound is remarkable using the SROM method. It is interesting to see that the spread of I_{R3} in Fig. 6-12 for the 4-D case is wider than that in Fig. 6-9 for the 2-D case. This is because there are many more possible occurrences in the 4-D case.

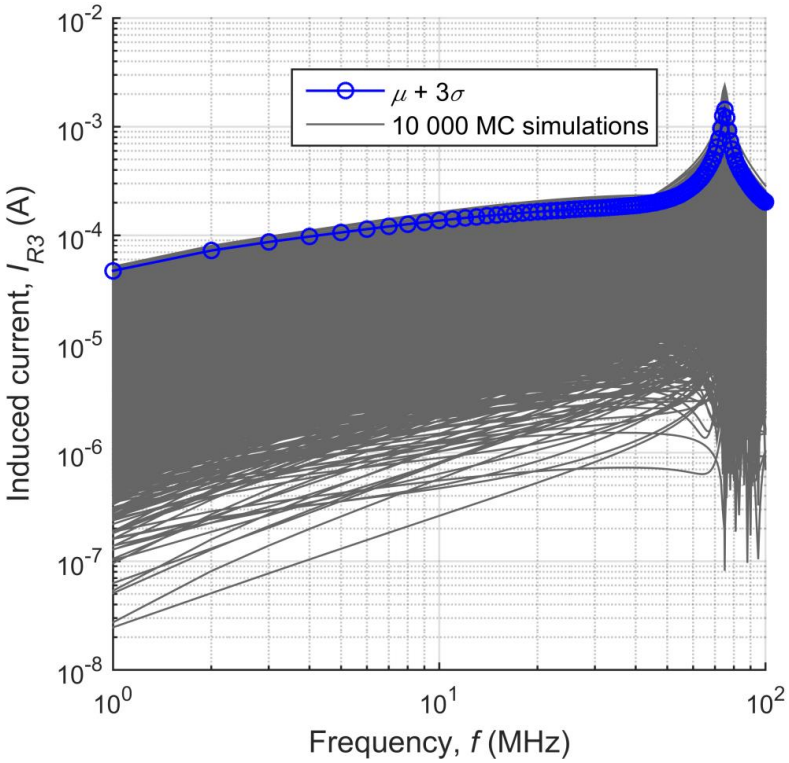

Fig. 6-12. Upper bound of the induced current I_{R3} obtained using the SROM method with only 41 samples, in the presence of the four random variables: θ, ψ, E_0, and η.

6.4 Discussion

This section presents in-depth discussions on the performances of SROM and SC in the 2-dimensional and 4-dimensional examples. It is clear that both the SROM and SC methods are much more efficient than the MC method. Also, the comparison between SROM and SC shows that the SROM method has a faster convergence to produce accurate statistics of the induced current I_{R3}. On the other hand, as shown in the 4-D case, the SC method may generate non-physical induced currents, making the SC result considerably deviate from the reference. However, please note that the presented SC result is given by using the sparse-grid sampling technique, but improved SC variants (such as the adaptive sparse-grid collocation method [74]) are possible, and may produce better performance. The non-intrusive PCE method [64] may also outperform the SROM method in terms of accuracy and computational cost. However, the comparison with every competing technique would be too exhaustive. There is no intention of contriving the examples and results in this chapter to make SROM appear as superior. The demonstrated goodness of the SROM method over the SC method

only holds true in the scope of this chapter, and may become overstated in other cases.

It should be pointed out that the distribution of the output is described via CDF using the SROM method. In fact, the probability density function may be better to show the shape of the distribution tails and estimate the spreading of the system response. But due to the nature of the SROM-based output (i.e., consisting of a set of discrete sample-probability pairs), it may be unfeasible to produce a continuous PDF directly by SROM. Please note that the performance of MC regarding mean, standard deviation, and CDF prediction is neglected in the examples. This is because at such sample sizes, performing a MC analysis with the same number of samples for different values of the random variables considered gives very different results.

Although both the SROM and SC methods need to repeatedly call the deterministic solver, the overall complexity of each method is different. This is because the core of the SROM implementation is to construct an accurate SROM-based input. Then, the statistics of the output can be straightforwardly obtained using (2.56)-(2.58). In contrast, the SC method needs to first select collocation points based on sparse grids, and then derive the approximated response of the output before quantifying the output uncertainty. Table 6-2 shows the computation time required by each method to converge within the error of 2%, and the speed-up factor compared with MC, based on a CPU of 3.4 GHz and RAM of 8 GB. The MC simulation time in Table 6-2 refers to 9000 simulations for the example $\boldsymbol{X} = [\theta, \psi]$ and 23000 simulations for $\boldsymbol{X} = [\theta, \psi, E_0, \eta]$. It is clear that the SROM implementation is faster than SC, and much faster compared to the MC method.

Table 6-2. Computation Time Required by SROM, SC, and MC

EXAMPLE		$\boldsymbol{X}=[\theta, \psi]$	$\boldsymbol{X}=[\theta, \psi, E_0, \eta]$
SROM	Time (s)	0.4	5.9
	Speed-up	367×	63×
SC	Time (s)	8.3	22.1
	Speed-up	18×	17×
MC	Time (s)	146.7	372.5
	Speed-up	-	-

Some questions about the SROM method are still waiting to be solved. For example, there is still no clear guideline on how to choose the optimal sample size m of $\widetilde{\boldsymbol{X}}$, given probability distribution types and the number of dimensions. Also, the performances of the SROM and SC methods in Section 6.3 are based on *a-posteriori* evaluation. This means that the accuracy of each method can only be revealed after comparing the result to the reference. In fact, an *a-priori* evaluation approach would be more desirable. However, this task is extremely difficult. The reason is that the accuracy of the SROM solution is not solely dependent on the SROM approximation of the real input, but also affected by the deterministic mapping (i.e., the problem under investigation). As a result, the *a-priori* accuracy evaluation should be tailored to each specific EMC problem. At the current stage, proposing a general guideline still remains as a bottleneck. On the other hand, it will be worth investigating how the SROM method scales with the number of random variables, given a practical computational resource. However, it may be difficult to yield a general conclusion. This is because the sensitivity of the output to random variables is different in each problem, which could affect the efficacy of the SROM method.

It is worth noting that the cable in this chapter is assumed to be a uniform transmission line with lossless and bare wires. It would certainly be more practical and convincing to consider the cable with some real features. However, this assumption is acceptable in the scope of this chapter. This is because all the uncertainty sources are assumed to be embedded in the incident plane-wave field. This random field is the nucleus component of the statistical analysis. The cable itself is only used as a victim for the current to be induced to.

6.5 Summary

In this chapter, a non-intrusive statistical approach referred to as the SROM method has been applied to efficiently estimate the statistics of the induced current in transmission lines excited by a random incident plane-wave field. The robustness of the SROM method has been validated by assuming the incident wave to be fully statistically characterised. With the SROM method, the accurate statistical information of the induced current (such as the CDF, mean value, standard deviation, and the upper bound) has been obtained with great efficiency.

The performance of the SROM method has been thoroughly compared with other non-

intrusive statistical approaches (SC and MC) for the prediction of the field-to-wire coupling phenomenon. It has been found that the SROM method is more efficient than the SC method in terms of reducing the number of simulations, and much more efficient than the MC method in the examples considered. The advantages and limitations of the SROM method have been thoroughly discussed, such as the implementation simplicity and the difficulty of developing the *a-priori* error evaluation mechanism.

Having demonstrated the impressive accuracy and efficiency of the SROM method in a typical field-to-wire coupling problem, the idea of the SROM method can be suggested to expedite statistical irradiation analysis in complex platforms (such as the cable in aircrafts).

Chapter 7 Efficient Measurement of Stochastic Multipath Field-to-Wire Coupling Using the Reverberation Chamber

7.1 Introduction

In Chapter 6, the variability of the induced current in the cable excited by a random illuminating field has been successfully quantified using the advocated *stochastic reduced order model* (SROM) method. However, it is worth noting that only one incident field illuminating the cable interconnecting system was assumed in the statistical analysis presented in Chapter 6. In fact, this assumption may not be true in many practical cases. This is because multipath electromagnetic waves arriving at the receiver commonly exist in real-world scenarios.

Taking the military aircraft shown in Fig. 7-1 for example, it is very likely to have multiple electromagnetic fields impinging on the aircraft simultaneously from radars or hostile aircrafts. In such a case, the electromagnetic energy coupled into the cable in the fuselage of the aircraft is contributed by all the impinging electromagnetic fields from different directions. Therefore, the multipath illuminations should be considered in the electromagnetic compatibility (EMC) performance test of various devices.

Having understood the significance of considering multipath illuminations, the randomness feature of the multipath illuminating fields needs to be emphasised. This is because the multipath illumination is very sensitive to the uncertainty of the environment. In other words, any variation in the environment may trigger the change in the incident direction, polarisation angle, and field strength of each incident wave. As already demonstrated in Chapter 6, the effect of the random incident wave on the cable coupling is usually very noticeable.

Therefore, it is of great significance to take into account the uncertainty of the multipath illuminating fields.

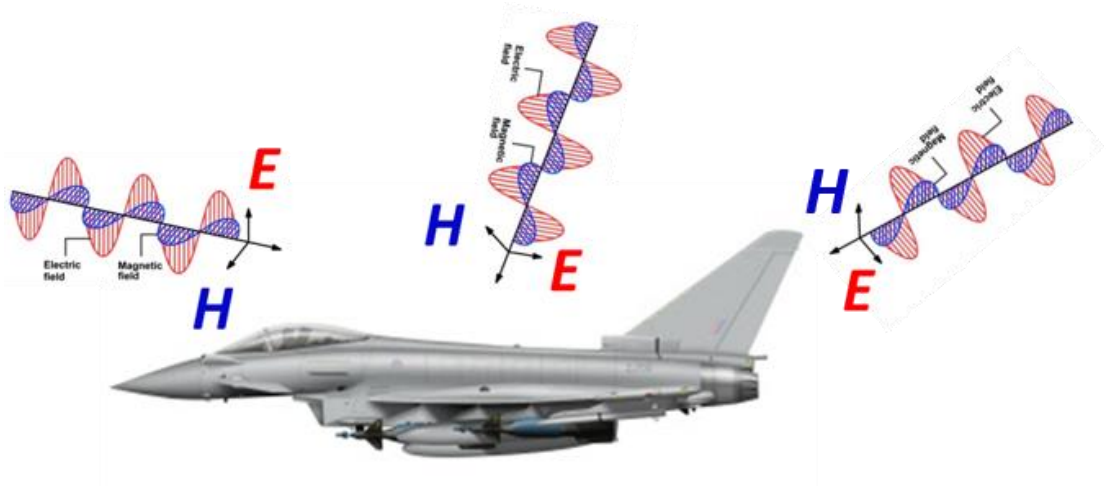

Fig. 7-1. Multipath illumination of electromagnetic waves on the military aircraft under test.

However, due to the complexity of the multipath illuminating problem, it is very difficult to derive the governing equation of the deterministic solver. Therefore, analysing the interference caused by multipath illuminations via simulation may not be suitable, especially when trying to take into account the uncertainty.

On the other hand, using the reverberation chamber [31] is an ideal solution to experimentally analyse the multipath field-to-wire coupling problem, and also to include the effect of the uncertainty of the multipath illumination. This is because in the reverberation chamber, multiple incident waves arrive at the device under test (DUT) simultaneously from different directions. As a result, this feature confirms the validity of using the reverberation chamber to generate the multipath illuminating electromagnetic fields. Also, the randomness of each incident wave can be included in the experiment by rotating the metallic paddles installed in the reverberation chamber to different positions.

Therefore, the reverberation chamber is used in this chapter to quantify the variability of the cable interference introduced by multipath illuminations with parametric uncertainty. The remainder of this chapter is organised as follows: Section 7.2 presents a concise introduction of the principle of the reverberation chamber. The experiment setup of the multipath field-to-wire coupling is described in Section 7.3. The experiment result is discussed in Section 7.4 to demonstrate the efficacy of using the reverberation chamber to statistically analyse the cable

interference caused by uncertainty-embedded multipath illuminations. Finally, the summary of this chapter is given in Section 7.5.

7.2 Principle of the Reverberation Chamber

Essentially, the reverberation chamber (RC) is a shielded room covered with metallic walls in each facet of the room. Typically, the metallic paddle referred to as a stirrer is installed in the chamber to rotate around its axis. At different stirrer positions, the boundary conditions of the electromagnetic fields in the RC are different. This is because the rotation of the stirrer changes the boundary conditions in the RC, resulting in a statistical environment to perform versatile EMC tests.

The RC can be used for a very wide range of applications, such as the radiated emission measurement, the radiated immunity test, the shielding performance evaluation of the cable, and the measurement of the antenna efficiency. In this chapter, the RC is used to measure the radiated emission from the multipath electromagnetic fields to the cable.

Taking the RC in the University of Liverpool for example, the stirrer is installed to a central rotational shaft, and rotates in a stepwise manner. As a result, the boundary conditions of the electromagnetic fields in the RC are changed whenever the stirrer rotates. Accordingly, the location of the peaks and troughs of the fields distributed in the RC is changed as well. In other words, any point in the working volume of the RC will experience strong and weak strengths of the multipath illuminating fields when continuously rotating the stirrer. As a result, the uncertainty of the multipath field strength can be created and taken into account using the RC.

In addition to imitating the uncertainty of the field strength, the RC can also be used to create the random incident angles (i.e., the angle of arrival) of the multipath reflected waves. Again, when rotating the stirrer stepwise, the multipath illumination can impinge on the device under test (DUT) from every possible direction. In fact, the probability of the incident angle taking any direction is equal, yielding the uniform distribution of the incident angle of the multipath electromagnetic fields in the RC. Similarly, the polarisation of the multiple reflected waves in the RC also varies randomly due to the rotation of the stirrer, and follows the uniform distribution. The theoretical explanation of the aforementioned statistics of the multipath electromagnetic fields in the RC can be found in [31] and [107] .

It is worth noting that the aforementioned stirring technique is referred to as the mechanical stirring mechanism. However, there are other stirring mechanisms available, such as the innovative *source stirring* technique proposed in [107] and [108]. For the *source stirring* technique, the incident direction, polarisation angle, and magnitude of the multipath electromagnetic waves are changed by placing the excitation source at different positions in the RC. The aim of these stirring techniques is the same: to make the electromagnetic fields in the RC uniformly distributed and isotropic when averaged over sufficient rotation steps. As a result, the uncertainty in the incident angle, polarisation angle, and field strength of the multipath electromagnetic waves can be created and investigated using the RC. Therefore, the RC is a very useful facility to experimentally analyse the stochastic multipath field-to-wire coupling problem. Also, the result from the RC is repeatable due to the use of statistical analysis.

To ensure that the result of the statistical analysis performed in the RC is valid, one needs to stir the multipath electromagnetic fields as diffusely as possible, in order to make the statistical environment homogenous and isotropic in the RC. This can be achieved by increasing the number of rotation steps of the stirrer when using the mechanical stirring technique. Clearly, the most accurate result of the statistical analysis is given by rotating the stirrer for one cycle (i.e., 360°) with 360 rotation steps (in this case, the stirrer is rotated by 360°/360 = 1° in each rotation step).

For this reason, in this chapter, the statistics of the multipath field-to-wire coupling level given by 360 rotation steps are regarded as the reference result. On this basis, this chapter is dedicated to study the minimum number of rotation steps yet giving the accurate statistics of the coupling level. As a result, the superior efficiency of using the RC to solve uncertainty-embedded multipath field-to-wire coupling problems can be validated. Here, the number of rotation steps represents the number of rotations to cover one cycle. For example, if the number of rotation steps is 180, then the stirrer is rotated by 360°/180 = 2° in each rotation step.

7.3 Experiment Setup

Fig. 7-2 shows the configuration of the RC in the University of Liverpool. The dimension of the RC is of 3.6 m × 5.8 m × 4.0 m. As can be seen in Fig. 7-2, two metallic paddles (i.e.,

stirrers) have been installed to statistically stir the electromagnetic fields in the RC. One stirrer is mounted to a vertical shaft and rotates around this shaft. The other stirrer is designated to rotate around a horizontal shaft placed close to the ceiling. The rotation of the stirrers is driven by motors controlled by the operating system outside the RC.

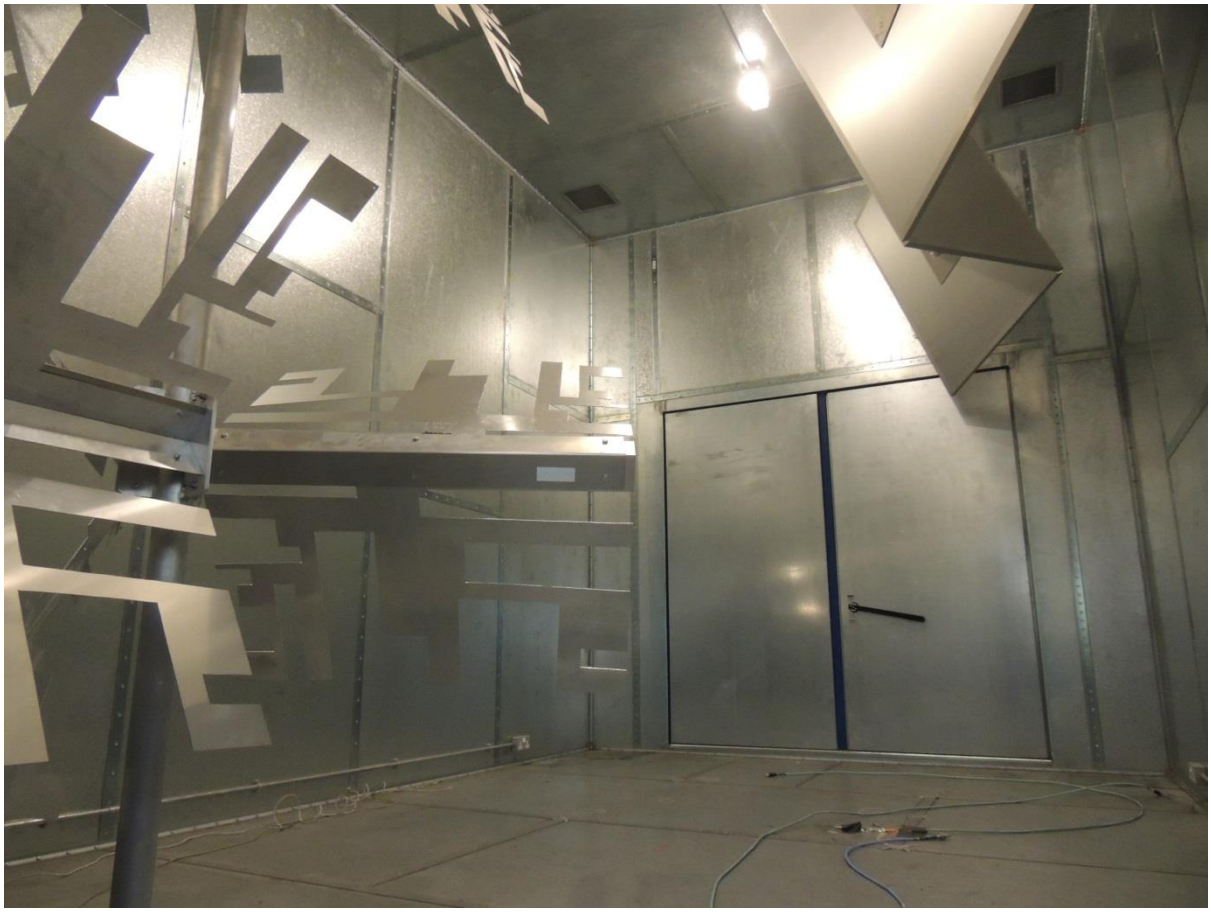

Fig. 7-2. Configuration of the RC in the University of Liverpool.

The configuration of the cable interconnecting system as the DUT in the RC is shown in Fig. 7-3. As can be seen, the cable under test consists of a pair of twisted wires. Each end of the wire is terminated by a radio frequency (RF) termination load with the impedance of 50 Ω. As shown in Fig. 7-3, two vertical aluminium plates are placed at the two ends of the aluminium ground plane. The geometric dimensions of the vertical aluminium plate and the ground plane are of 250 mm × 200 mm and 1500 mm × 500 mm, respectively. Each end of the wire is terminated by an RF load via a bulkhead SMA (Subminiature version A) connector penetrating the vertical plate. The diameter and length of each wire are 1 mm and 1440 mm, respectively. The TWP is placed at the height of 75 mm above the ground plane.

In this study, the twisted-wire pair (TWP) is chosen to model the cable structure. This is because the TWP configuration is widely used to transmit signals (e.g. in the internet cable) due to its good immunity to the external electromagnetic field. Therefore, the immunity of the TWP to random multipath illuminations is worth studying in this chapter.

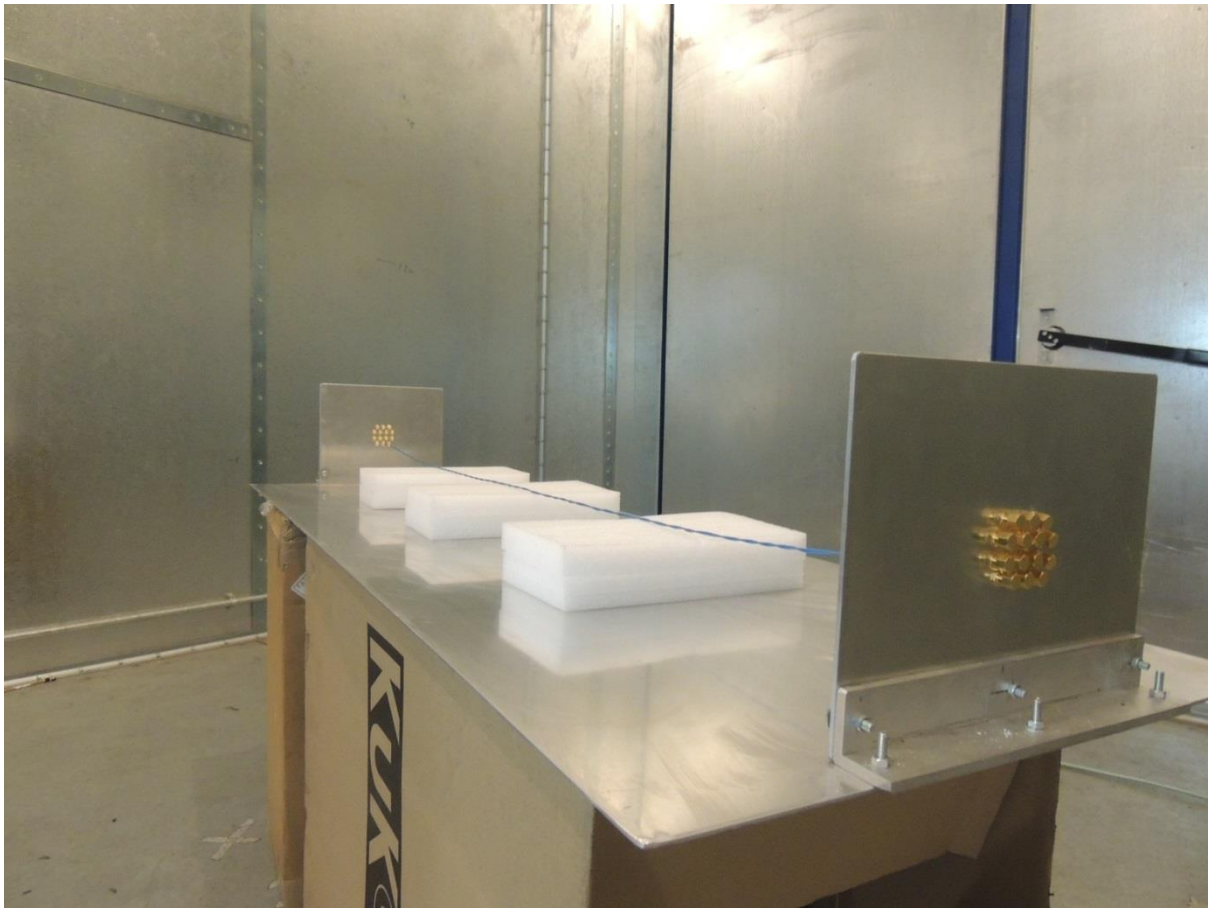

Fig. 7-3. Cable interconnecting system as the DUT.

The experiment setup is shown in Fig. 7-4. Specifically, a log-periodic antenna (type: R&S® HL223) is connected via a cable to Port 1 of a vector network analyser (VNA) placed outside the RC. A current probe (type: ETS-Lindgren 94111-1L) is connected via another cable to Port 2 of the VNA (type: Keysight Fieldfox N9917A). The electromagnetic energy is injected into the RC using the log-periodic antenna. The current probe is clamped around the TWP to measure the coupling from the multipath electromagnetic fields to the TWP. The detailed configuration of the log-periodic antenna setup is shown in Fig. 7-5. In this study, the coupling level is represented using the scattering parameter (or rephrased as the S-parameter [109]) as S_{21}. The DUT is placed in the working volume of the RC to ensure the validity and repeatability of the result.

The frequency range of interest is chosen as: [200 MHz, 1000 MHz], in order to satisfy the lowest usable frequency (150 MHz) of the RC and the operating frequency of the current probe and the log-periodic antenna.

Fig. 7-4. Experiment setup of the random multipath field-to-wire coupling.

7.4 Experimental Results

Having understood the experiment setup in Section 7.3, the experiment result is discussed in this section. First, let us understand the process of deriving the result from an experiment. In the experiment of using N rotation steps, the stir is rotated by a degree of $360/N$ for N times. At each rotation step, the coupling level S_{21} is obtained for each frequency in the range [200 MHz, 1000 MHz]. Therefore, when the experiment is finished, N samples of S_{21} are collected at each frequency. Averaging the N samples at each frequency gives the mean value of the coupling level S_{21} at each frequency. The standard deviation of the interference level at each frequency can be obtained in a similar manner. As mentioned in Section 7.2, the most

accurate result is given by using 360 rotation steps, as all the uncertainties in the incident direction, polarisation angle, and field strength are included in this scenario.

Fig. 7-5. Setup of the transmitting log-periodic antenna.

Now let us focus on the efficiency of using the RC to statistically analyse the coupling to the cable from random multipath electromagnetic illuminations. Specifically, Fig. 7-6 demonstrates the efficiency of using the RC to obtain the accurate mean value and standard deviation of the coupling level S_{21} at the frequency of 200 MHz. Herein, the relative error is used to evaluate the accuracy of the statistics of S_{21} given by each experiment. As can be seen in Fig. 7-6, only 90 rotation steps are required for the resulting statistics of S_{21} to converge within the error of 2% with respect to the reference result given by 360 rotation steps. This superior efficiency is also seen in Fig. 7-7 at the frequency of 300 MHz. As shown in Fig. 7-7, the stirrer only needs to be rotated for 90 times to produce the accurate statistics of the coupling level S_{21} within the error of 2% at 300 MHz. Therefore, although the reference statistics of the interference due to random multipath illuminations are given by 360 rotation

steps, in practice, reasonably accurate statistics can actually be obtained using the RC far before reaching 360 rotation steps.

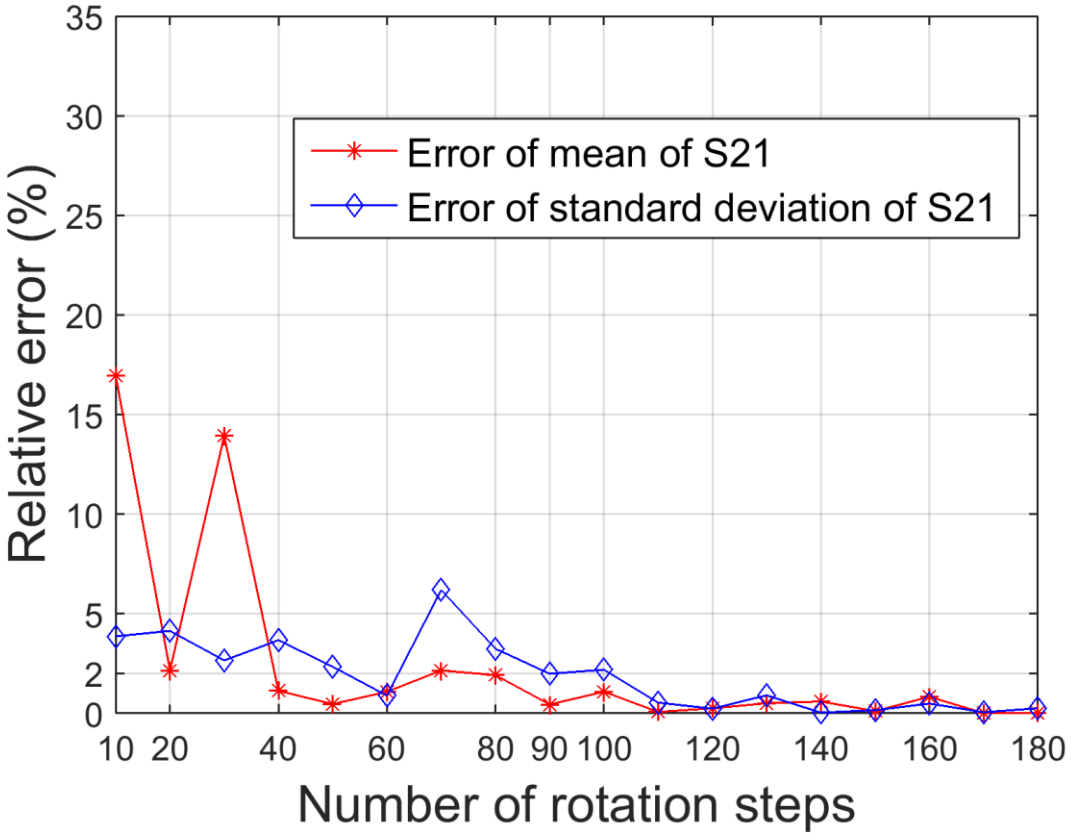

Fig. 7-6. Convergence rate of the mean value and standard deviation of the coupling S_{21} at the frequency of 200 MHz.

In addition to revealing the accurate statistics of the coupling level, the RC is also an efficient facility to obtain the worst-case coupling level affected by random multipath illuminations. As shown in Fig. 7-8, the upper boundary of the cable coupling due to random multipath waves can be obtained using a very small number (i.e., 60 in this case) of rotation steps. In the experiment of using 60 rotation steps, the maximum of the 60 samples of S_{21} at each frequency is collected to produce the worst-case boundary shown as the black curve in Fig. 7-8. As can be seen, this worst-case boundary provides an upper bound to most of the 360 variations of S_{21} given by 360 rotation steps (each variation is a recording of S_{21} at a stirrer position for the frequency range [200 MHz, 1000 MHz]). Here, the result from 360 rotation steps is deemed to include the effect of all the possible cases of the random multipath illuminations. It is worth noting that an experiment with 60 rotation steps in the RC at the University of Liverpool typically lasts around 20 minutes. Therefore, performing the

experiment in the RC to statistically characterise the system response to fully random multipath waves is very time-saving.

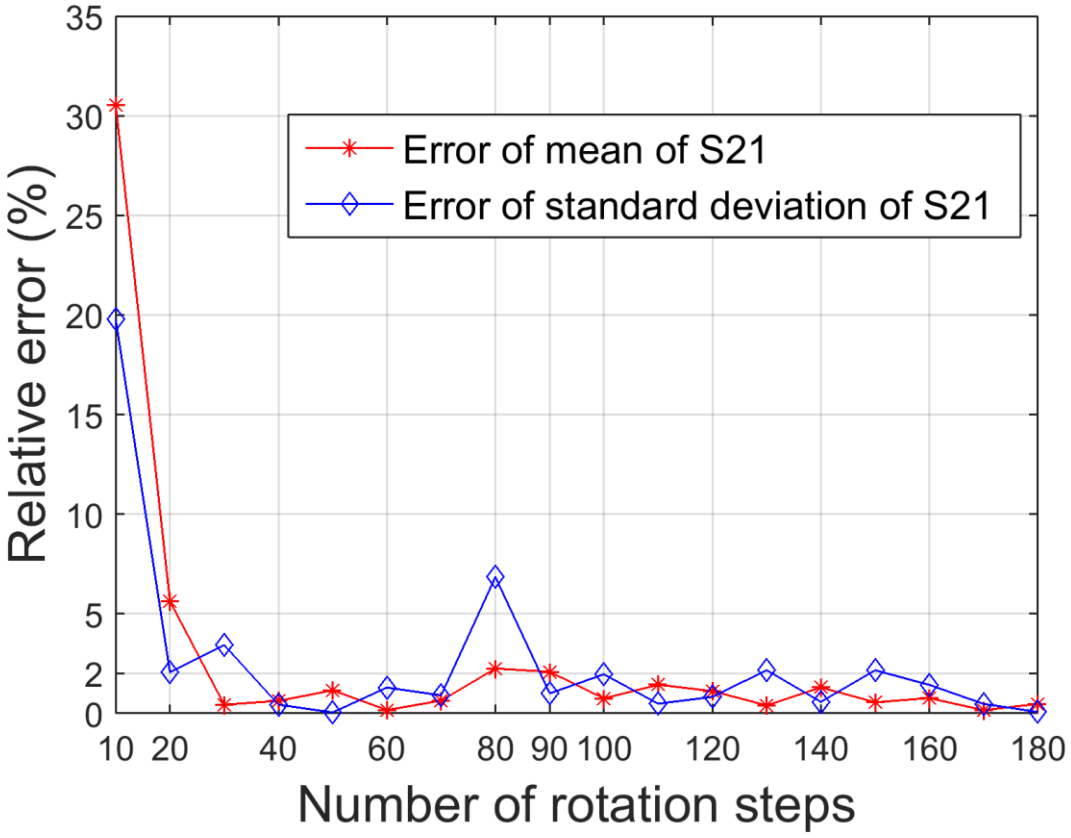

Fig. 7-7. Convergence rate of the mean value and standard deviation of the coupling S_{21} at the frequency of 300 MHz.

7.5 Summary

In this chapter, the necessity of considering random multipath electromagnetic illuminations for real-world EMC testing has been emphasised. Experimental analysis using the RC has been suggested as an efficient approach to solve random multipath field-to-wire coupling problems due to the capability of the RC to create a statistical electromagnetic environment by rotating the stirrer in the RC. To better understand the presented application of the RC, an informative but concise introduction of the RC has also been provided. The experimental results have been used to validate the efficiency of using the RC to obtain the accurate statistics of cable coupling due to the multiple electromagnetic waves with all possible incident directions, polarisation angles, and field strengths. Therefore, based on the results

presented in this chapter, the RC can be recommended as a very powerful facility to statistically characterise the system response affected by random multipath electromagnetic illuminations in other EMC problems.

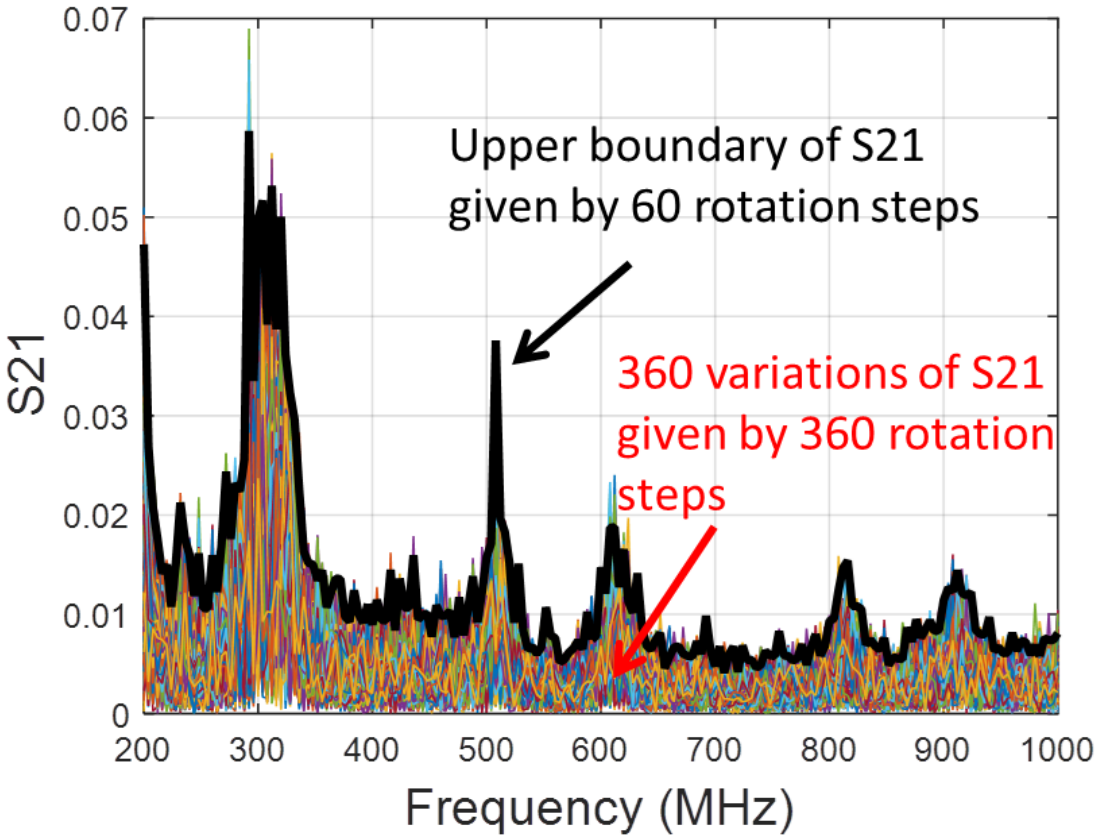

Fig. 7-8. Upper boundary of the coupling S_{21} obtained only using 60 rotation steps.

Chapter 8 Conclusions and Future Work

8.1 Summary of the Thesis

The interference to cables may cause the disastrous malfunction of the cable system. It is of great significance to predict the interference level before the installation of the cable in the system. Due to the inevitable variability residing in the cable implementation layout system, the cable interference becomes a random quantity, and therefore, a statistical description of the interference is required. However, a non-intrusive and efficient statistical analysis framework of cable interference was lacking. Due to this motivation, in this thesis, a novel framework for the statistical analysis of cable interference problems has been constructed using the *stochastic reduced order model* (SROM) method. The idea of the SROM method is to approximate the statistics of random input variables by using a very small number of selected samples assigned with probabilities. Thus, only these selected samples need to be examined without sacrificing accuracy. By using the SROM method, the uncertainty of the variables in the wire-to-wire and field-to-wire coupling scenarios has been successfully propagated to the cable interference. Also, the potential of the SROM method to solve other real-world electromagnetic compatibility (EMC) problems has been demonstrated due to its superior efficiency in dealing with a large number of random variables in the cable EMC problems investigated in this thesis. Now each chapter is summarised as follows.

In Chapter 1, the motivation of developing the statistical analysis framework to solve real-world cable EMC problems has been clearly explained, together with a detailed introduction of the essential terminologies regarding the EMC field.

An overview of the deterministic analysis of cable interference and the state-of-the-art statistical methods (including the advocated SROM method in this thesis) has been presented in Chapter 2. The introduction of the deterministic analysis has given an insightful

understanding of the modelling of cable EMC problems, and laid the foundation on which the statistical method is employed.

In Chapter 3, a parametric study has been performed to investigate how the interference level responds to cable configurational changes. The result of this study has shown the noticeable effect of potential parametric variations on the cable coupling, and demonstrated that the coupling could be sensitive or insensitive to different cable variables. Thus, the necessity of conducting the statistical and sensitivity analyses of cable coupling has been validated.

In Chapter 4, the uncertainty of crosstalk due to potential configurational variations has been successfully quantified using the developed framework based on the SROM method. The performance of the SROM method has been carefully discussed by comparing to that simulated using brute Monte-Carlo (MC) and standard stochastic collocation (SC) methods. The result of this study has validated the efficiency and the straightforward applicability of the SROM method to deal with cable EMC problems affected by parametric uncertainty.

In Chapter 5, the sensitivity of crosstalk to different cable variables has been efficiently quantified using the SROM method. Then, the impacts of different cable variables on changing the crosstalk have been ranked. Based on this ranking, the feasibility of reducing the randomness dimension of the statistical problem by ignoring the weak parametric uncertainty has been explored.

Chapter 6 has demonstrated the application of the SROM method to predict the statistics of the induced current in the cable illuminated by a fully random impinging field. Even in this most complex case, the SROM method has demonstrated a remarkable reduction in the required computational cost for accurate results, compared to the conventional MC method and the state-of-the-art SC method.

In Chapter 7, the significance of considering multipath illuminations in field-to-wire coupling problems has been clarified. A concise description of the principle of the reverberation chamber (RC) has been given to demonstrate its potential applicability in the efficient statistical analysis of the random multipath field-to-wire coupling problems. This potential applicability has been clearly validated using the experimental results. As a result, the RC has been found to be a very useful facility to create a statistical multipath field-to-wire coupling environment, and able to take into account the uncertainty in random multipath illuminations very efficiently.

8.2 Key Contributions

The research work presented in this thesis has produced a comprehensive and in-depth study of the uncertainty quantification of cable interference due to all the coupling mechanisms. The contribution is reflected by building the statistical analysis framework based on the SROM method to deal with cable EMC problems with large randomness dimension in a non-intrusive manner. Specifically, please see [13], [14], [21], [110], [111] for the two journal articles and three conference papers published in the top journals and conferences in the EMC field as the evidence of the contribution of this PhD work.

The most significant contributions as the new knowledge of this field have been presented in Chapter 4 and Chapter 6, and are listed below.

- **Chapter 4: Uncertainty Quantification of Cable Crosstalk**
  This chapter has presented the first successful application of the SROM method in the efficient statistical prediction of cable crosstalk subject to multiple uncertainty sources. The detailed illustration of the SROM implementation in this application is helpful for readers to fully understand the workflow of the SROM method. The demonstrated efficiency and the straightforward applicability should be inspiring for engineers to apply the SROM method in their problems of interest.

- **Chapter 6: Stochastic Analysis of Field-to-Wire Coupling Problems**
  In this chapter, the workflow of using the SROM method to predict the statistics of the induced current in the field-to-wire coupling problem has been clearly presented. This heuristic application has demonstrated the superior efficiency of the SROM method to quantify the variability of the system response affected by a random impinging field. Given its generality feature, the SROM method can be suggested to EMC engineers to accelerate the numerical analysis of the cable system response to a random radiation source.

Other novel contributions generated during this PhD work can be found as follows.

- **Chapter 2: Overview of Deterministic and Stochastic Analyses of Interference**
  A comprehensive literature review has been presented to outline the deterministic analysis for crosstalk prediction, as well as the state-of-the-art uncertainty

quantification methods and their applications in uncertainty-embedded cable EMC problems. This overview is considered very valuable for readers researching into cable crosstalk or general EMC problems affected by parametric uncertainty.

- **Chapter 3: Crosstalk Variations due to Cable Configurational Changes**
  The parametric study performed in this chapter can associate the increase and decrease of the coupling level with the contributing configurational changes. The result of this study is very useful to identify the possible causes for the excessive interference in the cable interconnecting system.

- **Chapter 5: Sensitivity Analysis of Cable Crosstalk**
  The result in this chapter can credit the SROM method as an efficient tool to predict the sensitivity of the output to different input variables. Thus, the weak and strong input variables can be identified. This information is very useful to understand the required accuracy of the value for each input variable in the simulation, or to reduce the computational cost of the statistical analysis using the randomness-dimension reduction technique.

- **Chapter 7: Measurement of Multipath Field-to-Wire Coupling in the RC**
  This chapter has clearly demonstrated the efficiency of using the RC to obtain the statistics of the cable interference due to random multipath illuminations. Therefore, it is promising to suggest using the RC as an efficient facility to experimentally solve other EMC problems affected by random multipath electromagnetic illuminations.

8.3 Future Work

Based on the limitations of the research work presented in this thesis, the future research direction can focus on the uncertainty quantification of crosstalk in more practical cable structures, and on the development of the SROM method. Specifically, the future research work can be conducted in the following areas:

- The first future work will be to investigate the advantage of the SROM method to quantify the crosstalk uncertainty subject to practical uncertainty sources in realistic cable bundles. It is worth noting that the demonstrated scenarios in this thesis are

based on the standard MTL, and therefore lacks practical uncertainty sources in a real random bundle. In order to show the efficacy of the SROM method on predicting crosstalk in a realistic cable bundle, we will need to consider typical uncertainty sources discussed in [25], such as the uncontrolled meandering path of each wire, and the presence of dielectric jackets and lacing cords. This is intended as the future work.

- On the other hand, some questions about the SROM method are still waiting to be solved. For example, there is no clear guideline on how to choose the optimal sample size for the uncertain input space, given that the probability distribution types and the number of random variables are already known. Therefore, in terms of the SROM method itself, the future work can be dedicated to: (1) investigating the maximum dimensionality of the random input space that the SROM method is practically able to handle; and (2) developing an *a-priori* evaluation of the errors of the SROM solution to choose the minimum SROM sample number which guarantees sufficient accuracy.

- Finally, as shown in Chapter 5, the accuracy of the output statistics after reducing the randomness dimension has been found to be dependent on the number of the ignored weak variables in the statistical analysis. Therefore, it is deemed useful to develop an evaluating mechanism to determine the number of weak variables to be ignored in the statistical analysis, with no sacrifice of accuracy.

END

Chapter 9 References

[1] C. R. Paul, *Introduction to Electromagnetic Compatibility,* 2nd ed. Hoboken, N.J., USA: John Wiley & Sons, 2005.

[2] C. Christopoulos, *Principles and Techniques of Electromagnetic Compatibility*, 2nd ed. Boca Raton, F.L., USA: CRC Press, 2005.

[3] C. R. Paul, *Electromagnetics for Engineers: with Applications to Digital Systems and Electromagnetic Interference*, 1st ed. Hoboken, N.J., USA: John Wiley & Sons, 2004.

[4] T. Costlow, "Trimming wiring harness becomes design focus", *Auto. Eng. Mag*., Aug. 2014.

[5] C. R. Spitzer, *The Avionics Handbook*, 1st ed. Boca Raton, F.L., USA: CRC Press, 2001.

[6] Volvo S80 Electrical System of the Future. Available: http://www.volvo.se/rt/trmag/vtr981/article1/a1no198.html. [Accessed: 8-Apr-2017].

[7] P. J. Rensburg and H. C. Ferreira, "Automotive power-line communications: favourable topology for future automotive electronic trends," in *Proc. 7th ISPLC*, Kyoto, Japan, Mar. 2003, pp. 103-108.

[8] G. Millet and D. Dejardin, "Aircraft electrical wiring monitoring system," in *Proc. Embedded Real Time Software and Systems*, Toulouse, France, Feb. 2008, pp. 1-10.

[9] M. Hinchey and L. Coyle, Eds., *Conquering Complexity*. London, UK: Springer, 2012.

[10] Aircraft Wiring and Engineering Services. Available: http://www.safran-group.com/site-safran-en/aerospace/aircraft-equipment/aircraft-power-systems/aircraft-wiring-and-engineering-1001/. [Accessed: 6-Apr-2017].

[11]Sumitomo Wiring Systems – Automotive Wiring Harness. Available: https://www.sws.co.jp/en/product/wireharness/. [Accessed: 6-Apr-2017].

[12] M. Malagoli and L. Cosqueric, "Space harness design optimization opportunities on ECSS derating rules," in *Proc. Space Passive Component Days, ESTEC*, Noordwijk, Netherlands, Sep. 2013, pp. 1-9.

[13] Z. Fei, Y. Huang, J. Zhou, and Q. Xu, "Uncertainty quantification of crosstalk using stochastic reduced order models," *IEEE Trans. Electromagn. Compat.*, vol. 59, no. 1, pp. 228–239, Feb. 2017.

[14] Z. Fei, Y. Huang, J. Zhou, and C. Song, "Numerical analysis of a transmission line illuminated by a random plane-wave field using stochastic reduced order models," *IEEE Access*, vol. 5, pp. 8741–8751, May 2017.

[15] C. R. Paul, "Solution of the transmission-line equations for three-conductor lines in homogeneous media," *IEEE Trans. Electromagn. Compat.*, vol. EMC-20, no. 1, pp. 216–222, Feb. 1978.

[16] S. Pignari and F. G. Canavero, "Theoretical assessment of bulk current injection versus radiation," *IEEE Trans. Electromagn. Compat.*, vol. 38, no. 3, pp. 469–477, Aug. 1996.

[17] F. Rachidi, "A review of field-to-transmission line coupling models with special emphasis to lightning-induced voltages on overhead lines," *IEEE Trans. Electromagn. Compat.*, vol. 54, no. 4, pp. 898–911, Aug. 2012.

[18] C. R. Paul, *Analysis of Multiconductor Transmission Lines*, 2nd ed. Hoboken, N.J., USA: Wiley-Interscience: IEEE Press, 2008.

[19] CST-Computer Simulation Technology. Available: http://www.cst.com/. [Accessed: 12-May-2014]

[20] FEKO-EM Simulation Software. Available: https://www.feko.info/. [Accessed: 8-Apr-2017]

[21] Z. Fei, Y. Huang, and J. Zhou, "Crosstalk variations caused by uncertainties in three-conductor transmission lines," in *Proc. LAPC*, Loughborough, UK, Nov. 2015, pp. 1–5.

[22] F-35 Joint Strike Fighter Official homepage. Available: http://www.jsf.mil. [Accessed: 8-Apr-2017].

[23] C. Maul, J. W. McBride, and J. Swingler, "Intermittency phenomena in electrical onnectors," *IEEE Trans. Compon. Packag. Technol.*, vol. 24, no. 3, pp. 370–377, Sep. 2001.

[24] P. Manfredi and F. G. Canavero, "Polynomial chaos for random field coupling to transmission lines," *IEEE Trans. Electromagn. Compat.*, vol. 54, no. 3, pp. 677–680, Jun. 2012.

[25] D. Bellan and S. A. Pignari, "Efficient estimation of crosstalk statistics in random wire bundles with lacing cords," *IEEE Trans. Electromagn. Compat.*, vol. 53, no. 1, pp. 209–218, Feb. 2011.

[26] A. Papoulis and S. U. Pillai, *Probability, Random Variables, and Stochastic Processes*, 4th ed., Internat. ed., Nachdr. Boston, Mass.: McGraw-Hill, 2009.

[27] M. Grigoriu, "Reduced order models for random functions. Application to stochastic problems," *Appl. Math. Model.*, vol. 33, no. 1, pp. 161–175, Jan. 2009.

[28] C. Robert and G. Casella, *Introducing Monte Carlo Methods with R*. New York, NY: Springer New York, 2010.

[29] D. Xiu and G. E. Karniadakis, "The Wiener-Askey polynomial chaos for stochastic differential equations," *SIAM J. Sci. Comput.*, vol. 24, no. 2, pp. 619–644, Jan. 2002.

[30] D. Xiu, "Efficient collocational approach for parametric uncertainty analysis," *Commun. Comput. Phys.*, vol. 2, no. 2, pp. 293–309, Apr. 2017.

[31] S. J. Boyes and Y. Huang, *Reverberation Chambers: Theory and Applications to EMC and Antenna Measurements*. Chichester, West Sussex, UK: Wiley, 2016.

[32] C. Paul and A. Feather, "Computation of the transmission line inductance and capacitance matrices from the generalized capacitance matrix," *IEEE Trans. Electromagn. Compat.*, vol. EMC-18, no. 4, pp. 175–183, Nov. 1976.

[33] C. R. Paul, "Useful matrix chain parameter identities for the analysis of multiconductor transmission lines," *IEEE Trans. Microw. Theory Tech.*, vol. 23, no. 9, pp. 756–760, Sep. 1975.

[34] X. Meng, P. Sewell, A. Vukovic, Z. W. Zhang, and T. Benson, "Experimental benchmarking of unstructured transmission line modelling (UTLM) method for simulations of explicitly meshed wiring," in *Proc. CEM*, Izmir, Turkey, Jul. 2015, pp. 46–47.

[35] P. D. Sewell, T. M. Benson, A. Vukovic, and X. Meng, "Complexity reduction of multiscale UTLM cell clusters," *IEEE J. Multiscale Multiphysics Comput. Tech*., vol. 2, pp.18-28, Feb. 2017.

[36] R. E. Matick, *Transmission Lines and Communication Networks: An Introduction to Transmission Lines, High-frequency and High-speed Pulse Characteristics and Applications.* Hoboken: Wiley-IEEE Press, 2000.

[37] S. A. Pignari, D. Bellan, and G. Spadacini, "Characterisation of crosstalk in terms of mean value and standard deviation," *IEE Proc. - Sci. Meas. Technol.*, vol. 150, no. 6, pp. 289–295, Nov. 2003.

[38] C. R. Paul, "Solution of the transmission-line equations under the weak-coupling assumption," *IEEE Trans. Electromagn. Compat.*, vol. 44, no. 3, pp. 413–423, Aug. 2002.

[39] C. R. Paul, "Derivation of common impedance coupling from the transmission-line equations," *IEEE Trans. Electromagn. Compat.*, vol. 34, no. 3, pp. 315–319, Aug. 1992.

[40] K. M. Coperich, J. Morsey, V. I. Okhmatovski, A. C. Cangellaris, and A. E. Ruehli, "Systematic development of transmission-line models for interconnects with frequency-dependent losses," *IEEE Trans. Microw. Theory Tech.*, vol. 49, no. 10, pp. 1677–1685, Oct. 2001.

[41] B. Cannas, A. Fanni, and F. Maradei, "A neural network approach to predict the crosstalk in non-uniform multiconductor transmission lines," in *Proc. ISCAS*, Phoenix-Scottsdale, USA, May 2002, pp. 573-576.

[42] C. R. Paul, "Decoupling the multiconductor transmission line equations," *IEEE Trans. Microw. Theory Tech.*, vol. 44, no. 8, pp. 1429–1440, Aug. 1996.

[43] F. Dai, G. H. Bao, and D. L. Su, "Crosstalk prediction in non-uniform cable bundles based on neural network," in *Proc. ISAPE2010*, Guangzhou, China. Nov. 2010, pp. 1043–1046.

[44] M. Gonser, C. Keller, J. Hansen, and R. Weigel, "Advanced simulations of automotive EMC measurement setups using stochastic cable bundle models," in *Proc. APEMC*, Beijing, China, Apr. 2010, pp. 590–593.

[45] C. Jullien, P. Besnier, M. Dunand, and I. Junqua, "Advanced modeling of crosstalk between an unshielded twisted pair cable and an unshielded wire above a ground plane," *IEEE Trans. Electromagn. Compat.*, vol. 55, no. 1, pp. 183–194, Feb. 2013.

[46] A. Shoory, M. Rubinstein, A. Rubinstein, C. Romero, N. Mora, and F. Rachidi, "Application of the cascaded transmission line theory of Paul and McKnight to the evaluation of NEXT and FEXT in twisted wire pair bundles," *IEEE Trans. Electromagn. Compat.*, vol. 55, no. 4, pp. 648–656, Aug. 2013.

[47] C. R. Paul, "Sensitivity of crosstalk to variations in wire position in cable bundles," in *Proc. IEEE Symposium on EMC*, Atlanta, GA, USA. Aug. 1987, pp. 1–5.

[48] S. Shiran, B. Reiser, and H. Cory, "A probabilistic method for the evaluation of coupling between transmission lines," *IEEE Trans. Electromagn. Compat.*, vol. 35, no. 3, pp. 387–393, Aug. 1993.

[49] A. Ajayi, P. Ingrey, P. Sewell, and C. Christopoulos, "Direct computation of statistical variations in electromagnetic problems," *IEEE Trans. Electromagn. Compat.*, vol. 50, no. 2, pp. 325–332, May 2008.

[50] M. Wu, D. Beetner, T. Hubing, Haixin Ke, and S. Sun, "Estimation of the statistical variation of crosstalk in wiring harnesses," in *Proc. IEEE Int. Sym. EMC 2008*, Detroit, MI, USA, Aug. 2008, pp. 1–7.

[51] X. Li, M. L. Wu, D. Beetner, and T. Hubing, "Rapid simulation of the statistical variation of crosstalk in cable harness bundles," in *Proc. IEEE Int. Sym. EMC*, Fort Lauderdale, FL, USA, Jul. 2010, pp. 614–619.

[52] M. Wu, D. G. Beetner, T. H. Hubing, H. Ke, and S. Sun, "Statistical prediction of reasonable worst-case crosstalk in cable bundles", *IEEE Trans. Electromagn. Compat.*, vol. 51, no. 3, pp. 842–851, Aug. 2009.

[53] M. S. Halligan and D. G. Beetner, "Maximum crosstalk estimation in lossless and homogeneous transmissionlLines", *IEEE Trans. Microw. Theory Tech.*, vol. 62, no. 9, pp. 1953–1961, Sep. 2014.

[54] M. S. Halligan and D. G. Beetner, "Maximum crosstalk estimation in weakly coupled transmission lines," *IEEE Trans. Electromagn. Compat.*, vol. 56, no. 3, pp. 736–744, Jun. 2014.

[55] I. Babuška, F. Nobile, and R. Tempone, "A stochastic collocation method for elliptic partial differential equations with random input data," *SIAM J. Numer. Anal.*, vol. 45, no. 3, pp. 1005–1034, Jan. 2007.

[56] S. Salio, F. Canavero, D. Lecointe, and W. Tabbara, "Crosstalk prediction on wire bundles by Kriging approach," in *Proc. IEEE Int. Sym. EMC*, Washington, DC, USA, Aug. 2000, pp. 197–202.

[57] S. Sun, G. Liu, J. L. Drewniak, and D. J. Pommerenke, "Hand-assembled cable bundle modeling for crosstalk and common-mode radiation prediction," *IEEE Trans. Electromagn. Compat.*, vol. 49, no. 3, pp. 708–718, Aug. 2007.

[58] O. G. Ernst, A. Mugler, H. J. Starkloff, and E. Ullmann, "On the convergence of generalized polynomial chaos expansions," *ESAIM Math. Model. Numer. Anal.*, vol. 46, no. 2, pp. 317–339, Mar. 2012.

[59] R. Askey and J. Wilson, "Some basic hypergeometric orthogonal polynomials that generalize Jacobi polynomials," *Mem. Am. Math. Soc.*, vol. 54, no. 319, pp. 1–10, Mar. 1985.

[60] N. Wiener, "The homogeneous chaos," *Am. J. Math.*, vol. 60, no. 4, pp. 897-936, Oct. 1938.

[61] R. G. Ghanem and P. D. Spanos, *Stochastic Finite Elements: A Spectral Approach*. New York, NY: Springer New York, 1991.

[62] J. A. S. Witteveen and H. Bijl, "Modeling arbitrary uncertainties using gram-schmidt polynomial chaos," in *Proc. AIAA*, Reno, Nevada, USA, Jan. 2006, pp. 1-17.

[63] X. Wan and G. E. Karniadakis, "Multi-element generalized polynomial chaos for arbitrary probability measures," *SIAM J. Sci. Comput.*, vol. 28, no. 3, pp. 901–928, Jan. 2006.

[64] M. Eldred, "Recent advances in non-intrusive polynomial chaos and stochastic collocation methods for uncertainty analysis and design," in *Proc. 50th AIAA*, Palm Springs, California, USA, May 2009, pp. 1-37.

[65] M. Eldred, C. Webster, and P. Constantine, "Evaluation of non-intrusive approaches for wiener-askey generalized polynomial chaos," in *Proc.49th AIAA*, Schaumburg, IL, USA, Apr. 2008, pp. 1-22.

[66] P. Manfredi and F. G. Canavero, "General decoupled method for statistical interconnect simulation via polynomial chaos," in *Proc. EPEPS*, Portland, OR, USA, Oct. 2014, pp. 25–28.

[67] I. S. Stievano, P. Manfredi, and F. G. Canavero, "Stochastic analysis of multiconductor cables and interconnects," *IEEE Trans. Electromagn. Compat.*, vol. 53, no. 2, pp. 501–507, May 2011.

[68] I. S. Stievano, P. Manfredi, and F. G. Canavero, "Parameters variability effects on multiconductor interconnects via hermite polynomial chaos," *IEEE Trans. Compon. Packag. Manuf. Technol.*, vol. 1, no. 8, pp. 1234–1239, Aug. 2011.

[69] D. Vande Ginste, D. De Zutter, D. Deschrijver, T. Dhaene, P. Manfredi, and F. Canavero, "Stochastic modeling-based variability analysis of on-chip interconnects," *IEEE Trans. Compon. Packag. Manuf. Technol.*, vol. 2, no. 7, pp. 1182–1192, Jul. 2012.

[70] D. Xiu, "Stochastic collocation methods: a survey," in *Handbook of Uncertainty Quantification*, R. Ghanem, D. Higdon, and H. Owhadi, Eds. Cham: Springer International Publishing, 2015, pp. 1–18.

[71] D. Xiu and J. S. Hesthaven, "High-order collocation methods for differential equations with random inputs," *SIAM J. Sci. Comput.*, vol. 27, no. 3, pp. 1118–1139, Jan. 2005.

[72] J. Bai, G. Zhang, D. Wang, A. P. Duffy, and L. X. Wang, "Performance comparison of the SGM and the SCM in EMC simulation," *IEEE Trans. Electromagn. Compat.*, vol. 58, no. 1, pp. 1739–1746, Sep. 2016.

[73] J. E. Warner, W. Aquino, and M. D. Grigoriu, "Stochastic reduced order models for inverse problems under uncertainty," *Comput. Methods Appl. Mech. Eng.*, vol. 285, pp. 488–514, Mar. 2015.

[74] B. Ganapathysubramanian and N. Zabaras, "Sparse grid collocation schemes for stochastic natural convection problems," *J. Comput. Phys.*, vol. 225, no. 1, pp. 652–685, Jul. 2007.

[75] S. A. Smolyak, "Quadrature and interpolation formulas for tensor products of certain classes of functions," *Sov. Math. Dokl.*, vol. 4, pp. 240–243, 1963.

[76] Sparse Grid Interpolation Toolbox. Available: http://www.ians.uni-stuttgart.de/spinterp. [Accessed: 5-May-2016].

[77] S. J. Julier and J. K. Uhlmann, "Consistent debiased method for converting between polar and cartesian coordinate systems," in *Proc. AEROsENSE'97*, Orlando, FL, USA, Jul. 1997, pp. 110–121.

[78] L. R. A. X. de Menezes, A. Ajayi, C. Christopoulos, P. Sewell, and G. A. Borges, "Efficient computation of stochastic electromagnetic problems using unscented transforms," *IET Sci. Meas. Technol.*, vol. 2, no. 2, pp. 88–95, Mar. 2008.

[79] R. V. Field, M. Grigoriu, and J. M. Emery, "On the efficacy of stochastic collocation, stochastic Galerkin, and stochastic reduced order models for solving stochastic problems," *Probabilistic Eng. Mech.*, vol. 41, pp. 60–72, Jul. 2015.

[80] M. Grigoriu, "Effective conductivity by stochastic reduced order models (SROMs)," *Comput. Mater. Sci.*, vol. 50, no. 1, pp. 138–146, Nov. 2010.

[81] J. E. Warner, M. Grigoriu, and W. Aquino, "Stochastic reduced order models for random vectors: Application to random eigenvalue problems," *Probabilistic Eng. Mech.*, vol. 31, pp. 1–11, Jan. 2013.

[82] M. Grigoriu, "Solution of linear dynamic systems with uncertain properties by stochastic reduced order models," *Probabilistic Eng. Mech.*, vol. 34, pp. 168–176, Oct. 2013.

[83] S. Sarkar, J. E. Warner, W. Aquino, and M. D. Grigoriu, "Stochastic reduced order models for uncertainty quantification of intergranular corrosion rates," *Corros. Sci.*, vol. 80, pp. 257–268, Mar. 2014.

[84] Q. Du, V. Faber, and M. Gunzburger, "Centroidal voronoi tessellations: applications and algorithms," *SIAM Rev.*, vol. 41, no. 4, pp. 637–676, Jan. 1999.

[85] Mathworks. Available: http://www.mathworks.com/. [Accessed: 31-May-2014]

[86] A. Ciccolella and F. Canavero, "Statistical simulation of crosstalk in bundles," in *Proc. IEEE Int. Symp. EMC*, Zurich, Switzerland, Aug. 1995, pp. 51–56.

[87] S. Pignari, D. Bellan, and L. Di Rienzo, "Statistical estimates of crosstalk in three-conductor transmission lines," in *Proc. Int. Symp. EMC 2002*, Minneapolis, MN, USA, Aug. 2002, pp. 877–882.

[88] D. Xiu, "Fast numerical methods for stochastic computations: a review," *Commun. Comput. Phys.*, vol. 27, no. 3, pp. 842–851, Feb. 2009.

[89] C. Paul, "Estimation of crosstalk in three-conductor transmission lines," *IEEE Trans. Electromagn. Compat.*, vol. EMC-26, no. 4, pp. 182–192, Nov. 1984.

[90] A. Diouf and F. Canavero, "Crosstalk statistics via collocation method," in *Proc. IEEE Int. Sym. EMC*, Austin, USA, Aug. 2009, pp. 92–97.

[91] F. N. Fritsch and R. E. Carlson, "Monotone piecewise cubic interpolation," *SIAM J. Numer. Anal.*, vol. 17, no. 2, pp. 238–246, Apr. 1980.

[92] E. Meijering, "A chronology of interpolation: from ancient astronomy to modern signal and image processing," *Proc. IEEE*, vol. 90, no. 3, pp. 319–342, Mar. 2002.

[93] H. Osnes and J. Sundnes, "Uncertainty analysis of ventricular mechanics using the probabilistic collocation method," *IEEE Trans. Biomed. Eng.*, vol. 59, no. 8, pp. 2171–2179, Aug. 2012.

[94] C. Taylor, R. Satterwhite, and C. Harrison, "The response of a terminated two-wire transmission line excited by a nonuniform electromagnetic field," *IEEE Trans. Antennas Propag.*, vol. 13, no. 6, pp. 987–989, Nov. 1965.

[95] C. Paul, "Frequency response of multiconductor transmission lines illuminated by an electromagnetic field," *IEEE Trans. Electromagn. Compat.*, vol. EMC-18, no. 4, pp. 183–190, Nov. 1976.

[96] R. B. Armenta and C. D. Sarris, "Efficient evaluation of the terminal response of a twisted-wire pair excited by a plane-wave electromagnetic field," *IEEE Trans. Electromagn. Compat.*, vol. 49, no. 3, pp. 698–707, Aug. 2007.

[97] S. A. Pignari and G. Spadacini, "Plane-wave coupling to a twisted-wire pair above ground," *IEEE Trans. Electromagn. Compat.*, vol. 53, no. 2, pp. 508–523, May 2011.

[98] G. Spadacini, F. Grassi, F. Marliani, and S. A. Pignari, "Transmission-line model for field-to-wire coupling in bundles of twisted-wire pairs above ground," *IEEE Trans. Electromagn. Compat.*, vol. 56, no. 6, pp. 1682–1690, Dec. 2014.

[99] M. Omid, Y. Kami, and M. Hayakawa, "Field coupling to nonuniform and uniform transmission lines," *IEEE Trans. Electromagn. Compat.*, vol. 39, no. 3, pp. 201–211, Aug. 1997.

[100] G. Spadacini and S. A. Pignari, "Numerical assessment of radiated susceptibility of twisted-wire pairs with random nonuniform twisting," *IEEE Trans. Electromagn. Compat.*, vol. 55, no. 5, pp. 956–964, Oct. 2013.

[101] G. Antonini, S. Cristina, and A. Orlandi, "PEEC modeling of lightning protection systems and coupling to coaxial cables," *IEEE Trans. Electromagn. Compat.*, vol. 40, no. 4, pp. 481–491, Nov. 1998.

[102] D. Bellan and S. Pignari, "A probabilistic model for the response of an electrically short two-conductor transmission line driven by a random plane wave field," *IEEE Trans. Electromagn. Compat.*, vol. 43, no. 2, pp. 130–139, May 2001.

[103] D. Bellan and S. Pignari, "Probability density function of load voltages in randomly excited multiconductor transmission line," *Electron. Lett.*, vol. 36, no. 19, pp. 1606-1607, Sep. 2000.

[104] M. Larbi, P. Besnier, B. Pecqueux, and F. Puybaret, "Plane wave coupling to an aerial electrical cable. Assessment of extreme interference levels with the controlled stratification method," in *Proc. Int. Sym. EMC EUROPE*, Wroclaw, Poland, Sep. 2016, pp. 112–117.

[105] S. Pignari and D. Bellan, "Statistical characterization of multiconductor transmission lines illuminated by a random plane-wave field," in *Proc. IEEE Int. Sym. EMC*, Washington, DC, USA, Aug. 2000, vol. 2, pp. 605–609.

[106] G. Spadacini, F. Grassi, and S. A. Pignari, "Statistical properties of low frequency voltages induced by a plane-wave field across the terminal loads of a random wire-bundle," in *Proc. IEEE Int. Sym. EMC*, Dresden, Germany, Aug. 2015, pp. 824–829.

[107] Y. Huang, "The investigation of chamber for electromagnetic systems," Ph.D. dissertation, Dept. of Eng. Sci., Univ. of Oxford, Oxford, U.K., 1993.

[108] Y. Huang and D. J. Edwards, "A novel reverberating chamber: the source-stirred chamber," in *Proc. 8th Int. Conf. EMC*, Edinburgh, UK, Sep. 1992, pp. 120–124.

[109] Y. Huang and K. Boyle, *Antennas: From Theory to Practice*. Chichester, UK: John Wiley & Sons, Ltd, 2008.

[110] Z. Fei, Y. Huang, J. Zhou, and Q. Xu, "Statistical analysis of crosstalk subject to multiple uncertainty sources using stochastic reduced order models," in *Proc. Int. Sym. EMC EUROPE*, Wroclaw, Poland, Sep. 2016, pp. 690–694.

[111] Z. Fei, Y. Huang, J. Zhou, and Q. Xu, "Sensitivity analysis of cable crosstalk to uncertain parameters using stochastic reduced order models," in *Proc. IEEE Int. Sym. EMC*, Ottawa, ON, Canada, Jul. 2016, pp. 385–389.